

VIBRATIONAL SUM FREQUENCY SPECTROSCOPIC INVESTIGATIONS
OF SULFUR DIOXIDE ADSORPTION TO
ATMOSPHERICALLY RELEVANT AQUEOUS SURFACES

by

STEPHANIE TOMOKO OTA

A DISSERTATION

Presented to the Department of Chemistry
and the Graduate School of the University of Oregon
in partial fulfillment of the requirements
for the degree of
Doctor of Philosophy

June 2011

DISSERTATION APPROVAL PAGE

Student: Stephanie Tomoko Ota

Title: Vibrational Sum Frequency Spectroscopic Investigations of Sulfur Dioxide Adsorption to Atmospherically Relevant Aqueous Surfaces

This dissertation has been accepted and approved in partial fulfillment of the requirements for the Doctor of Philosophy degree in the Department of Chemistry by:

Dr. Paul C. Engelking	Chair
Dr. Geraldine L. Richmond	Advisor
Dr. Jeffrey A. Cina	Member
Dr. Thomas R. Dyke	Member
Dr. Alan D. Johnston	Outside Member

and

Richard Linton	Vice President for Research and Graduate Studies/ Dean of the Graduate School
----------------	---

Original approval signatures are on file with the University of Oregon Graduate School.

Degree awarded June 2011

© 2011 Stephanie Tomoko Ota

DISSERTATION ABSTRACT

Stephanie Tomoko Ota

Doctor of Philosophy

Department of Chemistry

June 2011

Title: Vibrational Sum Frequency Spectroscopic Investigations of Sulfur Dioxide Adsorption to Atmospherically Relevant Aqueous Surfaces

Approved: _____
Dr. Geraldine L. Richmond

Aqueous aerosol surfaces are an important platform for chemical reactions through which gases are transported in the atmosphere. The chemical complexity of aqueous aerosols is well-established, but many questions remain about the molecular nature of their surfaces, particularly with respect to the uptake of gases. The pollutant sulfur dioxide, SO_2 , has been implicated in environmental phenomena such as acid rain, climate change, and cloud formation. SO_2 is fundamentally interesting because it forms spectroscopically identifiable complexes with water at aqueous surfaces. This dissertation aims to understand how temperature and aqueous composition impact the formation of surface complexes between water and SO_2 . Vibrational sum frequency spectroscopy (VSFS), a surface specific technique, is used to probe the vibrational modes of water and small organic molecules, investigating changes to the overall orientation, bonding environment, and structure of interfaces when aqueous surfaces are exposed to SO_2 .

SO_2 adsorption to water at tropospherically relevant temperatures (0–23 °C) is examined first. The results show enhanced SO_2 surface affinity at colder temperatures,

with most of the topmost water molecules showing evidence of binding to SO_2 at $0\text{ }^\circ\text{C}$ compared to a much lower fraction at room temperature. Surface adsorption results in significant changes in water orientation at the surface but is reversible at the temperatures examined.

The surface and vibrational specificity of these studies can be used to distinguish between the effects of surface adsorption compared to bulk accommodation. This distinction is utilized to demonstrate that SO_2 complexation is independent of solution acidity, confirming that bulk absorption is unnecessary for surface adsorption to occur.

Finally, the impact of the organic species succinic acid and formaldehyde on the formation of surface SO_2 complexes is examined. These experiments indicate that SO_2 surface complexation occurs primarily with water but that surface active organic species may interact with gases under certain circumstances, namely when the organic species are more chemically reactive towards the gas. These studies have important implications for atmospheric chemistry and the uptake of gases, particularly in the complex aqueous environments expected in the troposphere.

CURRICULUM VITAE

NAME OF AUTHOR: Stephanie Tomoko Ota

GRADUATE AND UNDERGRADUATE SCHOOLS ATTENDED:

University of Oregon, Eugene, Oregon
Carleton College, Northfield, Minnesota

DEGREES AWARDED:

Doctor of Philosophy in Chemistry, 2011, University of Oregon
Master of Science in Chemistry, 2005, University of Oregon
Bachelor of Arts in Chemistry, 2000, Carleton College

AREAS OF SPECIAL INTEREST:

Atmospheric Chemistry, Physical Chemistry, Surface Science, Laser Spectroscopy,
Science Education & Teaching

PROFESSIONAL EXPERIENCE:

Research Assistant in the Richmond Laboratory, University of Oregon, Eugene,
OR , (2005–present)

Visiting Instructor in Chemistry, Equilibrium and Analysis Laboratory, Carleton
College, Northfield, MN (Spring 2008)

Graduate Teaching Assistant, Advance General Chemistry Laboratory,
University of Oregon, Eugene, OR (2004–2005)

Teacher, Physical Science and Pre-Calculus, The College Preparatory School,
Oakland, CA (2000–2004)

Lab Assistant, General Chemistry, Carleton College, Northfield, MN (1999–2000)

Research with Dr. Marion Cass, Carleton College, Northfield, MN (1998–2000)

PUBLICATIONS:

Ota, S. T., and Richmond, G. L. (2011) Chilling Out: A Cool Aqueous Environment Promotes the Formation of Gas–Surface Complexes. *J. Am. Chem. Soc.* *133*, 7497–7508

Tarbuck, T. L., Ota, S. T., and Richmond, G. L. (2006) Spectroscopic Studies of Solvated Hydrogen and Hydroxide Ions at Aqueous Surfaces. *J. Am. Chem. Soc.* *128*, 14519–14527

ACKNOWLEDGEMENTS

The research presented in this dissertation would not have been possible without the advice and encouragement of many people including friends, family, co-workers, and mentors. I am grateful to all of them for their support throughout graduate school. I feel incredibly lucky to have had the opportunity to work in the Richmond Lab, and was privileged to have had the support of a wonderful advisor, Dr. Geraldine Richmond. Geri, you set high standards for research while leading a balanced life; I really appreciate your support of my personal interests both in and outside of the lab. The Richmond lab members, both past and present have been invaluable to me as a source of both academic and moral support - they have been a constant source of inspiration and fun.

I was fortunate to be mentored by Dr. Teresa Tarbuck, whose work in the lab provided the inspiration for my own research, and whose friendship has I value deeply. Teresa and Melissa - thank you for helping me keep things in perspective during my first few years in the lab with yoga, Toshi's and lots of laughs. Cathryn - graduate school would not have been the same without you. Thank you for the advice, support, and many cheese-related snacks and outings. You are an incredible friend. Dan, Jill, Joe, and Lulu - I don't know if I would have finished without your support - thank you for being my family down the street. Dan - thank you for always being a willing sounding board for my research questions and ideas in addition to being a great friend. Hristina, Katy, Ellen, Davida, Pat, Eric, Adam, and Dave - thank you for making the lab a great place to work.

These experiments would never have succeeded without the technical skills and advice of many people. Kris, John, and Jeffrey in the machine shop built and designed

the sample cell, and were incredibly patient with me as I learned to make small modifications on my own. Fred, Dennis, and Matt helped me implement Labview for the data acquisition, answering my numerous computer-related questions with the utmost patience. The modifications to the laser system would not have been possible without the support and advice of Larry Scatena. Larry - thank you for being a great sounding board and resource for my many optics related questions. My committee members, Professors Paul Engelking, Jeff Cina, Tom Dyke, and Dana Johnston were invaluable for their support and advice as my research project evolved over the past few years.

My friends and family members outside of the lab have provided an important sense of balance to my life during graduate school. I am grateful to them for helping me to keep things in perspective and for providing a welcome diversion from the basement. Finally, I would like to thank my mom for pushing me to go back to school. Her sincere love of learning, and genuine curiosity about everything has instilled in me a strong appreciation for education. Thank you for keeping me well supplied with blueberries and tofu, and for being a constant source of love and support.

This research was funded by the National Science Foundation.

TABLE OF CONTENTS

Chapter	Page
I. INTRODUCTION	1
II. AN OVERVIEW OF VIBRATIONAL SUM FREQUENCY SPECTROSCOPY AND SPECTRAL FITTING	5
2.1 Introduction	5
2.2 Vibrational Sum Frequency Spectroscopy	5
2.3 Analyzing Vibrational Sum Frequency Spectra	8
III. EXPERIMENTAL CONSIDERATIONS	12
3.1 Introduction	12
3.2 The Picosecond Laser System	12
3.3 Sample Preparation and Analysis	19
IV. THE VAPOR/WATER INTERFACE	22
4.1 Introduction	22
4.2 Interpreting VSF Spectra of the Vapor/Water Interface	23
4.3 Isotopic Dilution Experiments	27
4.4 Conclusions	29

Chapter	Page
V. THE EFFECTS OF TEMPERATURE ON THE UPTAKE OF SO ₂ TO WATER	30
5.1 Introduction	30
5.2 SO ₂ at the Vapor/Water Interface: An Overview	31
5.3 SO ₂ at the Vapor/Water Interface	34
5.4 The Vapor/Water Interface After Exposure to SO ₂ (g)	40
5.5 Conclusions	42
VI. UPTAKE OF SO ₂ TO THE VAPOR/WATER INTERFACE AT LOW PH	44
6.1 Introduction	44
6.2 The Uptake of SO ₂ to Sulfuric Acid	45
6.3 Conclusions	49
VII. UPTAKE OF SO ₂ TO AQUEOUS SUCCINIC ACID	50
7.1 Introduction	50
7.2 Succinic Acid at the Vapor/Water Interface	52
7.3 Isotopic Substitution Experiments	54
7.4 Uptake of SO ₂ to Succinic Acid	58
7.5 Conclusions	60

Chapter	Page
VIII. THE UPTAKE OF SO ₂ TO AQUEOUS FORMALDEHYDE	62
8.1 Introduction	62
8.2 Formaldehyde at the Vapor/Water Interface	65
IX. CONCLUSIONS	82
APPENDICES	
A. CALCULATED CONCENTRATIONS FOR ISOTOPIC DILUTION STUDIES	85
B. FITTING PARAMETERS FOR SUCCINIC ACID	87
C. FITTING PARAMETERS FOR FORMALDEHYDE	89
REFERENCES CITED	91

LIST OF FIGURES

Figure	Page
2.1. Schematic of the sum frequency experiment	8
3.1. Schematic of the Picosecond Sum Frequency Laser System	13
3.2. IR Energy Profiles using KTP versus KTA	16
3.3. Illustration of Temperature-Controlled VSFS	17
3.4. IR polystyrene absorbances and VSFS uncoated gold	20
4.1. Isotopic dilution series of water at 0 °C	25
4.2. Contributions from fitted OH stretching regions as a function of temperature	27
5.1. Spectra of the OH stretching region before, during, and after exposure to SO ₂ at 23 °C and 0 °C.	33
5.2. Isotopic dilution series at 0 °C with SO ₂ flowing	35
5.3. ssp-spectra with SO ₂ flowing as a function of temperature.	38
5.4. Isotopic dilution series taken after purging SO ₂ from the system	41
5.5. Relative contributions from the fitted OH stretch region, after exposure to SO ₂ , as a function of temperature	41
5.6. Cartoon of the SO ₂ :H ₂ O interface.	43
6.1. 2.5 M H ₂ SO ₄ at 23 °C and 0 °C	45
6.2. Overall fit and resonant components for H ₂ SO ₄	47
7.1. VSF Spectra of 0.25 M Succinic Acid	53
7.2. VSF Spectra of Succinic Acid in D ₂ O.	55
7.3. VSF Spectra of 0.25 M (CD ₂ (COOH)) ₂	56
7.4. Spectra of Succinic Acid with SO ₂	59

Figure	Page
8.1. VSF Spectra of 3.2 % w/v formaldehyde. Water is shown in gray for comparison.	66
8.2. Global Fits to spectra of CH ₂ O(aq) as a function of concentration.	67
8.3. Fit to ssp-polarization spectra of 3.2 % w/v formaldehyde with resonant components	68
8.4. Spectra of 3.2 % w/v formaldehyde with SO ₂ flowing and after exposure to SO ₂	71
8.5. Spectra of 16 % w/v formaldehyde. Evolution of the CH stretching region as a function of time.	72
8.6. ssp-polarization spectra of HMS	74
8.7. 3.2 % w/v formaldehyde before (green), during (red), and after (blue) exposure to SO ₂ . Data acquired at ~0 °C. a. ssp-polarization spectra b. sps-polarization spectra.	76
8.8. Comparison of spectra taken in the ssp and sps polarization schemes while SO ₂ is flowing at 0 °C.	77
8.9. Cartoon depiction of the evolution of aqueous formaldehyde with SO ₂ exposure over time	81
B.1. The evolution of succinic acid exposed to SO ₂ . Fits and resonant components.	87

LIST OF TABLES

Table	Page
A.1. Calculated Isotopic Dilution Concentrations	86
B.1. Fitting Parameters for Succinic Acid Resonant Peaks	88
C.1. Fitting Parameters for Formaldehyde CH-stretch Region	90

CHAPTER I

INTRODUCTION

The importance of water on Earth is unrefuted. It is undeniably one of the most important molecules for chemistry on both the ground and in the atmosphere. We are continually learning more about the reactivity of atmospheric constituents in the gas phase and in the chemical soup that is comprised within aqueous aerosols. For example, ions such as salts and acids are commonly solvated in the aqueous phase of aerosols, whereas organic species, including dicarboxylic acids, aldehydes, and surfactants, are expected to accumulate closer to the surface.^{1,2} Atmospheric chemistry often involves both gaseous and solvated species, and studies of heterogeneous reaction are the focus of many recent reviews.³⁻⁸ Yet a comprehensive understanding of the role of the surface separating the gas and liquid phases in the uptake process remains elusive.⁹ Does it operate as a barrier to reactivity, as a free pathway for entry, or as a temptress that promotes gas uptake? And how are interfacial interactions affected by the lower temperature of the atmosphere, which can not only affect surface condensation but also bulk solubility and bulk reactivity? In the absence of reaction, the solubility of most gases is inversely proportional to temperature but it is unknown whether an increase in bulk solubility at lower temperatures is accompanied by enhanced surface interactions as well. In addition to physical properties such as temperature, the chemical composition of aqueous aerosols increases the complexity of these surface interactions. Do organic species act to inhibit or enhance gas uptake, and how does the nature or the interaction, chemical or physical, influence surface complexation? The answers to these types of questions are important for accurately modeling gas uptake and reactivity in the atmosphere.

Sulfur dioxide gas, SO_2 , is an atmospheric pollutant with both industrial and terrestrial sources. Uptake of gases such as SO_2 by aqueous aerosols depends on many factors including gas-phase diffusion, bulk solubility, mass accommodation probability (the probability of entering the bulk after striking the surface), and bulk reaction rates. Additional complexity arises because all of these factors may be dependent on additional factors such as temperature, pH, and droplet composition¹⁰⁻²⁹.

The role of surface intermediates is relevant to understanding the results of previous studies that measured the dependence of SO_2 uptake rates on pH, temperature, and aqueous composition.^{6,10,14,16,19,22,23,30-33} These early studies initiated an important discussion regarding whether the effect of higher bulk solubility, via changes in either temperature or pH, is to reduce or enhance surface adsorption and complexation of SO_2 . They also highlight the importance of experimental techniques that can investigate surface behavior more directly. The ability to selectively probe surface complexes with water using vibrational sum frequency spectroscopy (VSFS) enables us to explore SO_2 surface adsorption when it is coupled to interactions with solvated species in solution.

The experiments described in this dissertation investigate the role of surface complexes in the atmosphere through experiments that probe SO_2 adsorption on water and aqueous solution surfaces at temperatures ranging from 0 to 23 °C. In particular, these studies were designed to answer three main questions: How does temperature impact SO_2 adsorption and complexation at the water surface? Are surface complexes inhibited by the same chemistry that inhibits bulk reactivity? And how do small surface active organic species impact surface adsorption of SO_2 ?

Prior to a discussion of the experimental results, Chapter II provides an overview of vibrational sum frequency spectroscopy, the technique utilized in this research.

Chapter III details the instrumentation and experimental parameters used in these experiments, followed by a discussion of how the data is analyzed. Chapter IV gives an overview of the vapor/water interface, followed by a discussion of how temperature affects the interfacial water environment.

Chapter V describes the use of VSFS to examine how temperature affects SO₂ complexation at water surfaces for six temperatures between 0 °C and 23 °C. At each temperature, the OH vibrational stretching region of surface water is examined before, during, and after exposure to SO₂ gas. These VSFS experiments address the question of whether surface affinity increases with bulk solubility as a function of temperature. Isotopic dilution experiments are conducted at 0 °C and, as in previous studies,³⁴⁻³⁶ used as a means of obtaining fitting parameters for the different interfacial environments. Global spectral fitting routines are employed to understand the molecular phenomena reflected in the data, and the results are discussed in the context of recent experimental and theoretical studies, and their implications for the environment.

In a subsequent set of studies, described in Chapter VI, the aqueous solution pH is varied to explore the mechanistic questions raised by the observation of earlier research that uptake enhancement varies with solution pH.¹⁶ These experiments are also used to distinguish spectral changes due to adsorption of SO₂ to the water surface from changes due to SO₂ solution reactivity. Changes to the molecular structure and bonding of surface water molecules upon variation of both temperature and pH with the addition of SO₂ are analyzed in reference to the structure of the neat vapor/water interface.

The experiments in Chapters VII and VIII are focussed on the question of how surface complexation of SO₂ to water changes if there are other molecules already

at the surface. The experiments in Chapter VIII examine the behavior of succinic acid, $(\text{HOOCCH}_2)_2$, a dicarboxylic acid with both biological and industrial sources that is commonly found in the atmosphere. Significantly, it is often a co-pollutant of SO_2 , resulting from the combustion of fuels. However, it is not expected to react with SO_2 , and can be used as a model system to study the surface adsorption of SO_2 in the presence of other surface species without the added complexity of additional chemical reactions. Chapter VII describes experiments examining the spectroscopic response of the vapor/succinic acid (aq) interface both with and without exposure to SO_2 .

The experiments described in Chapter VIII add another level of complexity, probing interactions between SO_2 and formaldehyde (CH_2O), which is known to react with HSO_3^- in solution. Both SO_2 and CH_2O have been detected at high levels in the fog and cloud water of the polluted environments near industrial areas. This has prompted numerous investigations into the importance of the reaction between CH_2O and HSO_3^- ions, which produces forms a stable S(IV) species in the atmosphere.³⁷⁻⁴² The results from the previous chapters will provide a context within which to understand the spectral response from aqueous formaldehyde solutions. The solutions will be probed with and without exposure to SO_2 gas.

Chapter IX provides an overview of the results from these experiments. The picture of aqueous surface complexes developed through these studies will be used to evaluate the importance of SO_2 surface adsorption in atmospheric chemistry. Finally, these findings will be discussed within the context of their overall environmental implications.

CHAPTER II

AN OVERVIEW OF VIBRATIONAL SUM FREQUENCY SPECTROSCOPY AND SPECTRAL FITTING

2.1 Introduction

This chapter provides a brief overview of vibrational sum frequency spectroscopy (VSFS), followed by a discussion of how sum frequency data is analyzed in this research. Vibrational sum frequency spectroscopy (VSFS) is well suited to the study of aqueous interfaces. As a selective vibrational technique, VSFS provides insight into bond strength, orientation, and intermolecular interactions at surfaces, and there are many resources available on the general aspects of the technique.^{5,43–56,56–66} This chapter will begin with a brief overview of how light interacts with matter, leading to a discussion of the specifics regarding VSFS. This is followed by a description of how the technique is implemented in this research, and a discussion of how the data is analyzed and interpreted.

2.2 Vibrational Sum Frequency Spectroscopy

2.2.1 Interactions Between Light and Matter

Spectroscopy can be broadly defined as the study of how light interacts with matter. When light impinges upon a medium, the electrons in that medium feel a force exerted by the oscillating electric field (\vec{E}) from the light, resulting in an oscillating polarization (\vec{P}) from the electrons in the medium. When the light intensity is relatively small, the amplitude of the material response is proportional to the amplitude of the impinging electric field.

$$\mathbb{P} = \mathbf{P}^{(1)} = \chi^{(1)} \mathbf{E} \quad (2.1.)$$

The linear spectroscopic regime gives rise to processes such as reflection and refraction. When more intense coherent light such as that from a laser is used the linear approximation is no longer sufficient and higher order terms must be considered. The total polarization can be expressed as a series expansion using the electric dipole approximation,

$$\mathbf{P} = \chi^{(1)} \mathbf{E} + \chi^{(2)} : \mathbf{E}\mathbf{E} + \chi^{(3)} : \mathbf{E}\mathbf{E}\mathbf{E} \dots + \dots \quad (2.2.)$$

where the material properties are represented by the first, and higher order, susceptibilities $\chi^{(n)}$. When the incident light is composed of two laser beams with different frequencies, ω_1 and ω_2 , the surface \mathbf{E} field can be expressed as

$$\mathbf{E} = \mathbf{E}_1 \cos(\omega_1 t) + \mathbf{E}_2 \cos(\omega_2 t). \quad (2.3.)$$

Thus, the second order polarizability term, $\mathbf{P}^{(2)}$ can be expressed as

$$\mathbf{P}^{(2)} = \chi^{(2)} (\mathbf{E}_1 \cos(\omega_1 t) + \mathbf{E}_2 \cos(\omega_2 t))^2, \quad (2.4.)$$

which can be expanded to yield

$$\mathbf{P}^{(2)} = \chi^{(2)} (\mathbf{E}_1^2 \cos(2\omega_1 t)) + \frac{1}{2} \chi^{(2)} \mathbf{E}_1 \mathbf{E}_2 [\cos(\omega_1 + \omega_2)t + \cos(\omega_1 - \omega_2)t] + \chi^{(2)} (\mathbf{E}_2^2 \cos(2\omega_2 t)). \quad (2.5.)$$

The first and last terms describe induced polarizations oscillating at twice the incident frequency (second harmonic generation), while the middle two terms describe the origins of sum and difference frequency generation. The non-linear oscillating

polarization emits coherent light propagating in a direction defined by conservation of momentum; ideally different from that of the incident electric fields.

2.2.2 The Second Order Susceptibility

The second order susceptibility term, $\chi^{(2)}$, is a rank three tensor containing up to 27 different elements ($\chi_{xxx}, \chi_{xxy}, \chi_{xxz} \dots$), but symmetry constraints can be used to reduce the number of non-zero, contributing elements. In a centrosymmetric environment, such as a bulk medium, all directions must be identical resulting in the relationship $\chi_{ijk}^{(2)} = \chi_{-i-j-k}^{(2)}$. This reversal of the axis system is equivalent to reversing the sign of the physical response, $\chi_{ijk}^{(2)} = -\chi_{-i-j-k}^{(2)}$. The only circumstance under which both of these relationships can be true is if $\chi_{ijk}^{(2)} = 0$. Thus, VSFS is forbidden in isotropic bulk media. However, this symmetry is necessarily broken at the boundary between two centrosymmetric media, such as air and water, with the result that such surfaces are VSF active. Liquid surfaces, such as that of water, are isotropic about the surface normal, giving them a C_∞ rotation axis, meaning that $z \neq -z$, but $x = -x$ and $y = -y$ (where the xy-plane is defined as the surface normal) as illustrated in Fig. 2.1.. Under these symmetry conditions, and using the same arguments made above, there are seven non-zero elements of $\chi^{(2)}$, which reduce to four unique elements because the x and y axes are interchangeable within the interfacial plane. These elements are the only components of the second order susceptibility that can contribute to VSF signal from a C_∞ surface.

$$\chi_{xxz}^{(2)} = \chi_{yyz}^{(2)}, \chi_{xzx}^{(2)} = \chi_{yzy}^{(2)}, \chi_{zxx}^{(2)} = \chi_{zyy}^{(2)}, \chi_{zzz}^{(2)} \quad (2.6.)$$

The macroscopic second order susceptibility, $\chi^{(2)}$, may contain both resonant and nonresonant contributions, each of which must be considered for the data analysis.

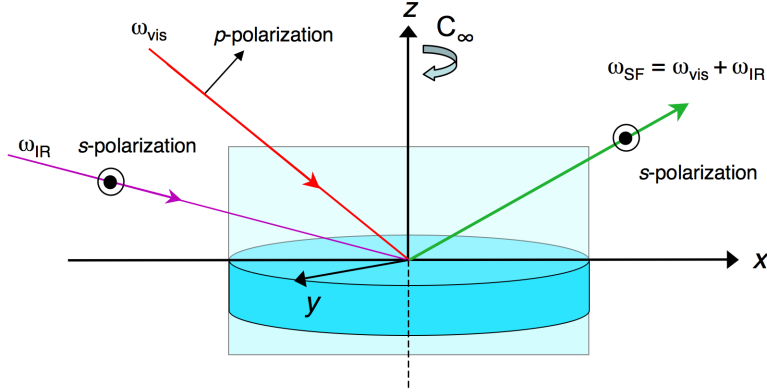


FIGURE 2.1. Schematic of laboratory frame and beam geometry for the sum frequency experiment.

$$\chi^{(2)} = \chi_{NR}^{(2)} + \sum_{\nu} \chi_{R(\nu)}^{(2)} \quad (2.7.)$$

2.3 Analyzing Vibrational Sum Frequency Spectra

In the VSFS experiment, a visible beam is spatially and temporally overlapped with a tunable infrared beam at the interface, resulting in the generation of VSF signal from the anisotropic surface region, as illustrated in Fig. 2.1.. The intensity of the emitted sum frequency signal, I_{SF} is proportional to the square of the induced macroscopic polarizability, $|\mathbf{P}_{SF}^{(2)}|^2$, which depends on the intensities of the incident beams.

$$I_{SF} \propto |\mathbf{P}_{SF}^{(2)}|^2 \propto |\chi_{sfg}^{(2)}|^2 I_{vis} I_{IR} \propto |\chi_{NR}^{(2)} + \sum_{\nu} \chi_{R(\nu)}^{(2)}|^2 I_{vis} I_{IR} \quad (2.8.)$$

As a coherent spectroscopy, the VSF signal contains both amplitude and phase information, and Eq. (2.8.) can be expressed as

$$I_{\text{SF}} \propto |\mathbf{P}_{\text{SF}}^{(2)}|^2 \propto |A_{\text{NR}}e^{i\psi_{\text{NR}}} + \sum_{\nu} A_{R\nu}e^{i\phi_{\nu}}|^2 I_{\text{vis}}I_{\text{IR}} \quad (2.9.)$$

The amplitude of the nonresonant component is determined by the medium, and does not vary with frequency. The resonant term is determined by the number of contributing molecules and the orientationally averaged molecular hyperpolarizability, $\langle\beta_{\nu}\rangle$.

$$\chi_{\text{R}(\nu)}^{(2)} = \frac{N}{\epsilon_0} \langle\beta_{\nu}\rangle \quad (2.10.)$$

where

$$\beta_{\nu} = \sum_{\nu} \frac{M_{IJ}A_K}{\omega_{\nu} - \omega_{\text{IR}} - i\Gamma_{\nu}}. \quad (2.11.)$$

In this equation, A_K is the IR transition moment, M_{IJ} is the Raman transition probability, ω_{ν} is the resonant mode frequency, and Γ_{ν} is the natural linewidth of transition. The orientational average over β has important implications, as the average molecular orientation for an isotropic medium is zero, meaning that molecules must adopt a net orientation to contribute sum frequency intensity. Due to the Lorentzian form of β , an enhancement in the sum frequency signal occurs when the frequency of the IR radiation is resonant with a sum frequency active vibration. Thus, by using a fixed frequency visible beam and a variable frequency IR beam, one can tune the IR to generate a vibrational spectrum of surface molecules.

The VSFS experiment can be set up to selectively probe the four non-zero susceptibility tensor elements by using different polarization schemes. The experiments presented in this dissertation probe two of these tensor elements, $\chi_{xzz}^{(2)}$ and $\chi_{xzx}^{(2)}$, by using the ssp and sps polarization combinations, where the polarization notations denote the sum-frequency, visible, and infrared polarizations, respectively.

Electric fields oscillating in the plane of incidence are designated p , while those normal to the plane of incidence are designated s . The ssp-polarization scheme probes components of the transition dipole that are perpendicular to the plane of the interface, while the sps- polarization scheme probes components of the transition dipole that are parallel to the plane of the interface.

2.3.1 Spectral Fitting

The sum-frequency intensity is proportional to the square of the second order susceptibility, $\chi^{(2)}$, which has both resonant and non-resonant components. Spectra must be fit to deconvolve the individual resonant modes, a non-trivial task. A fitting routine implemented by Moore et al,⁶⁷ allows us to account for both the homogeneous and inhomogeneous line widths of the vibrational modes using the expression in Eq. (2.12.), which was first proposed by Bain.⁶⁸

$$\chi^{(2)} = \chi_{\text{NR}}^{(2)} e^{i\psi} + \sum_{\nu} \int_{-\infty}^{+\infty} \frac{A_{\nu} e^{i\phi_{\nu}} e^{-[(\omega_{\text{L}} - \omega_{\nu})/\Gamma_{\nu}]^2}}{\omega_{\text{L}} - \omega_{\text{IR}} + i\Gamma_{\text{L}}} d\omega_{\text{L}} \quad (2.12.)$$

The first term in Eq. (2.12.) is the nonresonant second-order susceptibility. The second term is a sum over all resonant vibrational modes and is represented as $\chi_{R(\nu)}^{(2)}$. The resonant susceptibility, $\chi_{R(\nu)}^{(2)}$, is proportional to N , the number of molecules contributing to the sum frequency response, and $\langle\beta_{\nu}\rangle$, the orientationally averaged molecular susceptibility:

$$\chi_{R(\nu)}^{(2)} = \frac{N}{\epsilon_0} \langle\beta_{\nu}\rangle \quad (2.13.)$$

The second term in Eq. (2.12.), the resonant susceptibility (Eq. (2.13.)), is fit as a convolution of the homogenous line widths of the individual molecular transitions

(HWHM, Γ_L) with inhomogeneous broadening (fwhm, $\sqrt{2 \ln 2} \Gamma_\nu$). The transition strength A_ν is proportional to the product of the number of contributing molecules and their orientationally averaged IR and Raman transition probabilities. The frequencies of the IR, the Lorentzian, and the resonant modes are ω_{IR} , ω_L , and ω_ν , respectively. The phase of each resonant mode is ϕ_ν . The intensity of sum frequency spectra are complicated, and changes can arise from changes in the number of contributing molecules, changes in orientation, and/or a change in bond energies.

The parameters used to fit the neat vapor/water interface in ssp-polarization were determined in previous isotopic dilution studies.^{34,35,69} Each resonant peak contains 5 variables (2.12.), thus there may be non-unique fitting solutions. To reduce the number of variables associated with the fits: The phases are fixed at either π (for peaks between 3200–3600 cm^{-1}) or 0 (for peaks below 3200 or above 3600 cm^{-1}); lorentzian widths are fixed at 12 cm^{-1} (for the free OH), 5 cm^{-1} for the remaining OH stretches, or 2 cm^{-1} for the CH stretches; and global fitting routines are employed to constrain parameters where possible. The global fitting routine iteratively fits the data while constraining peak positions, phases, and gaussian widths such that the only variables for different samples are the peak amplitudes, lending higher confidence to the results. To account for changes due to perturbation by gas flow, ions, or organic solutes, spectra were first fit using the same parameters used for the neat water system, allowing only amplitudes to vary. Additional peaks were only added if they were both phenomenologically reasonable and necessary to achieve good agreement between the fits and the spectral response. Detailed discussions spectral fits and their interpretation are presented in conjunction with the pertinent experiments. The next chapter focusses on the experimental considerations and instrumentation used for these studies.

CHAPTER III

EXPERIMENTAL CONSIDERATIONS

The previous chapter detailed the theory describing VSFS, enabling us to understand why it is an appropriate technique for the investigation of surface complexes at the vapor/water interface. The following discussion will address the experimental considerations, beginning with an overview of the laser system used to implement these experiments, and a description of the sum-frequency experiment, including a discussions of how samples are prepared. This is followed by an overview of the techniques used for calibration and normalization of the raw sum frequency signal.

3.1 Introduction

As a second-order nonlinear process, the sum-frequency signal is proportional to the intensities of the incoming light, as well as the square of the non-linear susceptibility of the medium. The neat vapor/water interface has a small nonlinear susceptibility; thus good signal to noise ratios are achieved by maximizing the intensities without heating, and thus degrading, the sample. Pulsed lasers, such as the one used in these experiments, generate high peak powers that can be used to generate sum frequency without heating the surface.

3.2 The Picosecond Laser System

The laser system used for these experiments has been described in previous publications, and was originally designed and implemented by Dr. Derek Gragson and Dr. David Alavi in 1995^{70,71} Since its original implementation, the laser system

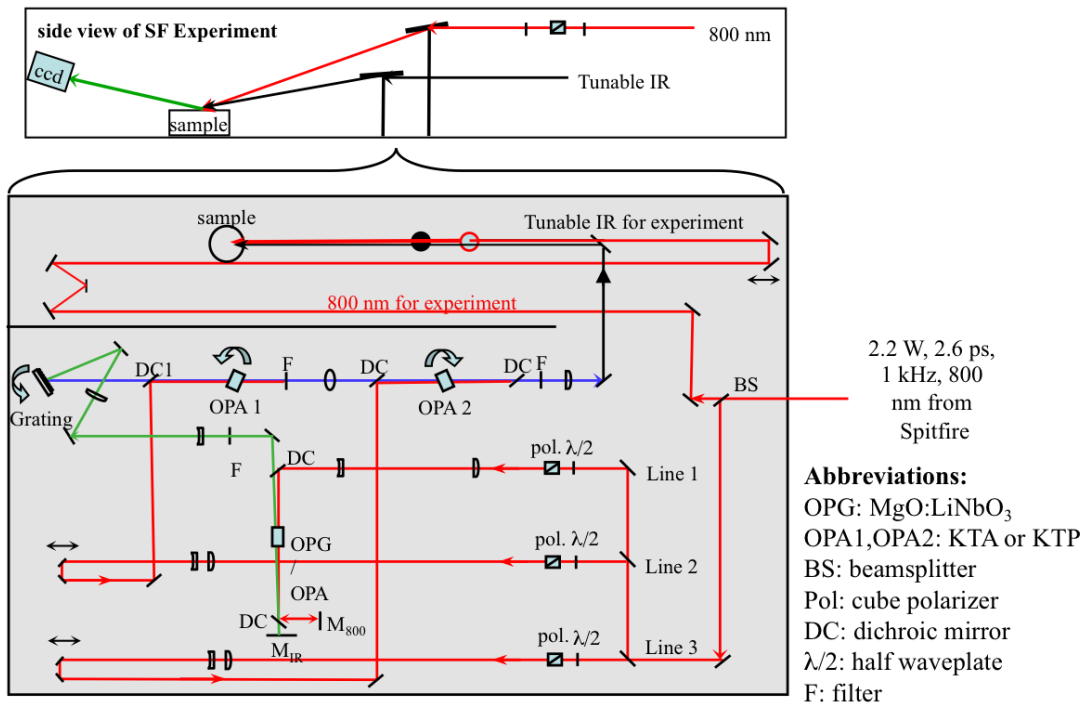
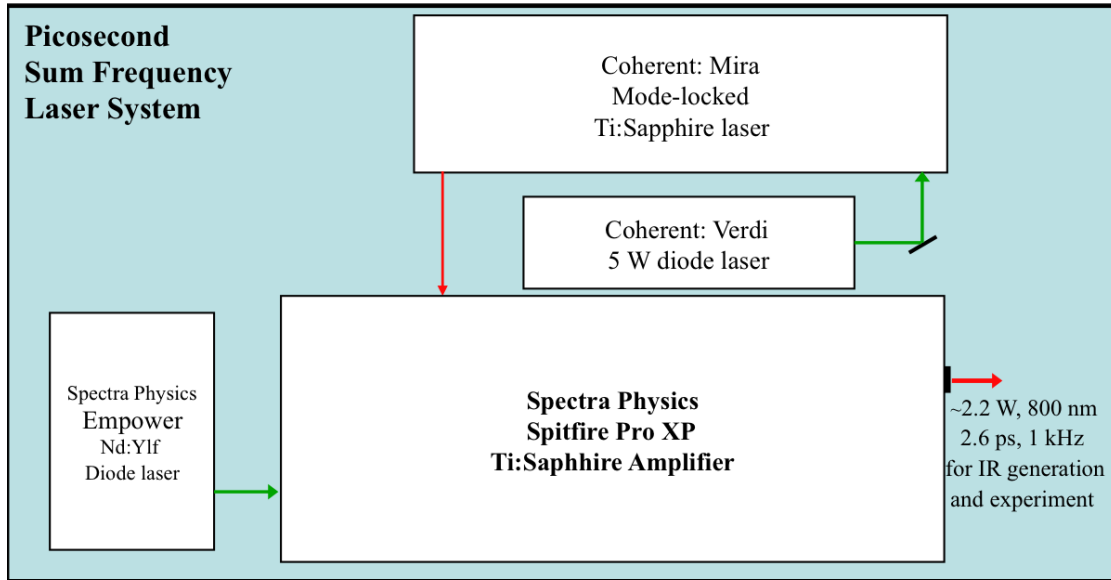


FIGURE 3.1. Schematic of the Picosecond Sum Frequency Laser System

has undergone several upgrades; the first of which was the implementation of an OPG/OPA stage to replace the original white-light generation cell and the use of a ccd detector.⁷² Continual upgrades to the laser system have been made to improve the power and stability of the visible light source, as well as to extend the tuning range of the IR light.

3.2.1 Visible Light Source

A schematic of the laser system used to generate the visible light used in these experiments is shown in Fig. 3.1. (top). Production of the 800 nm beam used for both the IR generation and the sum-frequency experiments begins with a Ti:Sapphire (Coherent Mira) passively mode-locked laser pumped with 5.5 W of a 532 nm laser beam from a Coherent Verdi laser. The resultant ~ 135 fs, 800 nm light is used to seed a Ti:Sapphire amplifier (Spectra Physics Spitfire Pro XP) pumped with 15 W of 527nm light (Spectra Physics Empower Laser), which produces a 2.6 ps beam at 800 nm (1 kHz repetition rate). The resultant 2.2 W is split by a 75/25 beam splitter; 25% is available for direct use in the VSF experiments, and the remaining 75% is used to generate the tunable IR.

The visible light source was upgraded in 2005 to take advantage of increases in the stability and reliability of commercially available laser systems. Functionally, the two Spectra Physics components used in the new configuration replace five Quantronix laser components described in previous publications.^{70,72} A diode-pumped Empower Nd:Ylf laser was incorporated to replace a flash-lamp pumped Quantronix 527 DP-H Nd:Ylf laser, leading to greater laser power and stability with much less maintenance. The Spitfire Pro XP system encompasses both the stretcher/compressor and regenerative amplification stages, which were previously housed separately. When

the femtosecond pulse enters the stretcher portion of the Spitfire Pro it is spectrally reflected off of a grating and aligned through a mask that is used to reduce the bandwidth of the incoming beam, resulting in the desired 2.6 ps pulse. With the improved efficiency afforded by this system, a second amplification stage (previously a double-pass Ti:sapphire amplifier) is no longer needed to produce the ~ 2.3 W of power used in these experiments, reducing the time spent maintaining and aligning the system.

3.2.2 Tunable Infrared Light Generation

The system used to generate the tunable IR light is depicted in Fig. 3.1. (bottom). Generation of the IR light is accomplished using three stages (labeled as lines one, two, and three), each of which use approximately 1/3 of the available 800 nm light. The first stage follows line one and uses a combination of optical parametric generation (OPG) and amplification (OPA). In this process, approximately 220 μJ of the 800 nm light passes through a MgO doped LiNbO_3 crystal, where it is split into two lower energy beams. The lower energy light (1.0-1.2 μm) is amplified as it reflects back through the crystal and is overlapped with the residual 800 nm light.

The resultant beam is spectrally dispersed using a grating (600 grooves/mm, blazed at 1 μm) on a computer controlled rotation stage. The rotation angle of the grating is tuned to select a portion of this light to be used as the seed for optical parametric amplification in the second stage (OPA 1). In this second line, ~ 160 μJ of 800 nm light is combined with the seed from the grating in a potassium titanyl phosphate (KTP) crystal using difference frequency generation. The grating and crystal are rotated to generate idler wavelengths from 2.4-3.8 μm (4000-2650 cm^{-1}). A long-pass filter is used to remove the high energy photons, and this light is amplified

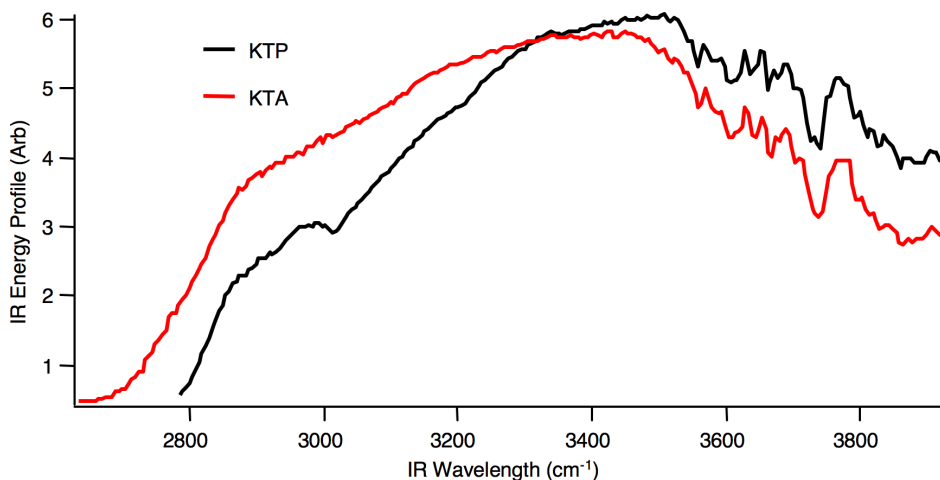


FIGURE 3.2. IR Energy Profiles showing OPA output using KTP (black) versus KTA (red).

by combining it with $\sim 250 \mu\text{J}$ of 800 nm light in a second KTP crystal (OPA 2). To compensate for beam walk-off, the second crystal is rotated in the opposite direction to that of OPA 1. A dichroic mirror and long-pass filter are used to remove the high energy photons from the resultant ($4000\text{-}2650 \text{ cm}^{-1}$) light, which is sent to the interface. The rotation angles for the grating, OPA 1, and OPA 2 stages are calculated based on the Sellmeier coefficients for KTP given by Vanherzeele et. al.⁷³

One of the limitations of KTP as a nonlinear optical material is its increasing optical opaqueness in the mid-IR region approaching 2900 cm^{-1} . This is not a problem when probing the water OH-stretch region, but can lead to strong reductions in IR energy in the CH-stretch region. For this reason, we have implemented the use of potassium titanyl arsenate (KTA), a crystallographic isomorph of KTP, in the OPA for studies involving organic solutes. The OPA is tuned in the same manner as with KTP, but the tuning angles are calculated using the Sellmeier coefficients published by Fenimore et. al.⁷⁴ Figure 3.2. shows representative IR energy profiles of the tunable IR produced using KTP (black) versus that using KTA (red). From the energy profiles,

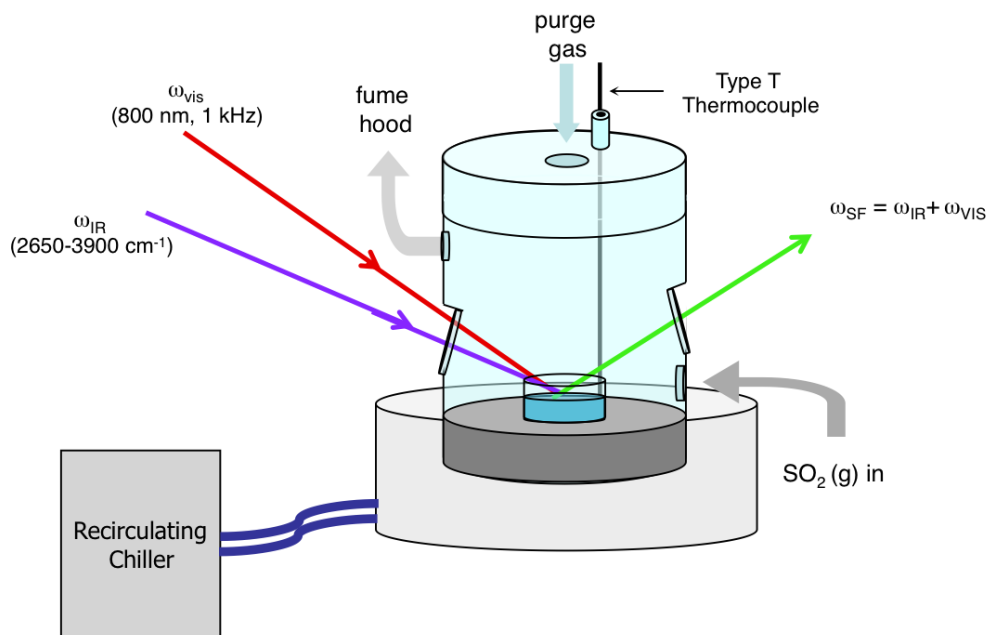


FIGURE 3.3. Illustration of the Experimental Set-up used for Temperature-Controlled VSFS Experiments

it is clear that the use of KTA can provide additional energy at the lower energy wavelengths while maintaining a wide tuning range.

3.2.3 The Interface

A schematic of the beam path for the sum frequency experiment is shown in Fig. 3.1.. Figure 3.3. shows a more detailed drawing of the sample configuration and the cell used for the temperature-controlled experiments. Sum frequency light is generated by overlapping and focussing $\sim 100 \mu\text{J}$ of 800 nm light (~ 2.6 ps, 1 kHz repetition rate) and $4\text{--}14 \mu\text{J}$ of tunable ($2700\text{--}4000 \text{ cm}^{-1}$) infrared light at the sample surface. The polarizations of the incident and collected light are set to either p- or s-polarization, representing light polarized in the plane of incidence (s) and normal to the plane of incidence (p). All of the spectra presented and discussed here were taken

using either the ssp- or sps-polarization schemes, which denote the sum-frequency, visible, and infrared polarizations, respectively. The incident IR and visible beams are co-propagated at 67° and 56° from the surface normal. Although the sum frequency light is spatially separated from the reflected visible and infrared light, some scattering does occur at the sample. An edge filter and a holographic notch filter are utilized to prevent stray light from entering the detector. After filtering, the resultant sum frequency light is collected with a thermoelectrically cooled CCD camera (Princeton Instruments: PIXIS 512).

Sum frequency experiments are particularly sensitive to organic contaminants. All surfaces making contact with experimental samples are cleaned by soaking in concentrated sulfuric acid solution containing Nochromix for at least 24 hours. After removal from the acid bath, materials are soaked overnight in ultrapure water from Barnstead E-pure system ($18\text{ M}\Omega\text{-cm}$) prior to being rinsed in copious amounts of water and dried in an oven. To minimize contamination, samples are poured into scrupulously clean glass dishes contained in a nitrogen purged Kel-f cell fitted with CaF_2 windows (Fig. 3.3.). The cell has three gas ports, two of which are used for gases; the remaining port is vented via teflon tubing to a fume hood. A smaller port in the cell lid accommodates the Teflon coated Type T thermocouple probe used to monitor sample temperature. The base of the cell is made of non-reactive stainless steel, which can undergo a rigorous cleaning process and is thermally conductive. The stainless base fits into a custom-made cooling plate containing coils that can be connected to a standard laboratory chiller. For low temperature studies, samples are thermally equilibrated for approximately an hour prior to data collection.

The data collection process is facilitated using a customized LabView program that controls the IR generation system while recording the CCD intensity and

monitoring the temperature for each data point. Sum frequency intensities are measured using a thermoelectrically cooled CCD camera with a 2 second exposure time. Intensities are recorded in 3 cm^{-1} steps over the desired tuning range, which can extend from 2650 to 3900 cm^{-1} . Gas flow experiments are conducted at atmospheric pressure with a constant SO_2 gas flow rate of 10 standard cubic centimeters per minute (sccm). Temperature is continuously monitored to ensure that the sample variation is within $1\text{ }^\circ\text{C}$ for each data point, and the temperature is recorded before and after each scan.

3.3 Sample Preparation and Analysis

Gases were purchased from AirGas: Argon (cylinder, 99.9%), Nitrogen (cylinder), and Air Liquide: SO_2 (lecture bottle, 99.99%). H_2SO_4 (5 M volumetric solution), H_2SO_3 (reagent grade), HCl, Na_2SO_3 (98%), and Succinic acid (99%) were purchased from Aldrich and used as received. D_2O (double-distilled) and $(\text{HOOC}(\text{CD}_2))_2$ (99% atom-D) were purchased from CDN Isotopes. Methanol-free formaldehyde (16 % w/v) was purchased in 10 mL ampules from Fisher and diluted as necessary with high purity water from a Barnstead E-pure system ($18\text{ M}\Omega\text{-cm}$).

3.3.1 Calibration and Normalization of Sum Frequency Spectra

The sum frequency system must be calibrated in order to produce compare-able experimental results. Every day sum frequency data is collected, three additional sets of spectra are acquired: three spectra of uncoated amorphous gold, three spectra of the neat vapor/water interface, and an IR spectrum of polystyrene. The gold and polystyrene spectra are used to calibrate the IR wavelengths for the VSF spectra, and the water spectra are used as a reference to compare the VSF intensities on different

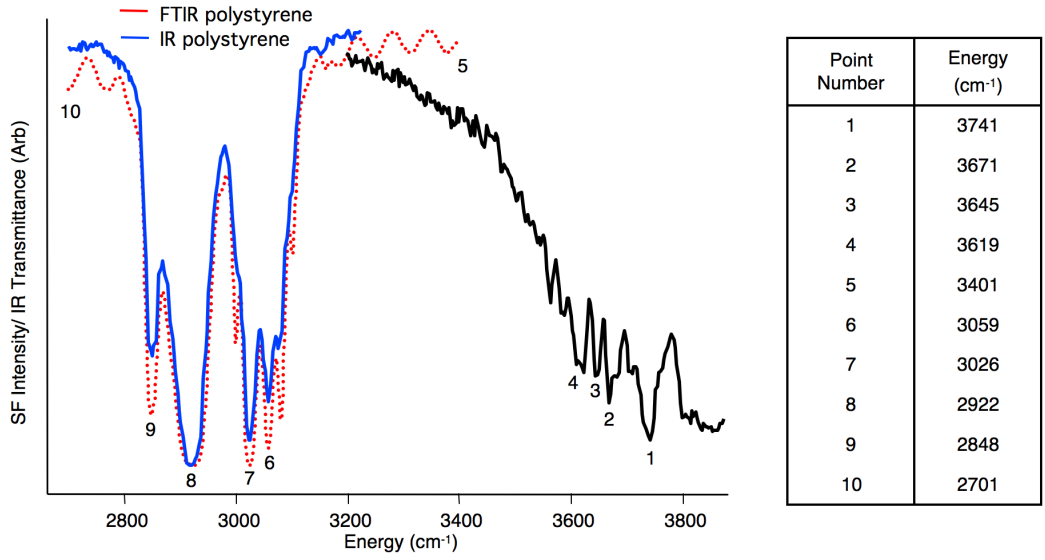


FIGURE 3.4. The tunable IR energy is calibrated daily using known IR polystyrene absorbances, and calibrated dips in the VSFS response from an uncoated gold surface.

days. The IR wavelengths are calibrated using the IR spectrum of polystyrene calibrated with an FTIR spectrometer and a VSF spectrum of gold calibrated with a monochromator. Figure 3.4. shows an example of a gold spectrum (right), a polystyrene spectrum (left), and the FTIR spectrum of polystyrene (dotted) used for the calibration. The numbers indicate the absorption wavelengths used for the calibration (far right). The IR generation is typically not optimized in the polystyrene region so overlaying the spectrum with the FTIR spectrum and rescaling the IR spectrum helps to identify the calibration energies. (Points 5 and 10 represent the end points from this rescaling). Depending on the the data acquisition range, one or both of the calibration standards are used. The known absorption wavelengths from gold and polystyrene are plotted against the uncalibrated points from the gold and IR data. The calibrated IR wavelengths are then calculated using the slope and intercept from a linear regression.

All VSF spectra are normalized for variations in SF intensity caused by spatial variation between the IR and visible beams, temporal lengthening of the IR pulses by water vapor, frequency dependent variations in the IR energy, and the frequency dependence of the optics used for filtering the sum-frequency signal. This is done by dividing each samples VSF spectrum by the average of three spectra of the nonresonant response from an unprotected gold surface obtained over the same frequency range. Spectra presented are averages of 3 to 12 spectra taken over multiple days to ensure reproducibility and to reduce the signal-to-noise ratio.

CHAPTER IV

THE VAPOR/WATER INTERFACE

Aqueous surfaces are ubiquitous in the environment, and in the atmosphere in particular. Aqueous aerosols are small (0.001 to 10,000 μm), and have relatively large surface areas. These surfaces serve as platforms for both reactive and non-reactive interactions, driving interest in interfacial chemistry in the atmosphere.^{1,2,75} The specific goals of this research are to examine the impact perturbations to an aqueous surface have on SO_2 uptake, but interpreting the spectral changes resulting from these perturbations requires us to first establish a baseline for understanding and fitting spectra of the neat vapor/water interface. This chapter begins with an overview of our current interpretation of the VSF response of the unperturbed (neat) vapor/water interface. This followed by a discussion of the use of isotopic dilution studies to establish appropriate fitting parameters when the water temperature is decreased. This chapter culminates in a discussion of how lowering the water temperature changes the interfacial response, setting the stage for studies of temperature and the uptake of SO_2 gas.

4.1 Introduction

To understand the role of interfacial chemistry and its implications for the environment, one must consider the many factors that govern the structure of aqueous aerosols and their surfaces. The current model of aerosols is an inverse micelle structure, where ions are solvated in an aqueous core surrounded by a hydrophobic organic exterior.⁷⁶ Aqueous aerosol particles are composed of numerous compounds including salts, sulfur compounds, and organics; the identification of specific organic

compounds has only recently been attempted.^{3,77-79} The chemical composition of aqueous aerosols influences environmental impact through radiative forcing, ozone depletion, and/or the formation of pollutants, such as acid rain.^{27,80} The role of interfacial chemistry in the atmosphere is the subject of much interest², as the uptake of potentially reactive compounds by aerosol particles is likely to be governed by the composition and orientation of molecules at the surface.

Given that aqueous surfaces have a prominent role in the atmosphere, it is important to have a solid molecular level understanding of the air/aqueous interfacial region. However, to develop a picture of behavior that accounts for the complexities of the aerosol surfaces, one must begin by looking at perturbations to the neat air/water interface. To begin, an overview of interfacial water structure will be presented based on current research in this field. This interpretation has mainly been developed from research conducted at room temperature, and will be followed by the presentation of isotopic dilution experiments conducted at 0 °C. These results will be discussed in conjunction with a series of spectra taken at intermediate between 0 and 23 °C, leading to a detailed discussion of vibrational assignments. The analysis and description of the neat vapor/water interface presented in this chapter will provide an important baseline for the experiments discussed in Chapters V–IX.

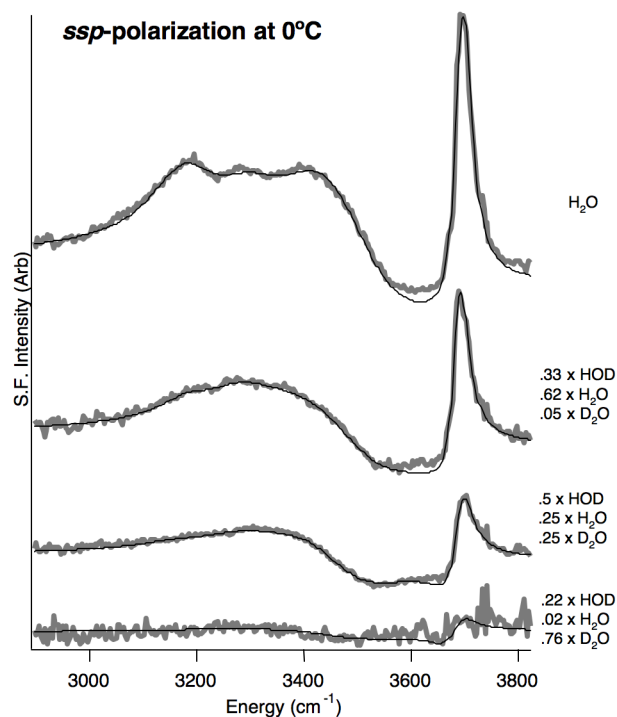
4.2 Interpreting VSF Spectra of the Vapor/Water Interface

It is difficult to give a simple molecular description of the vapor/water interface, as is evident in the many studies of molecular structure and hydrogen bonding at the water surface.^{34,69,81-107} Liquid surfaces are dynamic environments, and the continuum nature of surface water bonding can lead to collective behavior due to intermolecular coupling through hydrogen bonds. This makes the assignment of

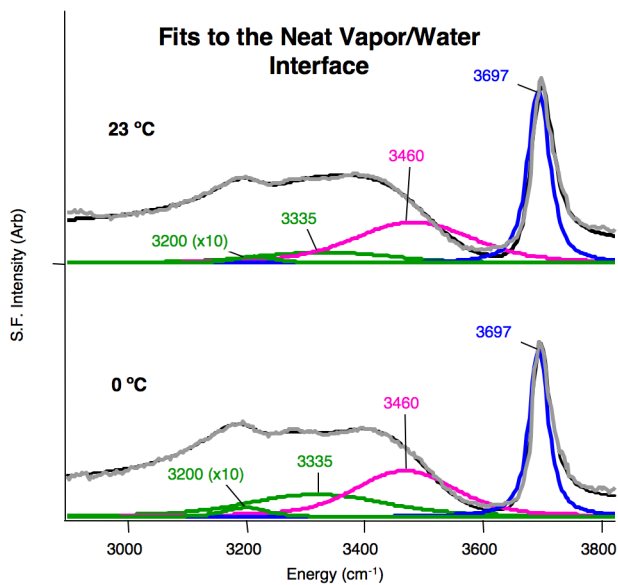
specific spectral features to particular water bonding geometries, coordinations, and strengths difficult. However, the results from computational and experimental studies by a number of groups indicate that there is a dominance of particular water species in localized interfacial regions. In general, the vapor/water interface can be described as a relatively narrow interfacial region, $\sim 6\text{--}9$ Å, where the average coordination of water molecules increases from ~ 2 bonds per molecule at the topmost surface layer to ~ 3.6 bonds per molecule in the bulk.^{34,87,88,107} Molecules with less coordination and fewer hydrogen bonds reside in the topmost water region, which is the easiest to interpret, and vibrate at higher frequencies ($3500\text{--}3700$ cm⁻¹). The highest level of coordination in the interfacial region is for the deeper tetrahedrally coordinated molecules corresponding to lower frequency vibrations ($3100\text{--}3500$ cm⁻¹).

We rely on a combination of spectral fitting and MD calculations to develop an overall picture that allows us to categorize interfacial response in terms of water orientation, coordination and hydrogen bonding. The neat vapor/water spectral assignments used in this study are based on previous isotopic dilution experiments^{34,36,69} and MD simulation results from our laboratory,^{94,96} and additional considerations from other studies.^{55,84–91,107–109} A representative fit to the neat vapor/water interface at room temperature is shown in Fig. 4.1.b (top), along with its component resonant features (colored). For simplicity, spectral contributions are described as arising from four dominant water environments, but each mode is actually comprised by contributions from several types of OH stretching environments.

The description of the vapor/water interface that is referred to throughout this study is as follows: I. The free OH peak, at ~ 3700 cm⁻¹, is attributed to unbound OH oscillators with an average orientation away from the bulk. This mode protrudes



(a)



(b)

FIGURE 4.1. a. Isotopic dilution series of water at 0 °C. Spectra are offset for clarity. Fits to the data (gray) are in black. b. Overall fits (black) to the neat vapor/water interface (gray) and resonant components (colored), at 23 °C (top) and 0 °C (bottom).

out of the surface and is highly sensitive to weakly bound species at the surface. II. The mode opposite the free OH mode (the companion OH) points into the bulk and gives rise to broad spectral intensity at $\sim 3460 \text{ cm}^{-1}$, a frequency consistent with measurements of the OH of uncoupled HOD in liquid water.¹⁰⁸ MD calculations support this conclusion and go further to indicate that such highly oriented water molecules interact weakly with neighboring molecules via hydrogen bonds through both the hydrogen and oxygen.^{86,94,96} Small contributions to this peak can also come from loosely coupled water molecules in the more coordinated region of the interface. III. Loosely bound water molecules that are mostly parallel to the interface are observed at $\sim 3580 \text{ cm}^{-1}$, and primarily contribute to data taken in the ssp-polarization scheme.^{86,96} IV. Slightly deeper in the interfacial region, one finds more coordinated water molecules, sometimes referred to as tetrahedrally bound water, which give rise to two modes at ~ 3300 and $\sim 3200 \text{ cm}^{-1}$. The assignment of the intensity at 3200 cm^{-1} has recently been attributed to a Fermi resonance between the overtone of the water bending mode at and the fundamental of the water symmetric stretch mode, re-igniting the debate over peak assignments in the water region.^{84,85,110,111} While discussion over the specific molecular origins of this intensity continues, the consensus from isotopic dilution studies of the OD^{84,85} and OH^{34,36,69} stretching regions, and recent MD simulations⁹⁶ is that the intensity of this mode increases with stronger hydrogen bonding and increased intermolecular coupling.

The recent development¹¹² and implementation of phase sensitive sum frequency measurements by a number of groups has raised questions about how sum frequency spectra, particularly of water, are fit.^{55,89-91,99,100,109} The main discrepancy between the recent phase measurements and the parameters we use to fit the water spectra is in the phase of the lower frequency region. Measurements by the Shen group

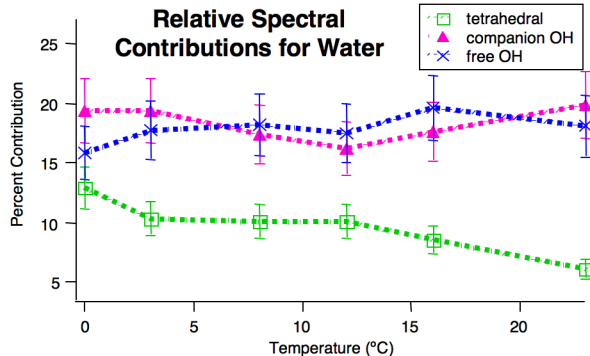


FIGURE 4.2. Relative contributions from fitted OH stretching regions as a function of temperature.

detect a phase change below 3200 cm^{-1} that was not previously included in fits to the vapor/water interface.^{55,89–91,109} We find that we can incorporate this phase change by adding an additional mode, but its amplitude is negligible for the neat vapor/water interface. Upon the addition of ions or gas to the interface, the intensity of this peak increases, and is taken into account when appropriate. This interpretation is consistent with a recent MD study that indicates the apparent phase change results from the anisotropic contribution to the polarizability, which increases in stronger hydrogen bonding environments.^{99,100} Similarly, previous VSF studies of strong acids¹¹³ and the vapor/ice interface^{114–116} attribute intensity at $\sim 3150\text{ cm}^{-1}$ to more coordination and stronger hydrogen bonding.

4.3 Isotopic Dilution Experiments

Prior to examining the influence of temperature on the uptake of sulfur dioxide to water, it is important to establish a baseline and fitting parameters for the VSFS response from the vapor/water interface at $0\text{ }^{\circ}\text{C}$ in the absence of SO_2 . As mentioned previously, isotopic dilution experiments have successfully been used in the past to isolate resonant components the water OH stretching region at room

temperature.^{34,36,69} Adding D₂O increases the HOD concentration, which simplifies the sum frequency response by reducing the effects of intra- and inter-molecular coupling. These solutions also provide us with spectral constraints, because the OH stretching region for each solution must be fit using the same parameters. The isotopic dilution experiments for water at 0 °C are presented in Fig. 4.1.a. The reported concentrations were calculated using an equilibrium constant of 4, which does not account for variations due to the zero point energies of the species present. Appendix A presents further details regarding the concentrations used in these solutions. The resultant fits to the data confirm that the previously determined fitting parameters for the neat vapor/water interface still apply at 0 °C. The overall fits and the component resonant modes for water are shown in Fig. 4.1.b at 23 °C (top) and 0 °C (bottom).

In conjunction with the isotopic dilution series at 0 °C, spectra of the neat vapor/H₂O interface were also obtained at 3, 8, 12, 16, and 23 °C. Figure 4.2. shows how the relative contributions from different OH stretching regions change with temperature. The relative contributions were calculated based on the peak areas for the resonant components as a percentage of the area of the overall fit. The tetrahedral region reflects the combined area of the peaks at 3200 and 3335 cm⁻¹. Percent errors were estimated for each temperature based on standard deviations in the fitted amplitudes for multiple data sets. These percentages (ranging from 5 to 30 %) were applied to the peak areas calculated for the averaged data sets. Characterizing the interfacial response in this manner allows us to investigate trends and changes with respect to water coordination and orientation when the temperature changes and/or gases or solutes are added. This facilitates our ability to determine which spectral regions are affected by a surface perturbation. For example, through changes in the tetrahedral region, we can infer information about how the perturbation affects the

most strongly coordinated molecular resonances somewhat deeper in the interface.⁹⁶ By contrast, changes in the free OH region are a clear indication that the topmost water layer is being perturbed.

4.4 Conclusions

From the results shown in Figs. 4.1. and 4.2. the behavior of the neat vapor/water interface parallels that of bulk water, with increased coordination as the temperature decreases. The most notable difference as the temperature decreases is an increase in the amplitudes of the peaks at 3200 and 3335 cm^{-1} . Their spectral contribution grows when the temperature approaches that of ice, while the contribution from the free and companion OH modes is relatively constant over the temperature range studied. The small changes to the water spectra shown in Fig. 4.1.b are consistent with changes reported by earlier studies at 0 °C,^{114–116} which showed a similar increase in the relative contribution from more highly coordinated OH stretching. As there are no changes in the overall electric field or composition of these solutions, the increased intensity of the tetrahedral mode is most likely due to an increase in the net water orientation as the temperature approaches that of ice. These interfacial changes are relatively small, but they provide us with the basic parameters necessary to begin analyzing the effect of temperature on the SO_2 /water system, which will be the focus of Chapter VI.

CHAPTER V

THE EFFECTS OF TEMPERATURE ON THE UPTAKE OF SO₂ TO WATER

SO₂ is an important atmospheric pollutant with great significance in the environment, particularly because of its propensity adsorb to and react with water. This chapter will begin with an overview of relevant SO₂ chemistry, as well as a discussion of previous studies showing that SO₂ forms surface complexes with water. These experiments will examine the effects of temperature on the formation of SO₂:H₂O surface complexes using isotopic dilution, and a series of temperature dependent spectra similar to those used for the neat water system. In addition to examining surface behavior during the gas uptake process, the surface is also examined after removal of SO₂ from the system. The analysis of these spectra will build on the results of the previous chapter to developing a more complex understanding of how aqueous surfaces are perturbed by gas uptake under atmospherically relevant temperatures. The resulting picture of gas uptake to neat water surfaces will provide a basis for understanding how other aqueous solutes impact interfacial activity, the focus of Chapters VI–IX.

5.1 Introduction

The uptake of gases such as SO₂ by aqueous aerosols depends on many factors including gas-phase diffusion, bulk solubility, mass accommodation probability (the probability of entering the bulk after striking the surface), and bulk reaction rates. Additional complexity arises because all of these factors may be dependent on additional factors such as temperature, pH, and droplet composition^{10–29}. The experiments described in this chapter will examine a system involving only water and

SO₂ to isolate the effect of temperature on interfacial water behavior. Nonetheless, the chemistry of this simple system is complex, and the chemistry between absorbed SO₂ and water cannot be ignored.

SO₂ reacts with water in a stepwise fashion¹:



The dominant reaction product (SO₂ (aq), HSO₃⁻, or SO₃²⁻) depends on the solution pH, but the Henry's law solubility (H) presented in Eq. (5.1.) does not account for further reaction equilibria. Nor does it attempt to distinguish SO₂ molecules at the surface from those fully solvated in the bulk aqueous phase. Surface species were first invoked to explain discrepancies between mass accommodation measurements and uptake rates calculated from predicted SO₂ solubility and bulk chemistry. Unpredictably high measured SO₂ uptake rates were attributed to surface intermediaries that facilitate gas uptake to water.^{16-18,30,32,33,72,117-121} In bulk water, SO₂ forms a gas hydrate structure with approximately seven water molecules¹²². This number is expected to be lower at the surface, but the nature of the surface complexes is not well understood.

5.2 SO₂ at the Vapor/Water Interface: An Overview

Recent experiments confirmed that when SO₂ gas comes into contact with liquid water it forms a surface complex that has recently been detected spectroscopically

via an examination of the interfacial VSF spectrum of water.^{123,124} The data in Fig. 5.1.a (top) displays evidence of this surface complex formation as was originally measured at 23 °C by Tarbuck et al.¹²⁴ These spectra correspond to the interfacial OH stretching region of water before (black), during (red), and after (blue) exposure to SO₂ gas. One of the most distinct changes to these spectra is the broadening of the sharp peak near 3700 cm⁻¹ that occurs only in the presence of flowing SO₂ (red). This broadening has been attributed to enhanced coordination between water molecules at the top most surface layer complexing to SO₂.^{123,124} In these earlier studies, the surface complex between SO₂ and the free-OH mode of water was found to be short-lived at room temperature, as it does not persist if the SO₂(g) is purged from the system (Fig. 5.1.a (blue)). Surface exposure is accompanied by an irreversible intensity increase in the coordinated water region below ~3400 cm⁻¹, an effect that has been attributed to solvated SO₂ and its reaction with water (Eqs. (5.1.) to (5.3.)). These previous studies demonstrate that SO₂ forms reversible surface complexes with water, and these complexes can be probed directly using VSFS. These surface complexes are believed to involve a single SO₂ molecule interacting with 1-3 water molecules in the topmost layer of the interfacial region.¹²³⁻¹²⁵

Using the experimental results in conjunction with MD and *ab initio* calculations, Baer et al¹²⁵ developed a picture of molecular structure that is consistent with both previous sum frequency measurements of interactions between water and SO₂ at the surface,^{123,124} and experimental^{31,126-130} and computational¹³¹⁻¹³⁵ studies of behavior in the bulk and at the surface.^{125,136} Their theoretical study supports the experimentally derived conclusions that, at room temperature, SO₂(g) has a weak affinity for the water surface, forming complexes with water molecules in the topmost interfacial layer. With confirmation of a unique SO₂:H₂O surface complex, the

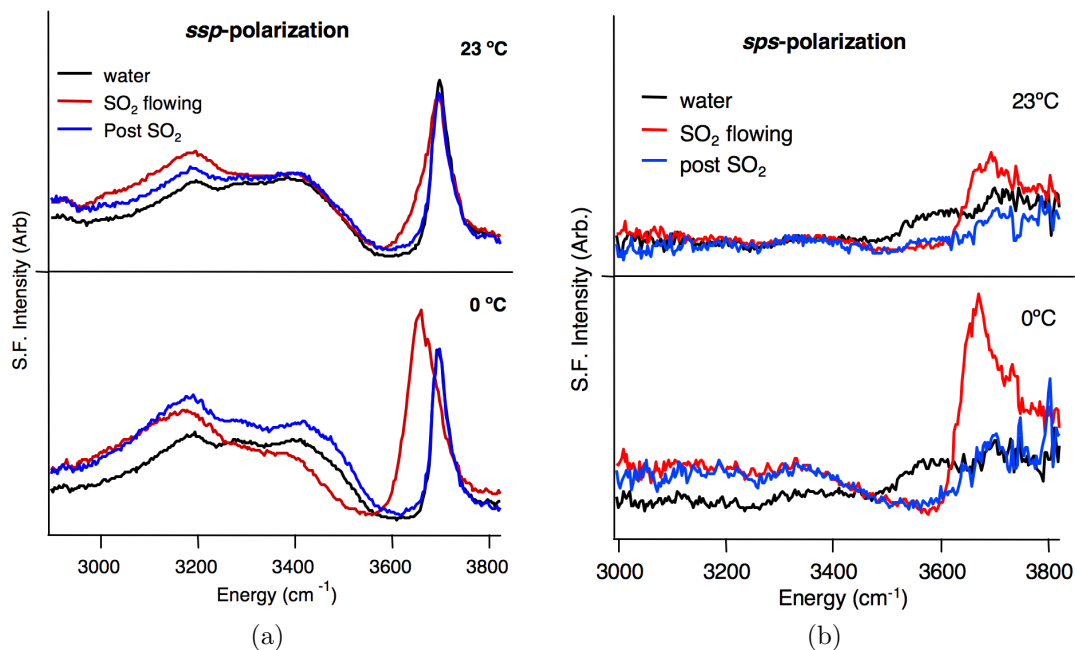


FIGURE 5.1. Spectra of the water OH stretching region before (black), during (red), and after (blue) exposure to SO₂ gas at 23 °C (top) and 0 °C (bottom). a. ssp-polarization, b. sps-polarization

primary question that arises is whether the formation of a surface complex is a necessary step in the uptake of SO₂ to water? Or is it simply a dominant pathway when solubility conditions are less favorable. If these surface complexes are required for uptake, is surface affinity determined by the same factors that determine bulk solubility? Or do physical properties, such as temperature, have different effects on surface affinity than chemical properties such as pH? Do surface active organic species change the way that SO₂ complexes to the water surface? If so, does their potential to react with SO₂ alter the nature of these interactions? Answers to questions such as these are essential to understanding the fate of SO₂ in the atmosphere.

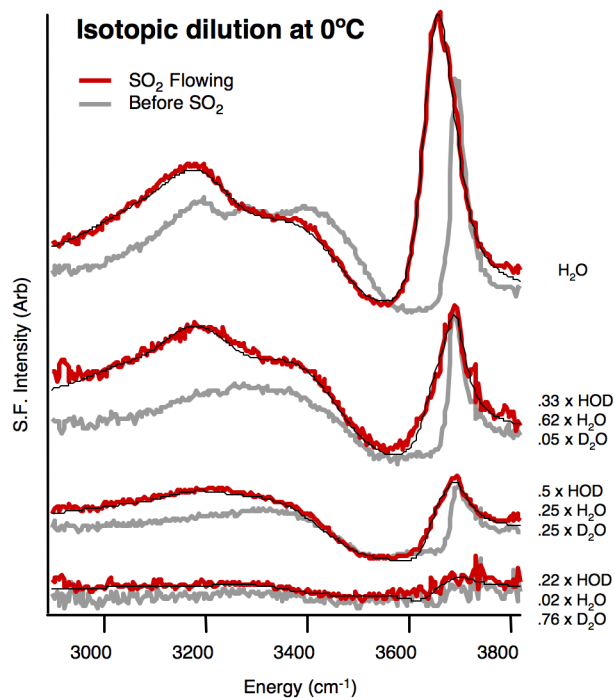
5.3 SO₂ at the Vapor/Water Interface

A preview of the interfacial behavior that will be examined in this chapter, Fig. 5.1.a (bottom), shows recently acquired spectra for SO₂ adsorption at a water surface maintained at 0 °C. Visual inspection of data taken at 0 °C shows more dramatic broadening of the 3700 cm⁻¹ peak upon exposure to SO₂, indicative of enhanced surface complexation at the lower temperature. However, as with the higher temperature, this adsorption is reversible. Spectra taken in the sps-polarization scheme (Fig. 5.1.b) show similar trends, with increased intensity in the 3700 cm⁻¹ region upon exposure to SO₂ when the temperature is decreased.

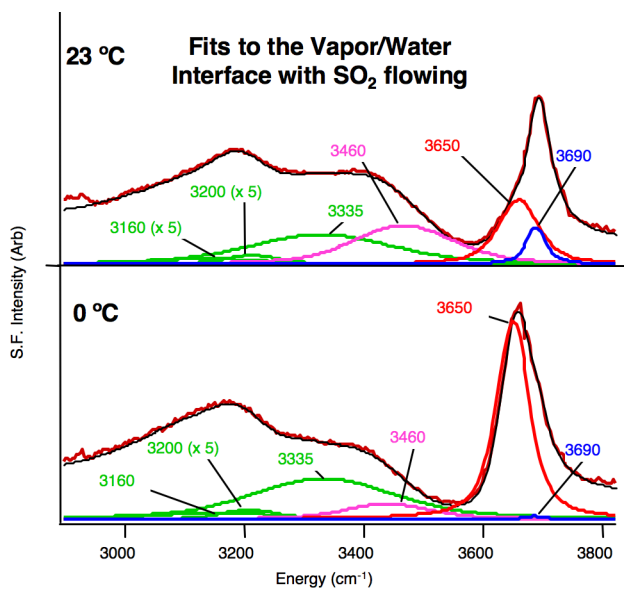
Understanding the contributions to the spectral changes observed in Figs. 5.1.a and 5.1.b requires more detailed studies as described below. Our approach is to employ isotopic dilution studies for the neat vapor/water interface at 0 °C (Fig. 4.1.), followed by identical studies conducted in the presence of SO₂ (Fig. 5.2.). Any conclusions drawn from the spectral changes observed must take into account that intensity increases can reflect changes in orientation, population, and/or transition strength of the surface species being measured.

5.3.1 Isotopic Dilution and Global Fitting

The adsorption behavior of SO₂ at the cold water surface (Fig. 5.1.) was investigated using both isotopic dilution experiments and global fitting routines. An analysis similar to that used for water in Fig. 4.1. was applied to analyze spectra taken while flowing SO₂ gas over the water surface. The isotopic dilution series used to determine the fitting parameters for spectra obtained with SO₂ flowing at 0 °C is shown in Fig. 5.2. (red), with corresponding water data (gray) for reference. From this data, we observe two main spectral changes; a broadening of the mode at ~3700 cm⁻¹



(a)



(b)

FIGURE 5.2. a. Isotopic dilution series at 0 °C with SO₂ flowing (red) with corresponding water solutions (gray). b. Fits (black) to the OH stretching region with SO₂ gas flowing (dark red) and resonant components (color) at 23 °C (top) and 0°C (bottom)

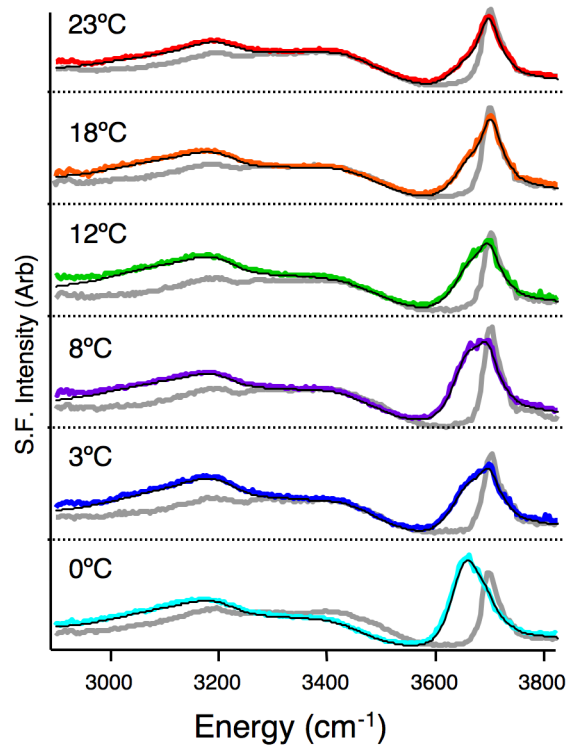
and increased intensity below $\sim 3400\text{ cm}^{-1}$. Fits to spectra taken while SO_2 gas is flowing cannot be achieved using only the standard four water bands. Two additional contributions are included to obtain an accurate global fit to the data in Figs. 5.1.a, 5.2. and 5.3.; a sharp peak attributed to surface complexes with molecular SO_2 at $\sim 3650\text{ cm}^{-1}$, which will be referred to as the complexed free OH, and a small broad peak at $\sim 3150\text{ cm}^{-1}$ that is likely due to enhanced OH coordination. These two peaks, in combination with the four water peaks, form the basis for the global fit used to interpret the spectral changes observed as a function of temperature. Lowering the temperature accentuates the spectral changes observed when the water surface is exposed to SO_2 at room temperature, proving that more surface adsorption occurs at colder temperatures. This surface enhancement can be seen in Fig. 5.3., which shows how the OH stretching region of water (gray) evolves when SO_2 is flowing (color) at intermediate temperatures between 0 and 23 °C.

In the initial analysis, three different approaches were used to fit the high frequency region above $\sim 3600\text{ cm}^{-1}$, all of which lead to the same conclusion regarding the free OH region. These approaches are: including peaks at $\sim 3650\text{ cm}^{-1}$ and $\sim 3700\text{ cm}^{-1}$ and varying their amplitudes while holding their frequencies and widths constant with temperature; treating the peak as a single resonant peak that varies in both frequency and width as the temperature decreases; or fixing the frequency of the $\sim 3700\text{ cm}^{-1}$ peak and varying the frequency and width of the peak at $\sim 3650\text{ cm}^{-1}$. For all three approaches, the net result is that the integrated intensity of this high frequency region increases as the temperature decreases.

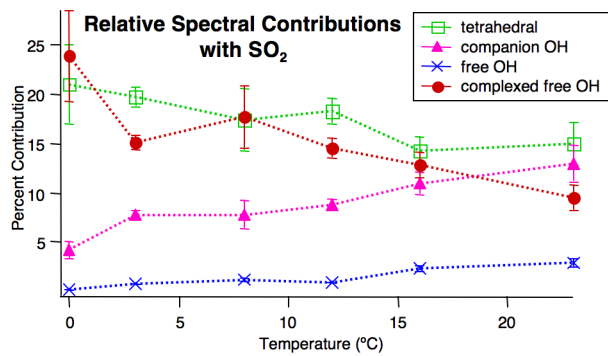
The first approach, holding the frequency and width constant, is used in this analysis, as it provides the best fit to the data in Figs. 5.2. and 5.3. while limiting the number of variable parameters and giving a measurable indicator of complex

formation. This approach is consistent with the picture that the surface spectra in this region are comprised of an unbound free OH peak and a lower energy peak corresponding to a $\text{SO}_2\text{:H}_2\text{O}$ surface complex. The lower energy peaks were fit using the parameters described above. The resultant fits obtained using a global fitting analysis are shown in Fig. 5.2.b with the corresponding resonant contributions (color) for data taken at 23 °C (top) and 0 °C (bottom). The relative contributions from the resonant peaks are displayed in Fig. 5.3.b as a function of temperature. The companion OH, free OH, and complexed free OH peaks are at ~ 3460 , ~ 3690 , and ~ 3650 cm^{-1} , respectively. The tetrahedral OH region on this plot refers to the combined contributions from the peaks at 3160, 3200, and 3335 cm^{-1} .

As shown in Fig. 5.2.b, when the temperature reaches 0 °C, the contribution from the peak at ~ 3650 cm^{-1} , which is attributed to water complexed to SO_2 , increases significantly. Meanwhile, the contribution from the peak at 3700 cm^{-1} becomes almost negligible. The observed bonding of SO_2 to essentially all the free OH bonds leads us to conclude that under low temperature conditions, the topmost surface region is fully involved in SO_2 complexation. The shift in intensity from the uncomplexed to the complexed free OH peak is attributed to an increase in surface SO_2 adsorption in conjunction with a change in overall water orientation as more water molecules bind to SO_2 . Support for this interpretation comes from data obtained using the sps- polarization scheme, which probes vibrations with components of the dipole in the plane of the interface (Fig. 5.1.b). Rigorous spectral fitting in the sps polarization scheme is difficult due to the high non-resonant background relative to the resonant signal for these experiments, but approximate fits were obtained using similar parameters to those used for data obtained in the ssp-polarization scheme. The main difference from the ssp-data is that loosely bound water molecules



(a)



(b)

FIGURE 5.3. a. ssp-spectra of the water OH stretching region with SO_2 flowing (color) and corresponding fits (thin black) as a function of temperature. The neat vapor/water interface at corresponding temperatures is in gray. b. Relative contributions of fitted OH stretching regions as a function of temperature

lying nearly parallel to the interface give rise to a peak at $\sim 3580 \text{ cm}^{-1}$ for the neat interface (black) that decreases significantly upon addition of SO_2 (red), becoming negligible when the temperature reaches $0 \text{ }^\circ\text{C}$. The intensity decrease at $\sim 3580 \text{ cm}^{-1}$ accompanies a corresponding intensity increase at $\sim 3650 \text{ cm}^{-1}$, similar to that seen in the ssp-data. These data indicate that the surface adsorption of SO_2 acts to reorient loosely coordinated water molecules in the topmost interfacial layer such that their OH oscillators are tilted more out of the plane of the interface, a change that is greatly enhanced at lower temperature.

The recent MD work by Baer et al suggests that SO_2 adsorption induces both reorientation and increased cooperation between surface water molecules.¹²⁵ Their simulations indicated that SO_2 forms complexes with multiple water molecules, with multiple coordination geometries consistent with a red-shifted free OH peak. The spectral implications of forming multi-water surface complexes are expected to extend below the free OH region. The peak at $\sim 3460 \text{ cm}^{-1}$ reflects contributions from the companion OH bonds of the water molecules containing free OH, as well as from loosely bound water molecules in the topmost surface layers.⁹⁶ In both the ssp and sps-polarization schemes, the integrated area of this peak decreases upon addition of SO_2 gas, and its overall spectral contribution decreases further with increased SO_2 bonding as the temperature decreases. The complexation of SO_2 to loosely bound water molecules in the interfacial region, and tighter water coordination results in a red-shift of intensity away from this peak.

Thus far, we have determined that cooler temperatures lead to increased surface accumulation of SO_2 , but how do these changes affect the interfacial region once the gas makes contact with the surface? How do the observed changes in behavior manifest themselves deeper into the interface? The solubility of SO_2 increases at

lower temperatures, driving increased production of both HSO_3^- and H^+ via the reactions shown in Eqs. (5.1.) to (5.3.). The spectral increases exhibited in the lower frequency tetrahedral region are consistent with increased ion concentrations, which induce greater water coordination. Both HSO_3^- ¹²³ and H^+ ^{36,137-139} are expected to accumulate in the interfacial region, and elicit similar spectroscopic responses, namely, an increase in the intensity below $\sim 3400\text{ cm}^{-1}$. HSO_3^- is a relatively large polarizable anion capable of hydrogen bonding to water via strong ion-dipole interactions, and protons are known to elicit strong electrostatic interactions. Figure 5.3.b shows that the contribution from tetrahedrally coordinated OH oscillators increases when the temperature is decreased. This is consistent with the increased coordination and electric field expected at higher HSO_3^- and H^+ concentrations. Spectra taken after the removal of SO_2 from the system support the assertion that these changes are due to reactions between SO_2 and water in the bulk, and not due to the flow of gas.

5.4 The Vapor/Water Interface After Exposure to $\text{SO}_2(\text{g})$

As noted earlier, after SO_2 is absorbed by water it reacts to form HSO_3^- in solution (Eq. (5.2.)). A decrease in temperature corresponds to an increase in SO_2 solubility, shifting this reaction to produce higher levels of HSO_3^- . The SO_3^{2-} concentration is expected to be negligible under these pH conditions. Figure 5.1.a (blue) shows that when SO_2 is removed the free OH mode returns to its original narrow state, but there is a large increase in the intensity below 3600 cm^{-1} , which is enhanced as the temperature decreases. The sps data supports the reversibility of these surface interactions; the peak at $\sim 3580\text{ cm}^{-1}$ must be included to fit the high energy spectral region in Fig. 5.1.b (blue). Interestingly, this reversibility is observed for all the temperatures examined in these experiments.

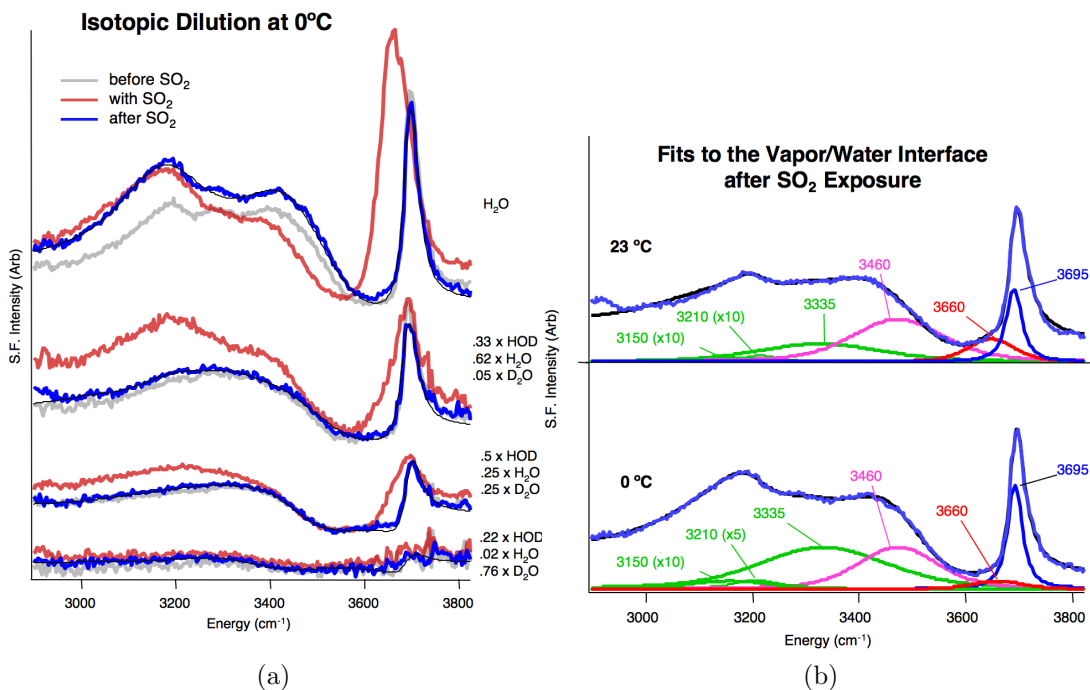


FIGURE 5.4. a. Isotopic dilution series taken after purging SO₂ from the system (blue) with corresponding spectra taken before (gray) and during (red) SO₂ exposure. b. Resonant modes and fits to spectra of the vapor/water interface after exposure to SO₂ at room temperature (top) and 0 °C (bottom).

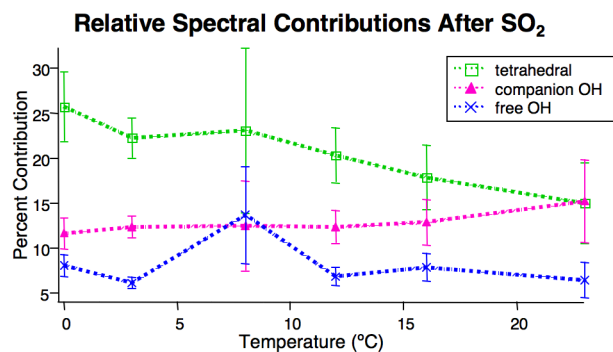


FIGURE 5.5. Relative contributions from the fitted OH stretch region, after exposure to SO₂, as a function of temperature

As confirmed by isotopic dilution (Fig. 5.4.a), the post-SO₂ ssp-spectra can be fit using six peaks: the same four parameters used for water with a small peak at 3150, which is attributed to more coordination between water molecules, and a small peak at 3660 cm⁻¹ that is attributed to water solvating interfacial protons and HSO₃⁻ (Fig. 5.4.b). The solvation mode is much broader than the coordinated free OH peak due to complexation to SO₂, and its parameters are consistent with solvation modes seen in previous studies of ion containing solutions.^{35,36,123}

After the removal of SO₂, the interfacial water structure reflects the water composition dictated by SO₂ solubility in the bulk. As displayed in Fig. 5.5., the contribution from the tetrahedral region increases at lower temperature, consistent with the expected increase in HSO₃⁻ concentration. That the free and companion OH peaks stay relatively constant with temperature indicates that temperature has no effect on the structure of the topmost water layer in the absence of SO₂. The surface SO₂ complex is reversible throughout the temperature region studied here, and does not persist after the gas is removed from the system.

5.5 Conclusions

The SO₂:H₂O surface complexation observed at room temperature in previous studies^{123,124} is significantly enhanced when the temperature is lowered. Whereas at room temperature only a fraction of topmost surface water molecules complex with SO₂, as the temperature is lowered to 0 °C nearly all of the surface water molecules with their free OH bonds protruding into the air complex with SO₂. Although it is known that bulk absorption of SO₂ increases with decreased temperature, this is the first evidence that the intermediate step to this uptake, surface complexation, is also enhanced. Complexation with water molecules in the topmost layer is accompanied

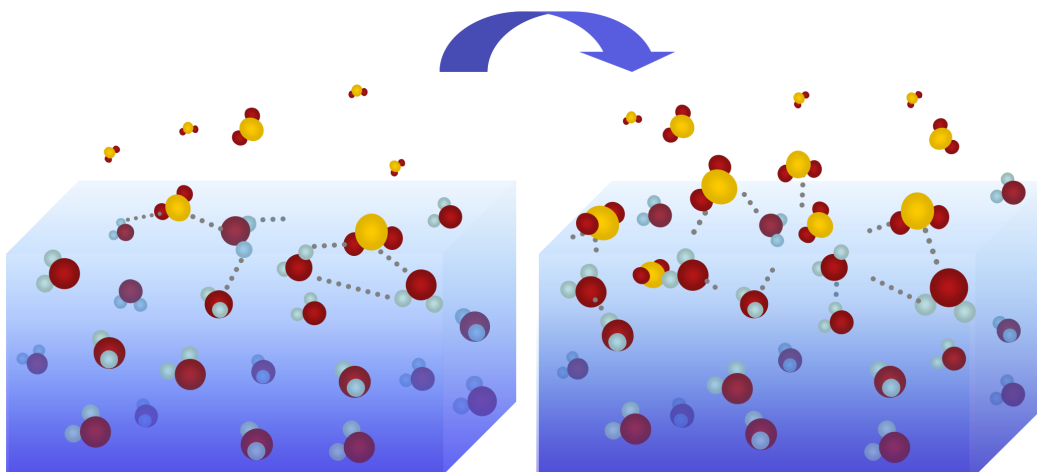


FIGURE 5.6. Cartoon representation of the SO_2 (yellow and red): H_2O (light blue and red) interface. When the temperature is cooled (right) from room temperature (left), more SO_2 accumulates

by changes in the orientation of the SO_2 bound water molecules prior to the eventual dissolution and reactivity in the bulk aqueous phase. However, even at the lower temperatures, surface complex formation does not necessarily lead to accommodation into the bulk solution as evidenced by the reversible nature of the surface complex formation when the ambient gas is removed. 5.6. provides a simple depiction of SO_2 :water surface complexation.

From these results, we conclude that low atmospheric temperatures will favor the accumulation of SO_2 on aqueous aerosol surfaces. However, the question remains of whether surface adsorption is tied to bulk reactivity. Thus far, the results have shown that under conditions of low temperature, where solubility is higher, surface adsorption is also higher. The next chapter will address the question of what happens when bulk absorption is inhibited by lowering the pH? These pH studies will also confirm whether the lower energy intensity changes observed here are due to solvated species, and not the surface complexes themselves.

CHAPTER VI

UPTAKE OF SO₂ TO THE VAPOR/WATER INTERFACE AT LOW PH

The experiments presented in this chapter examine the uptake of SO₂ to acidic water. The aqueous solution pH is varied to explore the mechanistic questions raised by the previous observation that an enhancement in uptake occurs when the temperature is lowered. These experiments are also used to distinguish spectral changes due to adsorption of SO₂ to the water surface from changes due to SO₂ solution reactivity. Changes to the molecular structure and bonding of surface water molecules upon variation of the temperature and pH with the addition of SO₂ are analyzed in reference to the structure of the neat vapor/water interface. This chapter culminates in an overview of pH effects on the SO₂-water system and its relevance to atmospheric systems and aerosol composition.

6.1 Introduction

There is considerable ambiguity regarding the nature of SO₂ surface complexation under the acidic conditions relevant to aerosol chemistry. Some studies report unpredictably high uptake rates compared to expected bulk reactivity, indicating that surface complexes may be important;^{13,16} another study indicates that surface reactions are insignificant at high H₂SO₄ concentrations.²³ This chapter presents spectra showing surface accommodation of SO₂ to 2.5 M sulfuric acid solutions. To ensure that the results were not dependent on the type of acid used, the experiments were repeated using HCl to adjust the solution pH. Similar results were also obtained using aqueous solutions that were made highly acidic with SO₂. Under low pH conditions the uptake of SO₂ into the bulk solution should be significantly

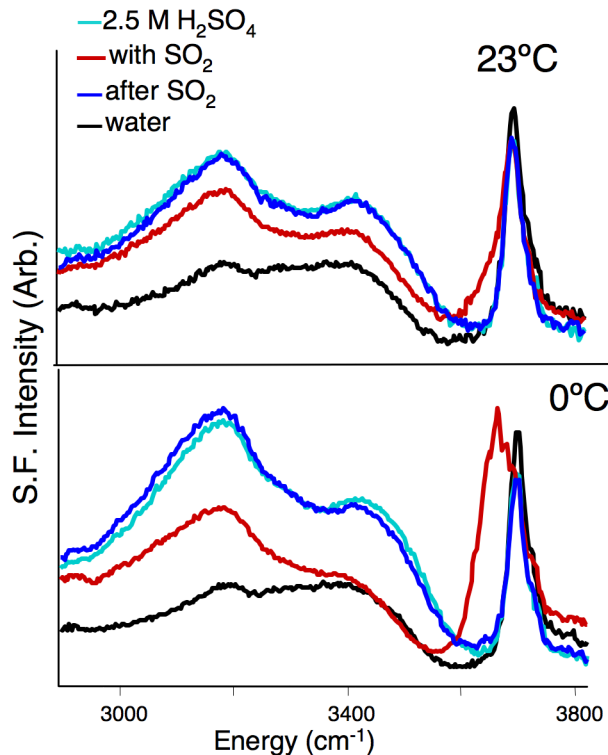


FIGURE 6.1. 2.5 M H_2SO_4 at 23 °C (top) and 0 °C (bottom). ssp- spectra were obtained before (light blue), during (red) and after (dark blue) exposure to SO_2 . Acid-free water (black) is shown for comparison.

lowered, because the formation of HSO_3^- is unfavorable.^{21–23,118} Hence these pH studies provide us with a mechanism for removing the ambiguity of previous results, while also elucidating the surface behavior upon inhibiting the reactive channel following uptake.

6.2 The Uptake of SO_2 to Sulfuric Acid

Figure 6.1. shows VSF spectra of 2.5 M H_2SO_4 solutions obtained before (light blue), during (red), and after (dark blue) exposure to SO_2 at 23 °C (top) and 0 °C (bottom). For reference, the vapor/water interface without added H_2SO_4 is shown in black for each of these systems. Visual inspection of the data in

Fig. 6.1. shows that at both temperatures, surface complexation occurs even in the presence of high bulk concentrations of H_2SO_4 , as manifested in the broadening of the free OH upon exposure to SO_2 (red), a broadening that is accentuated at lower temperature (bottom). Once the SO_2 is removed the VSF spectra (dark blue), at both temperatures, are essentially identical to those taken before adding SO_2 (light blue). This confirms that the surface chemistry is different from that of acid-free water (Fig. 5.1.a), where the effects of interfacial HSO_3^- ions are observed in the 3200 cm^{-1} spectral region after removal of SO_2 from the system.

To obtain a more detailed picture of these effects, spectral fitting analyses were performed for the H_2SO_4 data in Fig. 6.1.. Figures 6.2.a and 6.2.b contain the fitting results for the H_2SO_4 solutions prior to flowing SO_2 (light blue) and upon exposure to SO_2 (red), respectively, at $0\text{ }^\circ\text{C}$ (bottom) and $23\text{ }^\circ\text{C}$ (top). Focussing first on the H_2SO_4 solutions in the absence of SO_2 , Fig. 6.2.a, the $2.5\text{ M H}_2\text{SO}_4$ differs from the acid-free water spectrum by a larger VSFS response below $\sim 3400\text{ cm}^{-1}$ and a slight decrease in the free OH contribution at both temperatures. These results are consistent with previous VSF studies of H_2SO_4 solutions.^{140–146} When compared to neutral water, the main differences found from the fitting analysis are that for the acidic solution the peak at 3200 cm^{-1} is much larger, and there is an additional peak at 3150 cm^{-1} that is attributed to highly coordinated water molecules with increased hydrogen bonding interactions. Overall, these spectral changes reflect that the H_2SO_4 containing solution has a more structured water surface with orientation that extends deeper into the interfacial region. This is consistent with a molecular picture where solvated ions in the bulk induce an electric field that extends towards the water surface. At lower temperature, the amplitude increase at 3200 cm^{-1} is even more pronounced, consistent with an even greater increase in water coordination.

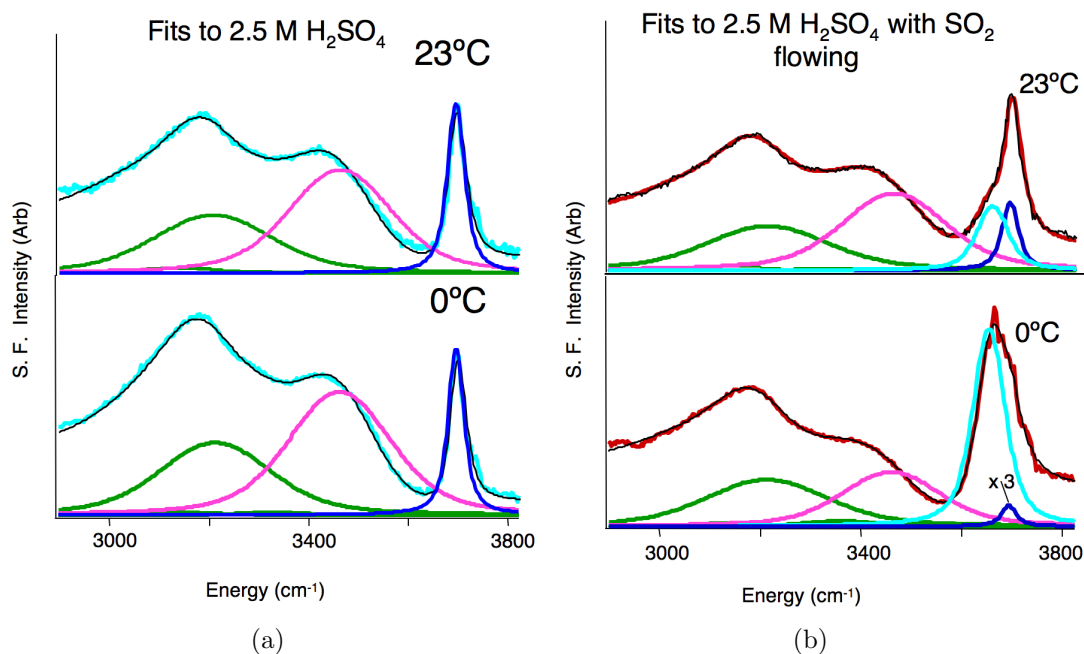


FIGURE 6.2. a. The overall fit (thin black) and resonant components (colored) for H_2SO_4 (light blue) at 23 °C(top) and 0 °C(bottom). b. The overall fit (thin black) and resonant components (colored) for H_2SO_4 with SO_2 flowing (red) at 23 °C (top) and 0 °C (bottom).

A similar analysis of the H_2SO_4 solution surface in the presence of SO_2 shows both similarities and differences when compared to the analysis of SO_2 at the acid-free water surface. A comparison of the data in Figs. 6.2.a and 6.2.b shows that the surface complex on the acid solution is manifested in spectral changes in the free OH peak similar to those observed for the neutral solution in Fig. 5.2., namely increased broadening and red-shifting of this peak when the temperature is lowered and complexation is increased. SO_2 complexation on the H_2SO_4 surface is also demonstrated by the decrease in the nearby companion OH mode which is evident in the decreased contribution from the peak near 3500 cm^{-1} in Figs. 6.2.a and 6.2.b. As for the neutral solution, this decrease upon exposure to SO_2 is attributed to an increase in the coordination and net orientation of loosely coordinated water molecules

in the topmost interfacial layer. The highly coordinated region below 3400 cm^{-1} is where the spectra of the acidic and neutral solutions differ upon exposure to SO_2 . The acidic solution intensity appears to decrease slightly due to interference with the diminishing companion OH peak, but the opposite trend is observed for acid-free solutions where the intensity increases with increased adsorption of SO_2 (Fig. 5.2.). The intensity increase for acid-free water is attributed to the reactive production of HSO_3^- ions. The contrasting behavior observed here provides further evidence that, under acidic conditions, the adsorption of SO_2 is localized to the topmost water layer and the level of solvated SO_2 and HSO_3^- in the interfacial region is negligible. As a whole, these measurements provide a means of distinguishing between surface water binding to SO_2 and changes due to solvated ions in the interfacial region.

These results demonstrate that the conditions that dictate interactions between SO_2 and H_2O at the surface are uncoupled from those that determine behavior in the bulk. As the data in Fig. 6.1. show, $\text{SO}_2:\text{H}_2\text{O}$ surface complexes continue to form under acidic conditions; clarifying the ambiguous results of previous studies that could not distinguish between surface and bulk interactions.^{13,16,23} Similar to the behavior at the neat water surface, SO_2 surface complexation is enhanced at lower temperatures, and occurs regardless of bulk absorption behavior. Further, the surface complexes are localized to the topmost surface layer, with little influence on the deeper interfacial region. The lower energy spectral region reflecting deeper more coordinated water molecules is thus an ideal indicator of solvated species such as HSO_3^- . Even though the acidic ions in a bulk H_2SO_4 solution are present in the interfacial region, as manifested through their impact on the hydrogen bonding characteristics water molecules therein, the presence of these ions has no effect on the complexation of SO_2 to the water surface at either room temperature or $0\text{ }^\circ\text{C}$.

Furthermore, the increased production of ions such as HSO_3^- in the interfacial region that is observed upon exposure of SO_2 to neutral solutions is not observed in the presence of acid. Hence the chemistry observed in the interfacial region is driven by the same equilibrium behavior as the bulk solution.

6.3 Conclusions

The experiments presented in this chapter show clear evidence of surface accumulation in the absence of bulk absorption, a phenomenon that has important implications for the cool low pH conditions typical of the atmosphere. The potential for surface complexation may be especially relevant to polluted environments where there is an abundance of both SO_2 and potentially reactive organic species. Under such conditions, does aqueous surface affinity still lead to surface complexation? How do organic species in the interfacial region change the propensity for surface complexes to form? Does the surface enhancement found at lower temperatures extend to surfaces containing other molecules? The next two chapters will detail experiments aimed towards learning about how other types of pollutants, namely organics, impact surface accumulation.

CHAPTER VII

UPTAKE OF SO₂ TO AQUEOUS SUCCINIC ACID

Chapters V and VI illustrated the complex nature of the interactions between SO₂ and water at the interface, expanding the description of surface adsorption to include environmentally relevant temperatures and pH. The experiments presented in this chapter add an additional layer of complexity by examining how succinic acid (HOOC(CH₂)₂COOH), a small surface active organic molecule perturbs interfacial behavior. The first part of this chapter details experiments examining the effect of succinic acid on the neat water surface. Isotopic substitution is used to isolate and assign specific spectral modes. The resultant fitting parameters, as well as those determined in Chapters IV-VI are then applied to understand spectral changes observed when the system is exposed to SO₂.

7.1 Introduction

The importance of organics in the atmosphere is well recognized and their effect on aerosol growth and chemistry is commonly studied.^{76,77,147-154} However, the nature of their influence on aerosol surface chemistry is still not well understood.^{3,79,155-157} In fact, a recent perspective studying the transport of persistent organic compounds in the atmosphere indicates that interfacial properties, such as adsorption probabilities and reaction potentials, are the least understood of the factors determining the fate of such species in the environment.¹⁵⁸ Part of the difficulty in characterizing the effects of organics on aqueous surface chemistry arises from the vast diversity of atmospherically relevant species, and the correspondingly high number of relevant behavioral pathways to explore. For example, long chain surfactants are expected

to behave quite differently from small, semi-soluble organic acids, and the level of surface coverage is likely to be important in determining whether, and how effectively, molecules act as a barrier to absorption of gases.¹⁵⁹ The varied functionality of organics adds another level of complexity, which is further complicated by different surface chemistry from that in solution. This makes it difficult to extrapolate information from early measurements, which were often in the bulk. Thus, many of the gaps in our understanding of aerosol surface chemistry are related to the behavior and influence of organic constituents on interfacial behavior.

Measurements of aerosol components have pointed to a prevalence of dicarboxylic acids, including succinic acid, in the troposphere.¹⁶⁰⁻¹⁶⁶ And there is substantial evidence indicating that the organic molecules most likely to persist on atmospheric surfaces tend to be short chain molecules with a relatively high oxygen:carbon ratio.¹⁶⁶ This has led to a number of studies aimed towards better understanding how these compounds, and their derivatives, behave in the atmosphere.¹⁶⁷⁻¹⁷⁵ In addition to being produced from the photo-degradation of larger organics in the atmosphere, succinic acid is a primary pollutant with both natural and industrial sources. The main anthropogenic sources of succinic acid are the combustion of wood, coal, and gasoline for heat and automobile fuel. Thus, it is a co-pollutant of SO₂, which is derived from many of the same sources.^{160-162,176}

The molecular structure of succinic acid has been characterized in the solid state using both IR and Raman spectroscopy^{177,178} and in aqueous solution using IR¹⁷⁸⁻¹⁸⁰, Raman¹⁸¹ and NMR spectroscopy.¹⁸² These spectroscopic studies have mainly focussed on the vibrational modes of the carbonyl and carboxylate groups, due to difficulties in assigning and interpreting the spectral response from the carboxylic OH and CH stretching modes. These modes are strongly dependent on the water

environment, and are often hidden beneath the stronger spectral response from water, a problem compounded by the low solubility of succinic acid. However, although surface tension measurements show that succinic acid accumulates at the water surface,^{171,183,184} and molecular dynamics simulations suggest that it has a higher propensity to reside at aqueous surfaces than in the bulk,¹⁸³ little is known about how succinic acid changes the interfacial environment.

The primary focus of the experiments presented here is to understand what role, if any, organic species play in the uptake of SO_2 to water. Succinic acid was chosen for these studies, because it is both surface active and chemically inert towards SO_2 . This limits the number of new vibrational modes to those from aqueous succinic acid and its interactions, if any, with SO_2 . The first set of experiments described here is aimed at understanding the VSF spectroscopic response of succinic acid at the vapor/water interface. This analysis will then be extended to examine changes to the interfacial region when the succinic acid solutions are exposed to SO_2 .

7.2 Succinic Acid at the Vapor/Water Interface

The spectra presented in Figs. 7.1.a and 7.1.b were acquired using 0.25 M succinic acid solutions at room temperature. These solutions are at the native pH, 2.4, and succinic acid is expected to be fully protonated. At this concentration, succinic acid is clearly present in the interfacial region, but remains solvated, and the spectral response from water is still strong. Similar experiments were attempted at lower temperatures, and with higher concentrations, but the low solubility of succinic acid causes it to crystallize out of solution, resulting in irreproducible spectra. Therefore, 0.25 M solutions were used for all of the experiments presented in the following discussion.

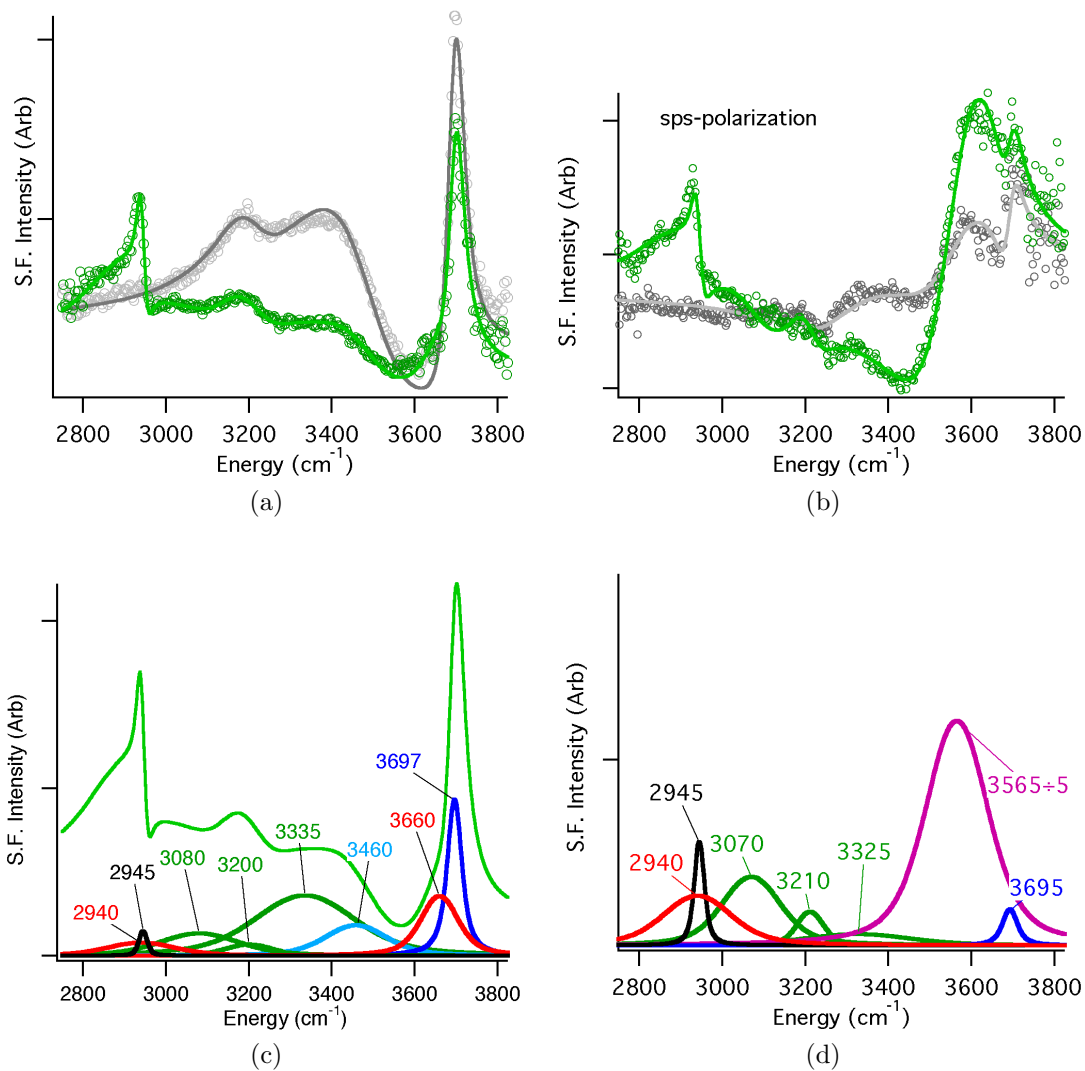


FIGURE 7.1. VSF Spectra of 0.25 M Succinic Acid (green) overlaying water (gray). a. ssp-polarization spectrum b. sps-polarization spectrum. c. Resonant components (colored) of fit(green) to ssp-spectrum d. Resonant components of fit to sps-polarization spectrum.

Figure 7.1. shows representative spectra of 0.25 M succinic acid solutions taken using the ssp- and sps-polarization schemes. Probing the spectral region between 2700 to 3900 cm^{-1} provides information about the water OH stretching modes, as well as the succinic acid CH_2 and OH stretching modes. Visual inspection of Figs. 7.1.a and 7.1.b shows that succinic acid perturbs the interfacial water environment, as seen in spectra taken using both the ssp- and sps- polarization schemes. The most obvious spectral changes are a decrease in the intensity of the water coordinated OH stretching region and a sharp feature at approximately 2900 cm^{-1} . This peak is seen in both polarization schemes, and is attributed to the succinic acid CH_2 stretching mode. However, as for the VSF spectra discussed in previous chapters, fitting these spectra is non-trivial. Thus, additional experiments were conducted using isotopic substitution to provide greater confidence in the spectral fits presented in Figs. 7.1.c and 7.1.d. These experiments and the corresponding analysis are the focus of the following discussion.

7.3 Isotopic Substitution Experiments

Deuterated analogs of succinic acid and water are chemically identical, but vibrationally distinct from their fully hydrogenated counterparts. Substituting hydrogen with the heavier deuterium atom results in lower energy vibrations, removing the corresponding spectral features from the region being probed. Replacing water with D_2O removes intensity due to water OH stretching from the spectral region, as the OD stretches are red-shifted by approximately 1000 cm^{-1} . In addition, exchange between the D_2O solution and the dicarboxylic acid groups results in a solution that contains mainly $\text{DOOC}(\text{CH}_2)_2\text{COOD}$ (Fig. 7.2.).

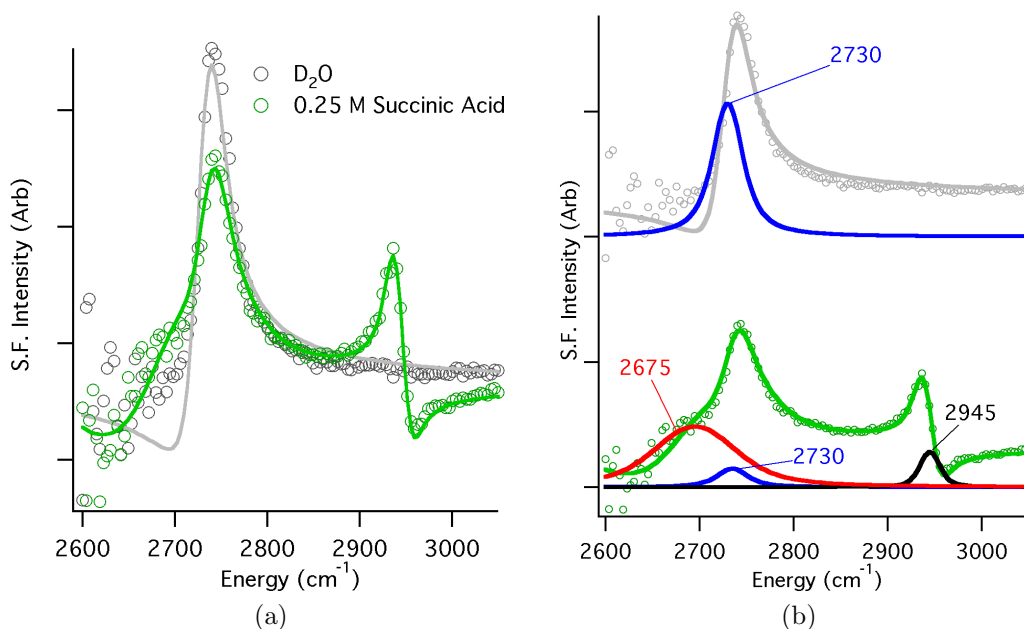


FIGURE 7.2. Spectra of Succinic Acid in D_2O . a. Spectra of succinic acid (green) and D_2O (gray) b. Resonant components of fits to D_2O (top) and succinic acid (bottom)

Figures 7.2.a and 7.2.b show spectra of 0.25 M succinic acid in D_2O (green) overlaying a spectrum of the vapor/ D_2O interface taken in the ssp-polarization scheme, and the corresponding fits. The intense peak at 2730 cm^{-1} , which is present in spectra of D_2O as well as that of succinic acid, is attributed to the free OD stretch, and is analogous to the free OH of H_2O . The succinic acid spectra also contains two other modes. A narrow peak at 2945 cm^{-1} , which is assigned to the CH_2 stretching mode and a second, broader peak at $\sim 2695\text{ cm}^{-1}$, which is attributed to D_2O solvating ions. This assignment is consistent with the analogous ion solvation peak at $\sim 3660\text{ cm}^{-1}$ identified in earlier studies,^{35,36,123} as well as the assignments used in Chapters V and VI of this work.

The spectral response from the succinic acid OH groups was isolated in a similar manner, using partially deuterated succinic acid of the form $HOOC(CD_2)_2COOH$ in water to remove the CH stretch response from the spectral region. In Fig. 7.3., spectra

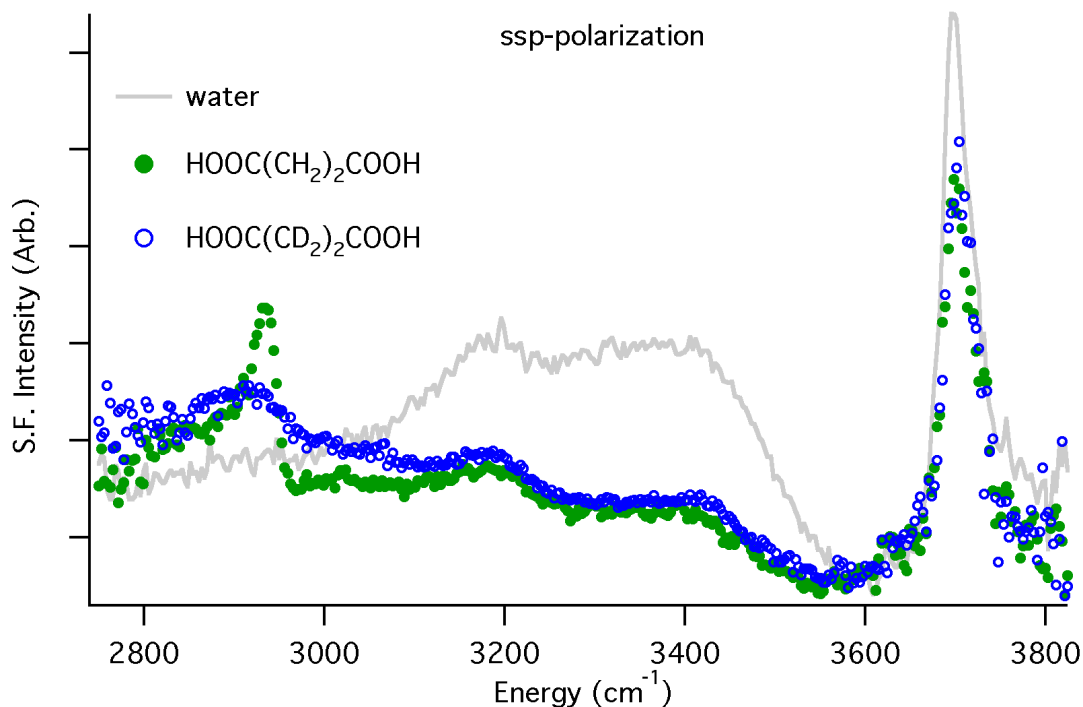


FIGURE 7.3. VSF Spectra of 0.25 M $(\text{CD}_2(\text{COOH}))_2$ (blue) and 0.25 M $(\text{CH}_2(\text{COOH}))_2$ (green) in water (gray)

of the partially deuterated (blue) and fully hydrogenated (green) analogs of succinic acid overlay the spectrum of water (gray). The main difference between spectra of the deuterated and protonated succinic acid is the sharp feature at 2945 cm^{-1} , which is assigned to the CH_2 stretch. The relatively broad peak in that same region does not change for the deuterated sample, but was absent from spectra taken in D_2O , indicating that it arises from the carboxyl OH stretching mode. In addition to the standard four water peaks, both of these spectra are fit with two other peaks; a peak at $\sim 3660\text{ cm}^{-1}$ that is attributed to ion solvation, and a peak at $\sim 3080\text{ cm}^{-1}$, which is attributed to water in highly coordinated hydrogen bonding environments.

The succinic acid spectral assignments were determined by first fitting the spectra for the deuterated analogs and applying the same fitting parameters to peaks for the fully hydrogenated compound. The resultant peak positions and their

corresponding gaussian widths are summarized in Table B.1.. Although previous Raman and IR studies of aqueous succinic acid mainly focussed on the carbonyl and carboxylate stretches, which are much lower in energy,^{126,180} the low frequency, and broad nature of the peak at 2940 cm^{-1} are consistent with assignments from an IR study of other aqueous dicarboxylic acids,¹⁷⁹ which attributed the low frequency to hydrogen bonding interactions between the carboxyl OH and water or neighboring acid molecules. This assignment is also consistent with measurements and calculations based on studies of crystalline succinic acid, where intermolecular hydrogen bonding is expected to decrease the energy of this vibration. In the gas phase, carboxylic acid OH stretches are seen at $\sim 3500\text{ cm}^{-1}$,¹⁸⁵ but the closest spectral feature observed here is the peak at $\sim 3660\text{ cm}^{-1}$, which is attributed to water molecules solvating ions. It is possible that this peak arises from carboxyl OH groups pointing out of the interface, in a similar manner to the water free OH, but this seems unlikely given its higher frequency relative to the gas phase vibrations. In addition, the CH_2 -stretching mode gives rise to a single peak, that is the same in both polarization schemes. If one of the carbonyl groups were pointed out of the interface, one might expect the two CH_2 groups to appear in different environments. However this is not observed here, and experiments investigating the orientation of the carbonyl mode are currently underway in this laboratory, and may shed more light on the matter in the future.

The sharp peak assigned to the CH_2 stretch mode is seen at 2945 cm^{-1} in both the ssp and sps-polarization schemes. This indicates that the CH_2 groups are angled relative to the surface normal such that there are components of the transition dipole along the interfacial plane, as well as directed out of it. The peak at $\sim 3080\text{ cm}^{-1}$, which is assigned to highly coordinated and strongly hydrogen bound water, supports an interfacial picture where water forms hydrogen bonds to succinic acid, thereby

increasing the level of water coordination deeper into the interface. The presence of succinic acid at the surface also explains the decrease in intensity in the spectral region between $\sim 3200\text{--}3500\text{ cm}^{-1}$. Figures 7.1.c and 7.1.d show that the spectral contributions from the tetrahedrally coordinated water molecules are still relatively high for the succinic acid solutions. However, interference with the solvation peak at $\sim 3660\text{ cm}^{-1}$ results in an apparent decrease in the intensity of this region. This is supported by the sps-polarization spectra, which shows a large increase in the peak due to weakly coordinated water molecules lying nearly parallel to the surface when succinic acid is added to the water. These spectral results point to an interfacial picture where the topmost region is populated by weakly coordinated water molecules solvating hydronium ions, with larger succinic acid molecules hydrogen-bonding to water slightly deeper in the interfacial region. The spectral assignments derived from these experiments can now be applied to examine changes to the spectral region when succinic acid solutions are exposed to SO_2 .

7.4 Uptake of SO_2 to Succinic Acid

Figures 7.4.a and 7.4.b display VSF spectra of $(\text{COOH}(\text{CH}_2))_2$ (a) and $(\text{COOH}(\text{CD}_2))_2$ (b) prior to (green) and during (red) exposure to SO_2 . The partially-deuterated and undeuterated forms of succinic acid show a similar spectral response to exposure to SO_2 . Flowing SO_2 over the succinic acid solutions results in two main spectral changes: increased broadening and red-shifting of the free OH, and increased spectral intensity below 3400 cm^{-1} .

Prior to exposure, the main difference between the spectral response for succinic acid and water in this region is the succinic acid ion solvation peak at 3660 cm^{-1} . These spectra can be fit using an analysis similar to that used for water, as discussed

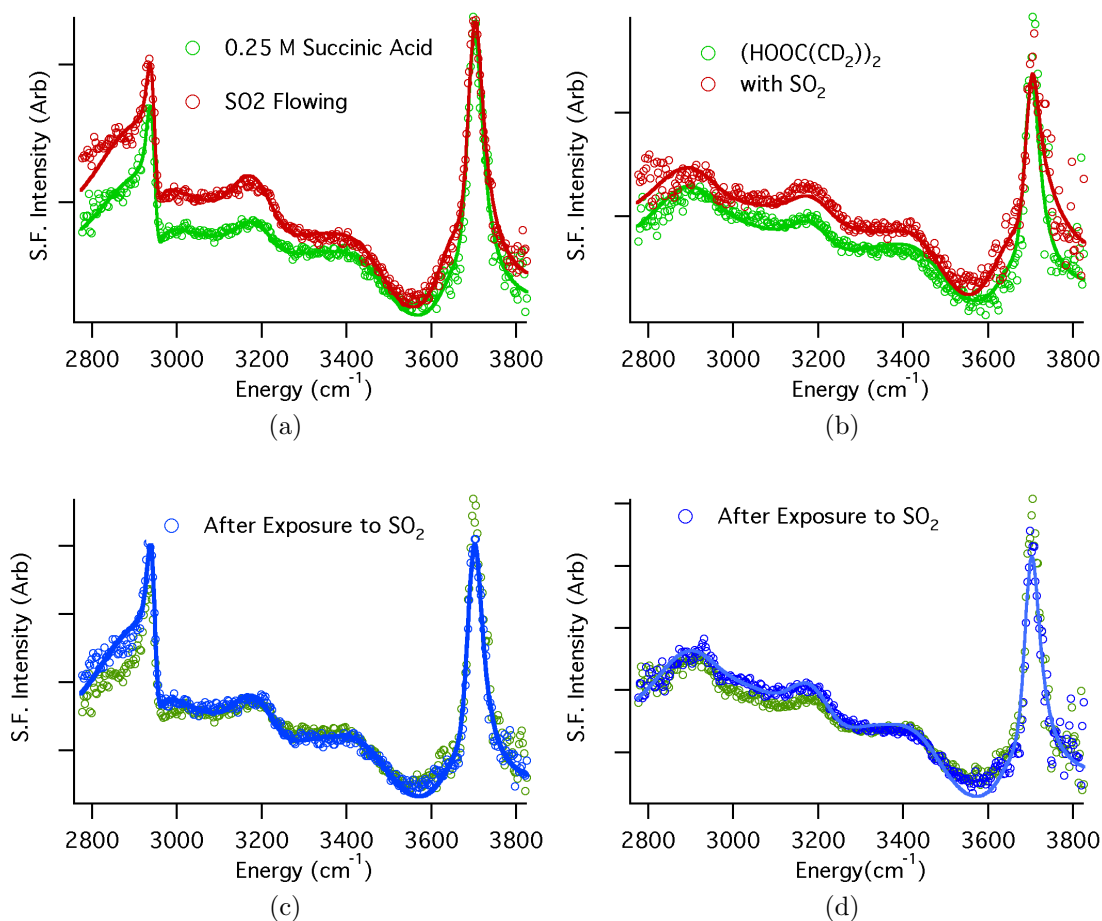


FIGURE 7.4. a. VSF Spectra of Succinic Acid (green) with SO₂ flowing (red) b. VSF Spectra of D4-Succinic Acid (green) with SO₂ flowing (red) c. VSF Spectra of Succinic Acid(green) after SO₂ Exposure (blue) d. VSF Spectra of Succinic Acid(green) after SO₂ Exposure (blue)

in Chapter V. Comparable fits to the free OH region can be achieved either by using a single, broad, red-shifted peak or by adding a second peak to account for the increased intensity below the free OH peak.

For consistency with the analysis in Chapters V & VI, two peaks were used to fit the succinic acid spectra, and the intensity due to water solvating ions is incorporated into the peak for the complexed free OH. This peak is broader and more intense than the solvation peak alone, consistent with previously observed behavior for surface

complexation between water and SO_2 in the presence of H_2SO_4 . The amplitudes of the peaks at ~ 3200 and $\sim 3080 \text{ cm}^{-1}$ also increase, consistent with the production of HSO_3^- and H^+ from the reaction between SO_2 and water (Eq. (5.2.)). However, the frequencies and widths of the succinic acid peaks at 2940 and 2945 cm^{-1} do not exhibit changes in either position or width upon exposure to SO_2 . Thus, it appears that SO_2 does adsorb to the water surface via the formation of surface water complexes. However, there is no evidence of an interaction between SO_2 and succinic acid in the interfacial region.

This interpretation is further supported by the spectra in Figs. 7.4.c and 7.4.d, which show the interface after the removal of SO_2 from the system (blue) overlaying spectra of the unperturbed succinic acid solutions green. The spectra of the unperturbed succinic acid solutions are very similar to those from solutions that have been exposed to SO_2 . The free OH region returns to its initial, narrower, shape showing that the reversibility of the $\text{SO}_2:\text{H}_2\text{O}$ has not changed. There is, however, a small increase in the amplitude of the peaks at ~ 3200 and $\sim 3080 \text{ cm}^{-1}$ compared to the unperturbed surface, indicating that some of the SO_2 has absorbed into, and reacted with, water in the interfacial region. These resonant components used in these fits are illustrated in Fig. B.1. and the fitting parameters are given in Table B.1. of Appendix B.

7.5 Conclusions

Aqueous solutions of the C4 dicarboxylic acid, succinic acid, have been used to study the uptake behavior of the atmospheric pollutant SO_2 to water surfaces. Succinic acid is abundant in the atmosphere, and has been shown here to be surface active in aqueous solutions. Figure B.1. shows the spectral evolution of succinic acid,

and the corresponding fits, prior to, during, and after exposure to SO_2 . Spectra of the neat vapor/succinic acid (aq) interface indicate that succinic acid forms hydrogen bonds to water in the interfacial region. However, the topmost surface layer appears to be populated with weakly coordinated water molecules solvating hydronium ions. Nonetheless, succinic acid does show a propensity for the interfacial region, inducing an increase in water coordination and hydrogen bonding. However, although succinic acid clearly perturbs the water surface, it does not appear to inhibit the uptake of/or surface complexation of, SO_2 to water. In fact, the interactions between SO_2 and water appear to be entirely independent of those between succinic acid and water. These results indicate that organic components can be present within aerosol particles without significantly impacting gas adsorption or uptake. However, these experiments raise the question of whether these gas adsorption interactions are related to the potential for reaction with the surface species. The experiments presented in the next chapter will examine the uptake of SO_2 to aqueous solutions containing formaldehyde, a molecule known to react with HSO_3^- in solution.

CHAPTER VIII

THE UPTAKE OF SO₂ TO AQUEOUS FORMALDEHYDE

The experiments described in Chapter VII demonstrated that succinic acid, a small dicarboxylic acid, has a limited impact on the formation of surface SO₂:H₂O complexes at aqueous surfaces. Although succinic acid does change the interfacial water environment, its surface insensitivity to SO₂ was apparent in its lack of interaction with that compound. Given these results, one might wonder whether SO₂ surface complexation is specific to water, or if other more reactive surface species have the ability to form similar complexes. The experiments presented here examine this question by studying the role of aqueous formaldehyde (CH₂O) in the adsorption of SO₂ to water. These experiments are conducted at two temperatures, 0 °C and 23 °C, and will begin with an examination of aqueous formaldehyde at room temperature. The ensuing analysis will be applied to better understand spectral perturbations introduced by flowing SO₂ over the formaldehyde solutions.

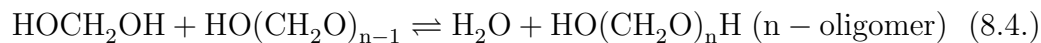
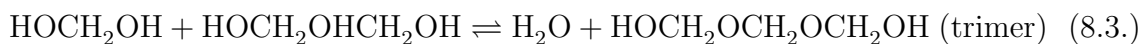
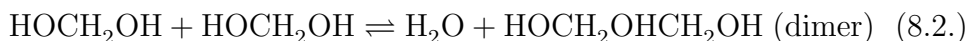
8.1 Introduction

The importance of organic compounds in the atmosphere cannot be overemphasized, and the experiments presented in Chapter VII probed a very small subset of the many questions regarding their behavior. The experiments presented here will examine the behavior of another oxygen-containing organic molecule, but one with very different chemistry from that of the dicarboxylic acids; the simple aldehyde, formaldehyde. Short chain aldehydes are found in both the gas phase and as a component of aqueous particles in clouds and fog water. As such, they have been identified as potential precursors in the formation of secondary organic aerosols

in the atmosphere.^{186–190} Formaldehyde is a common pollutant in urban, industrial areas, with high aqueous solubility, which is enhanced by its reaction with water to form methylene glycol (MG).¹⁹¹



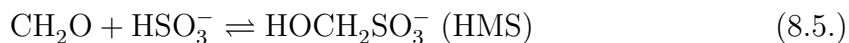
At higher CH_2O concentrations, methylene glycol can react to form oligomers as follows:



but solutions with CH_2O concentrations below 5 mol % contain primarily the diol methylene glycol. For the ensuing discussion, $\text{CH}_2\text{O}(\text{aq})$ will be used to refer to all solvated forms of formaldehyde, including MG and other oligomers that may be present. Due to its atmospheric importance, there have been many studies detailing the equilibrium between formaldehyde and water. Raman spectroscopy is commonly applied to probe the aqueous phase chemistry,^{113,191–195} while uptake studies, coupled with theoretical models, have examined the probability of formaldehyde partitioning to water and water ice surfaces.^{187,188,190,196–202}

Most of the studies presented here examine solutions with a CH_2O concentration of 3.2 % w/v, (approximately 3 mole % CH_2O), in order to reduce complications from oligomer formation.

In addition to its reaction with water, formaldehyde reacts with aqueous SO_2 in the following manner.¹



Measurements of hydroxymethanesulfonate (HMS) in the fog and cloud water of polluted areas have shown a strong correlation between high HMS concentrations and the high levels of formaldehyde and S(IV) species in the atmosphere.^{37,203} In contrast to HSO_3^- and SO_3^{2-} , HMS is stable against oxidation by hydroxide and hydrogen peroxide, the primary oxidants in aqueous aerosols.³⁸ In addition, it has been suggested that the formation of aldehyde-sulfite adducts in cloud and fog water particles could account for up to a two fold increase in wet deposition of SO_2 ,³⁹ and that such particles may act as a vehicle for long-range transport of SO_2 in the atmosphere.^{37,42,204} The kinetics of Eq. (8.5.) are highly dependent on pH. Under alkaline and slightly acid pH, the dehydration of methylene glycol is the rate limiting step in HMS formation,¹⁸⁹ whereas at low pH (less than 4), Eq. (8.5.) is believed to proceed via nucleophilic addition of SO_3^{2-} to formaldehyde.³⁸

In studies analogous to those for SO_2 ,^{6,10,14,16,19,22,23,30-33} uptake rates have been measured for the mass accommodation of CH_2O gas onto aqueous particles.^{196,197,201} These studies indicate that surface complexes between formaldehyde and water may form at low pH,¹⁹⁶ where earlier studies measuring uptake to aqueous SO_3^{2-} solutions had found no indication of surface complexation.²⁰¹ These studies primarily focussed on the uptake of CH_2O to aqueous surfaces at neutral or alkaline pH, and did not examine the reverse interaction; the uptake of SO_2 to aqueous formaldehyde. The surface specificity of the VSFS experiments presented here can help to illuminate

the details of surface interactions in the cooperative behavior of SO_2 and CH_2O at aqueous surfaces.

The effects of formaldehyde on the structure of the neat vapor/water interface are presented first, followed by an examination of SO_2 uptake to 3.2 % w/v formaldehyde at room temperature. This concentration was chosen to limit complications from the formation of higher order oligomers, but spectra acquired using higher concentrations of formaldehyde will also be used to aid the interpretation of the spectral response in the presence of SO_2 . This analysis will also include a comparison with to spectra of the aldehyde-bisulfite reaction product, HMS. The resultant spectral interpretation will be applied to better understand spectra acquired at 0 °C to study the interfacial behavior under more atmospherically relevant conditions. The chemistry of these solutions is quite complex compared to the solutions examined in previous chapters, which makes definite peaks assignments difficult. Thus, the analytical approach here will be to discuss peak assignments for formaldehyde within the context of the available literature, but to interpret the data as a function of the observed spectral perturbations as the solutions evolve under exposure to SO_2 .

8.2 Formaldehyde at the Vapor/Water Interface

Figure 8.1. shows VSF spectra of 3.2 % w/v formaldehyde (green) using the ssp (top) and sps (bottom) polarization schemes. For reference, the neat vapor/water interface is shown in gray. As for previous analyses, peaks were added only if necessary to achieve agreement between the fits and the data. For added confidence in the fitting parameters, a global fit was performed for ssp-polarization spectra taken of a range concentrations between 1.2–16 % w/v formaldehyde. Five peaks were used in addition to the standard four water peaks: A broad peak at $\sim 3050 \text{ cm}^{-1}$, an intense

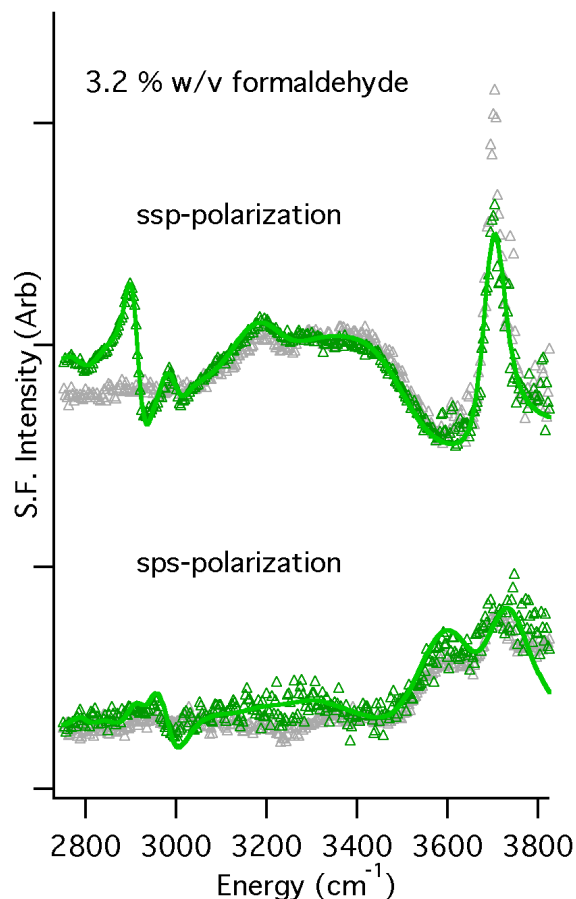


FIGURE 8.1. VSF Spectra of 3.2 % w/v formaldehyde (green). Water is shown in gray for comparison. Solid lines are fits to the data

peak at $\sim 2910\text{ cm}^{-1}$, and three weaker peaks at 2785 , 2870 , and 2995 cm^{-1} . The resultant fit to the 3.2 % w/v formaldehyde solution is shown as a solid line in Fig. 8.1., and the resonant components used in the fit are illustrated in Fig. 8.3.. For clarity, the lower frequency peaks are plotted alone in 8.3.a Visual inspection of the data indicates that formaldehyde (aq) does partition to the aqueous surface, and that the surface concentration increases with increasing bulk concentration. At room temperature, the sps-polarization spectrum closely resembles that of the neat vapor/water interface and the low signal to noise ratio, together with the relatively high non-resonant background, makes fitting this data difficult. Nonetheless, three

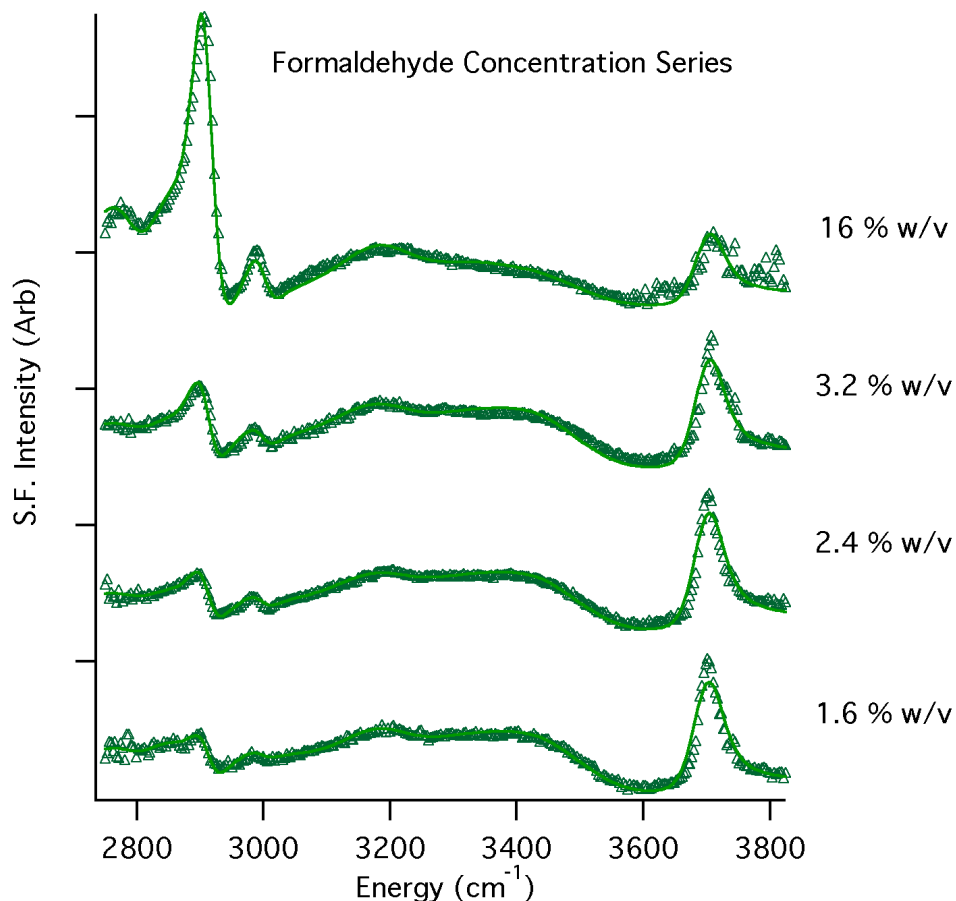


FIGURE 8.2. Global Fits to ssp-polarization spectra of the vapor/ $\text{CH}_2\text{O}(\text{aq})$ interface taken as a function of concentration. Solid lines are fits to the data

low amplitude peaks were added to the CH-stretching region at 2850, 2920, and 2975 cm^{-1} . These peak parameters were determined by using a global fit including data taken at $\sim 0^\circ\text{C}$, which will be discussed later, because the peaks were slightly more distinct at the lower temperature.

The addition of formaldehyde to water results in two overall spectral changes: a decrease in the contribution from loosely coordinated water molecules in the topmost region, and the appearance of new peaks, which are attributed to $\text{CH}_2\text{O}(\text{aq})$ in the CH stretching region. At 3.2 % w/v, the aqueous solution contains primarily $\text{CH}_2(\text{OH})_2$, methylene glycol. But it is unknown whether surface concentrations or species are

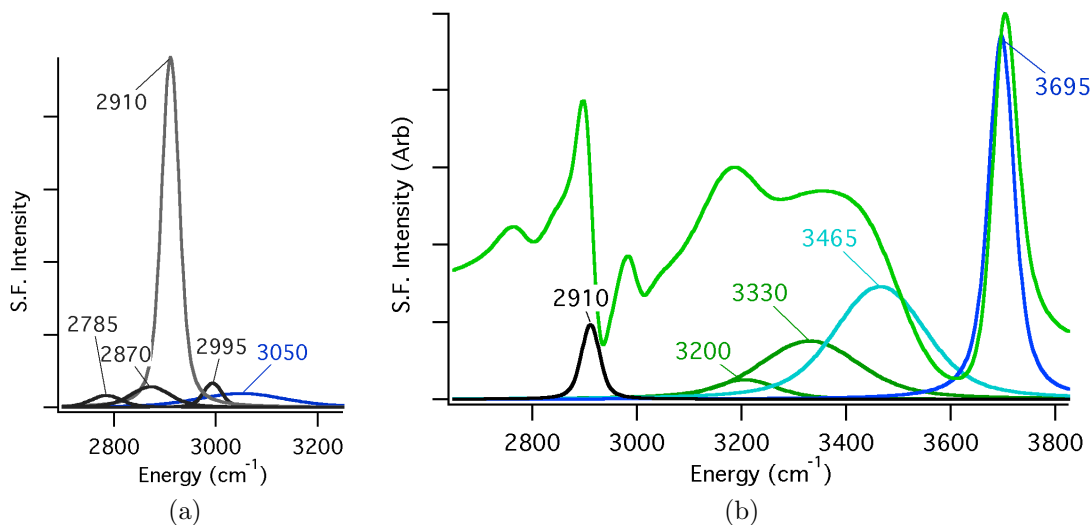


FIGURE 8.3. Fit to ssp-polarization spectra of 3.2 % w/v formaldehyde (green) with resonant components (color). a. Enlargement of CH region. b. Overall fits

different from those in the bulk, and it is likely that surface molecules are solvated by fewer water molecules from those in the bulk. And although there have been numerous Raman and IR studies of aqueous formaldehyde, spectral assignments vary for different experiments.^{191–195,205,206}

The broad peak at $\sim 3050\text{ cm}^{-1}$ can be attributed to either the methylene glycol OH stretching mode, or an enhancement in the overall water binding environment. Increased intensity in this region was observed for the succinic acid solutions, as well. The four peaks below $\sim 3000\text{ cm}^{-1}$ are attributed to methylene glycol and formaldehyde at the surface. The main contribution, a relatively sharp peak at $\sim 2910\text{ cm}^{-1}$, is assigned to the methylene glycol symmetric stretch mode, consistent with Raman measurements of aqueous MG.^{191,193} The frequency of the peak at $\sim 2995\text{ cm}^{-1}$ matches that of the $\nu_a(\text{HCH})$ mode assigned by Lebrun et. al.,¹⁹¹ but its phase, which matches that of the peak at $\sim 2910\text{ cm}^{-1}$ indicates that it may be a Fermi resonance of the symmetric CH_2 stretch. This assignment would be

consistent with the symmetry arguments from a previous VSFS study of longer chain diols by Le et al.²⁰⁷ The other two peaks, which are relatively small, can be attributed to either molecular CH₂O,¹⁹⁴ non-fundamental methylene glycol peaks,¹⁹¹ or longer-chain oligomers. The peak at 2785 cm⁻¹ is similar in frequency to the symmetric CH stretch of gas phase formaldehyde, an assignment that could be supported by the peak at 2850 cm⁻¹ in the sps-polarization scheme, which matches the frequency of the asymmetric CH stretch. However, in aqueous solution these modes are expected to blue-shift, and are predicted to be at ~2820 and ~2870 cm⁻¹, respectively making a definite assignment difficult.^{194,206} Clearly, the surface spectrum of formaldehyde is quite complex, but these parameters provide a baseline for assessing the changes to the spectral region when SO₂ is flown over the surface. These perturbations are the focus of the following discussion.

8.2.1 Uptake of SO₂

The spectrum in Fig. 8.4.a shows that the addition of SO₂ (red) significantly perturbs the aqueous formaldehyde (green) surface. Similar to the analysis in the previous section, a global fit was performed to determine fitting parameters for the spectral perturbations due to SO₂. The results of this fit are shown in Fig. 8.4.b. The primary differences between this spectrum and the one for the neat formaldehyde solution are the additional peak at ~3650 cm⁻¹, which indicates that SO₂:water surface complexes are forming, and a reduction in the number of peaks necessary to fit the CH-stretching region. However, from these spectra alone, it is difficult to understand the origin of these spectral changes. There are three plausible explanations for these spectral changes: SO₂ could be complexing to CH₂O(aq) at the surface; the new peaks could be due to product of the reaction between CH₂O and

SO₂, HMS; or a new surface complex could be forming between SO₂ and another species, such as HMS, at the interface.

Based on spectra taken after removing SO₂ from the system, which are shown in Fig. 8.4.c, it is unlikely that the peaks shown during SO₂ exposure are due to the reaction alone. The post SO₂ spectra appear quite different from those of either the fresh formaldehyde solutions, or those taken during exposure to SO₂. However, although their shapes are quite different, it is interesting to note the similarities between the components of the fits to the spectra taken during and after exposure to SO₂.

To examine the question of whether complexes are forming between formaldehyde and SO₂ at the surface, the evolution of a more concentrated formaldehyde solution was observed while exposing it to SO₂. The spectra in Fig. 8.5. were obtained using a 16 %w/v formaldehyde solution, with the assumption that the reaction between SO₂ and CH₂O would take longer to reach equilibrium with the more concentrated solution. The top spectrum was taken prior to exposure to SO₂. As mentioned earlier, the VSF response for the 16 %w/v formaldehyde solution can be fit using the same peaks as for the 3.2 %w/v solution, indicating that the surface species for the unexposed surfaces are the same. Spectra were obtained over the full spectral region, but for simplicity, only the CH-stretching region is shown. Each spectrum takes approximately 18 minutes to acquire, and spectra were taken continuously until the response was constant for at least three consecutive acquisitions.

The main CH peaks for spectra taken during the first hour of SO₂ exposure (light red) lose intensity, but do not shift position. By contrast, the broadening observed in the free OH region (not shown) occurs immediately upon exposure to SO₂. However, after an hour of exposure, the peaks do shift and remain shifted during subsequent

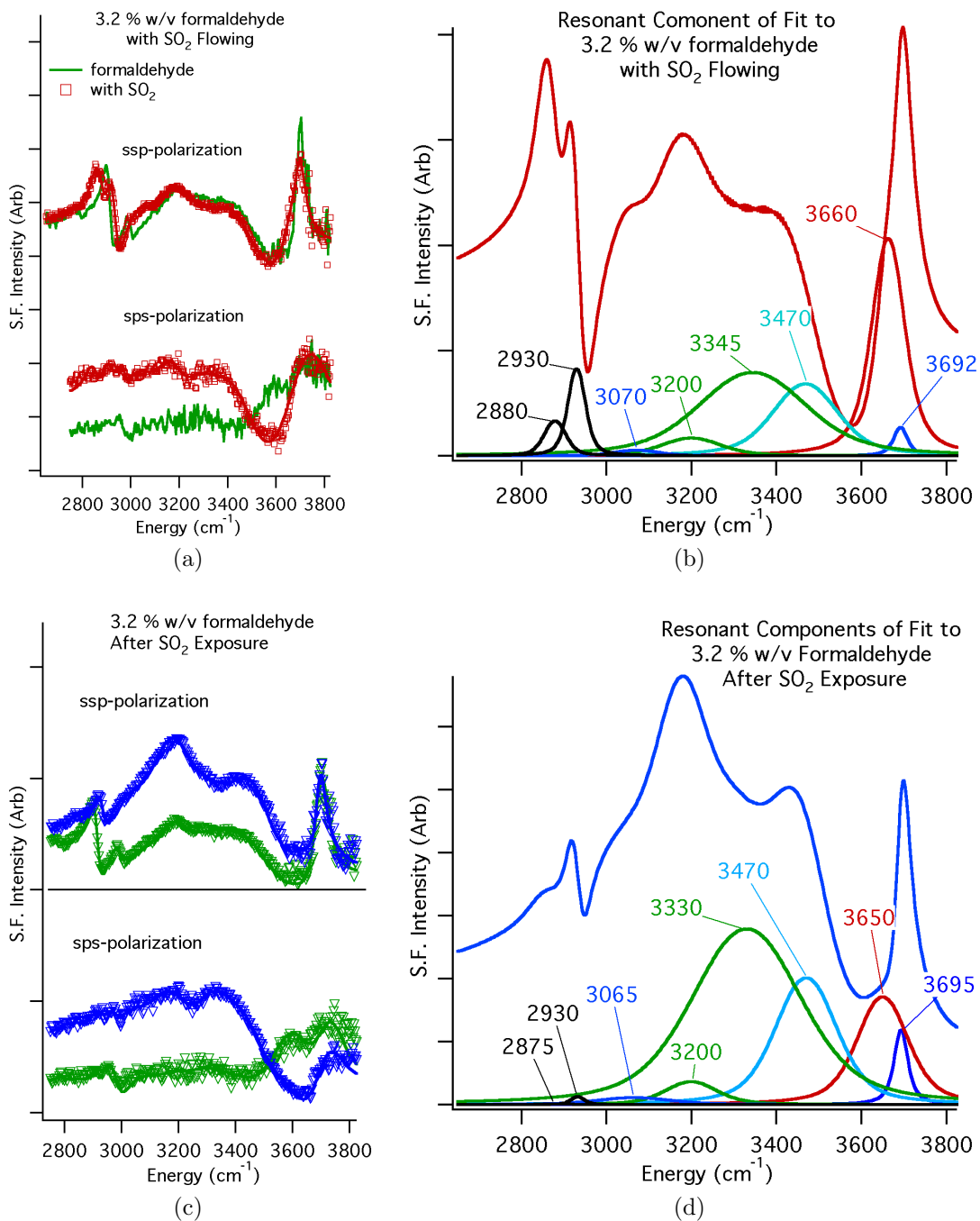


FIGURE 8.4. a. ssp (top) and sps (bottom)-polarization spectra of 3.2 % w/v formaldehyde with SO₂ flowing (red) with the vapor/formaldehyde interface (green) for reference. b. Resonant components of fit to data (red). c. ssp (top) and sps (bottom)-polarization spectra of 3.2 % w/v formaldehyde after exposure to SO₂ (blue). d. Resonant components (colored) of fit to the data (blue).

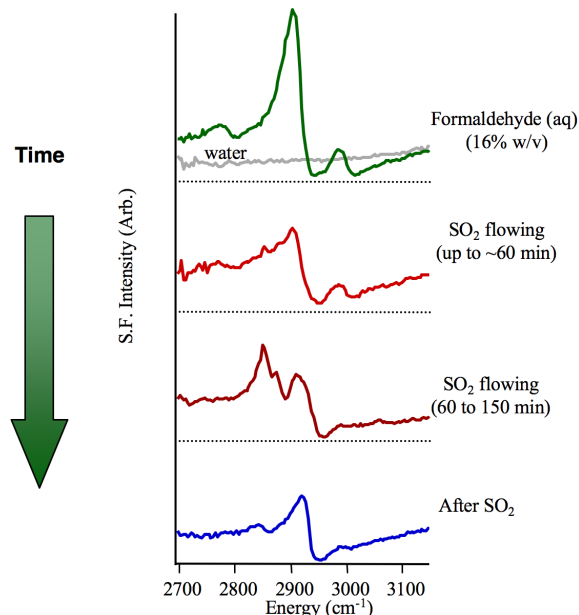


FIGURE 8.5. ssp -polarization spectra of 16 % w/v formaldehyde. Spectra show evolution of the CH stretching region during exposure to SO_2 as a function of time, and after removal of the gas.

exposure to SO_2 (dark red). The peak positions and widths for this solution match those for the 3.2 % w/v formaldehyde solutions shown in Fig. 8.4.b.

These results indicate that the reaction between HSO_3^- and H_2CO occurs in the bulk solution. The reaction reduces the amount of H_2CO in solution so the VSF intensity decreases. It is only after some of the formaldehyde has reacted that spectral evidence of the new reaction is seen in the CH region, which indicates that the new peaks could be due to HMS partitioning to the interface. Given the low pH of these solutions, and the polar nature of the HMS ions, they are unlikely to be strongly surface active. However, it is possible that the surface adsorbed SO_2 is complexing to HMS molecules, causing them to partition to the interfacial region.

To test this hypothesis, two solutions of HMS were made. The first solution was made by diluting a 16 % w/v formaldehyde solution to 3.2 % w/v in concentrated sulfurous acid (H_2SO_3). As the reaction is very similar to the one instigated by the

absorption of SO_2 into aqueous formaldehyde solutions, the results were also tested using an HMS solution made by dissolving Na_2SO_3 in 3.2 % w/v $\text{CH}_2\text{O}(\text{aq})$. The resultant HMS solutions are at different pHs, thus the VSF response from water was quite different for the two solutions. H_2SO_3 has a pH of less than 1, while the Na_2SO_3 solutions start at pH 12, and their interfacial behavior is consistent with the spectral response seen for previous pH studies.³⁶ The low pH solution has strong intensity in the coordinated water region, consistent with the accumulation of HMS and hydronium ions in the interfacial region, while the OH stretching region for alkaline solution is more similar to that of water. In addition, the spectral response from Na_2SO_3 solution changes upon the absorption of SO_2 , while the spectrum of the acidic solution returns to its initial shape after the removal of SO_2 . This difference is attributed to the absorption, and subsequent reaction, between SO_2 and water. The low pH solution, which is already saturated in SO_2 is unlikely to absorb more, consistent with the earlier observation that SO_2 does not absorb into the interfacial region of acidic solutions. By contrast, SO_2 absorbing into the alkaline solutions reacts with water, bringing the pH down to about 4.

Although the spectrum of the acidic HMS solutions is quite different from that of unexposed CH_2O , the two surfaces respond very similarly when exposed to SO_2 , and can be fit using the same peak parameters. For the HMS solution, this means a slight red shift-and narrowing of the CH peaks, which is accompanied by an intensity increase over time. Upon removal of SO_2 the interface returns to its initial state, as is indicated by the similarity between the green and blue spectra in Fig. 8.6.a, which represent the interface before and after exposure to SO_2 , respectively. This supports the picture that SO_2 gas is forming complexes with HMS at the water surface, consistent with the studies presented above. The evolution of the alkaline

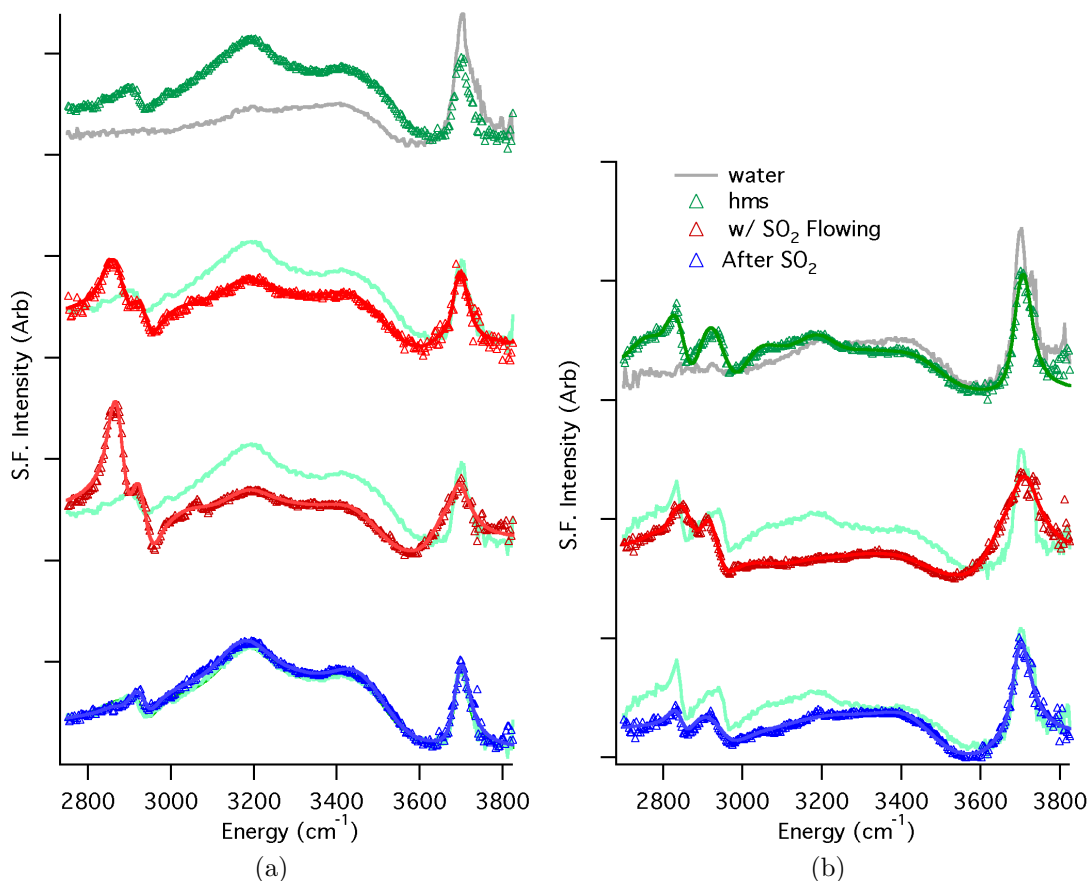


FIGURE 8.6. ssp-polarization spectra of HMS before (green), during (red), and after (blue) exposure to SO_2 . a. HMS solution made with $\text{CH}_2\text{O}(\text{aq})$ and $\text{H}_2\text{SO}_3(\text{aq})$. Darker red spectrum shows evolution over time with exposure to SO_2 . b. HMS solution made with $\text{CH}_2\text{O}(\text{aq})$ and Na_2SO_3

solutions is more difficult to interpret, as it is complicated the reactions between water and SO_2 . However, the spectral shifts in the CH region are consistent with SO_2 :HMS complexation at the surface; the two CH peaks become narrower and closer together when the solution is exposed together, but return to their original shape upon removal of SO_2 . The decrease in their intensities is attributed to changes in the water hydrogen bonding environment as the result of the HSO_3^- and H^+ ions introduced by the reaction with newly solvated SO_2 .

Based on the time dependence observed with the more concentrated formaldehyde solutions, and the similarities between the HMS solutions and those of CH_2O during SO_2 exposure, the picture that develops is as follows. SO_2 adsorbs to the vapor/ $\text{CH}_2\text{O}(\text{aq})$ interface via complexes with water molecules in the topmost interfacial region. This is followed by absorption into the bulk, where the HSO_3^- ions react with $\text{CH}_2\text{O}(\text{aq})$ to form HMS. HMS in the interfacial region complexes to the surface-adsorbed SO_2 , resulting the reversible accumulation of HMS to the interface. With time, the surfaced absorbed HMS concentration increases, and becomes more orientated, resulting in an increase in the intensity of the peaks in the CH region, without a concurrent energy shift, as illustrated in Fig. 8.6.a (dark red). Upon removal of SO_2 the spectra in Fig. 8.6.a (blue) are almost identical to those taken before SO_2 exposure (green). Similarly, both the free OH and CH peaks for the spectra in Fig. 8.6.b return to their initial shape after exposure to SO_2 .

From these spectral changes, it appears that SO_2 initially adsorbs to the interface and binds to water. SO_2 absorbing into the water reacts with CH_2O to form HMS, which can migrates to the surface and complex with SO_2 . The evolution of the surface over time suggests that SO_2 adsorption at the surface induces both surface adsorption and orientation of HMS. In addition, both surface complexes are reversible: upon removal of SO_2 they are no longer observed. Now that we have a general understanding of the surface chemistry between formaldehyde and SO_2 , these studies can be expanded to more atmospherically relevant temperatures.

8.2.2 Temperature and the uptake of SO_2

To study the role of temperature in the uptake of SO_2 to formaldehyde, VSF spectra were obtained at $\sim 0^\circ\text{C}$. Figure 8.7. shows the spectral evolution of the

3.2 %w/v formaldehyde solution in the ssp (a) and sps (b) polarization schemes before (green), during (red), and after (blue) exposure to SO₂.

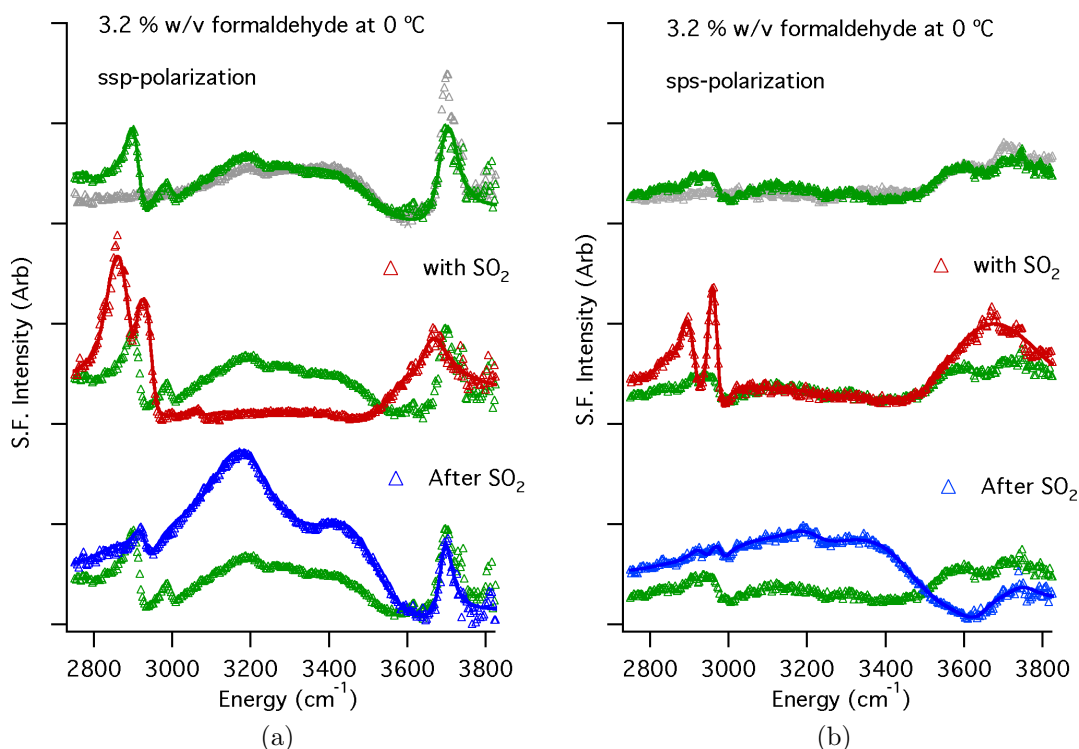


FIGURE 8.7. 3.2 % w/v formaldehyde before (green), during (red), and after (blue) exposure to SO₂. Data acquired at ~ 0 °C. a. ssp-polarization spectra b. sps-polarization spectra.

Lowering the temperature has very little impact on the surface of the vapor/CH₂O(aq) interface, and the ssp-spectrum taken at ~ 0 °C is almost identical to the spectrum at room temperature (Fig. 8.1.). In the sps-polarization scheme, the CH peaks are slightly more intense, and the data were fit using a global fitting routine to match the parameters to those at room temperature.

Similar to what was observed for the neat vapor/water interface in Chapter VI, the perturbations due to the lower temperature are much more dramatic when the solutions are exposed to SO₂ gas (red). The ssp- and sps- polarization spectra show

significant changes, both in comparison to the unexposed $\text{CH}_2\text{O}(\text{aq})$ surfaces and in comparison to the comparable spectra taken at room temperature. Figure 8.8. highlights the CH stretching region with an overlay of the spectra taken in the ssp (triangles) and sps (circles) polarization schemes. The solid lines act as a guide to the eye.

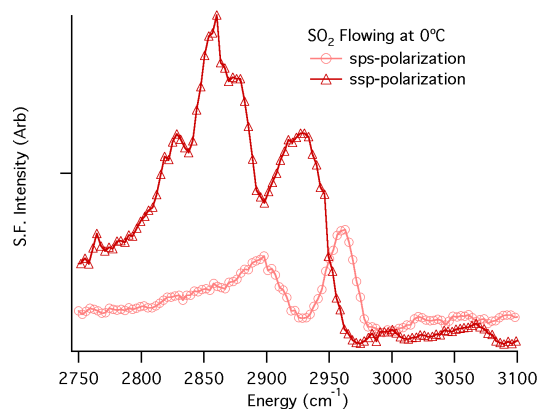


FIGURE 8.8. Comparison of spectra taken in the ssp and sps polarization schemes while SO_2 is flowing at $0\text{ }^\circ\text{C}$.

The most obvious change in this spectral region is that the peaks are more intense, and spectrally more resolved. An examination of the data in Fig. 8.8. shows that the peak intensities at ~ 2910 and $\sim 2970\text{ cm}^{-1}$ in the sps spectrum are blue-shifted, coinciding with dips in the intensity, for the ssp spectrum. Chemically, these surfaces are identical; thus the peaks in the sps-polarization are assigned to asymmetric modes corresponding to the symmetric stretches observed in the ssp-polarization. Accounting for these peaks in the fits to the ssp-spectra yields three primary peaks in this region: a broader peak at $\sim 2880\text{ cm}^{-1}$, a sharp peak at $\sim 2920\text{ cm}^{-1}$, and a sharp peak of the opposite phase at $\sim 2940\text{ cm}^{-1}$. However, it should be noted that this region can also be fit using a single peak at $\sim 2930\text{ cm}^{-1}$, consistent with the fits at room temperature, that incorporates the two peaks at 2920

and 2940 cm^{-1} . That the distinct peaks are only observed at the lower temperature indicates that the surface complexes is much more oriented with respect to the interfacial plane, giving rise to symmetric and asymmetric stretches that are more aligned with respect to the surface normal.

In both polarizations, the magnitude of the complexed free OH peak increases in a manner similar to what was observed for water in Chapter IV. But the broadening observed here is even more exaggerated. In the ssp-polarization scheme high energy region can either be fit using a single broad peak at 3630 cm^{-1} or using two peaks; a narrower peak at 3660 and a broad peak at 3580 cm^{-1} . Interestingly, this increase is accompanied by a loss of intensity in the coordinated water region, and the amplitudes of the companion OH and tetrahedrally coordinated water peaks are negligible in the presence of SO_2 . The changes to the high energy OH stretching region are also very different in the sps-polarization scheme. At room temperature, as the water molecules reoriented to complex with SO_2 there was a concurrent decrease in the intensity of the peak at $\sim 3580\text{ cm}^{-1}$. By contrast, at the colder temperature, the dominant feature in this region is a broad peak at $\sim 3580\text{ cm}^{-1}$, which has very little contribution from either the uncomplexed free OH or its companion mode at $\sim 3460\text{ cm}^{-1}$. As they were at room temperature, these changes are reversible in both polarizations, and the spectra taken after SO_2 adsorption (blue) closely resemble those taken of the HMS solution at room temperature.

Thus, the picture that arises is as follows. At cold temperature, SO_2 complexes to both water and HMS, but higher SO_2 solubility leads to even greater surface adsorption than is observed at room temperature.

The migration of HMS, and complexation with SO_2 at the surface disrupts the interfacial electric field caused by charge separation between the hydronium ions and

solvated sulfur species, which results in less coordination and orientation of the water molecules. This has two effects. First, it increases the number of loosely coordinated waters in the topmost surface region, which increases the intensity of the high energy peaks near 3500 cm^{-1} . Second, reducing the charge separation between interfacial ions causes the water molecules to reorient with less overall structure, as their dipoles no longer align with the interfacial electrical field. In addition, water molecules solvating HMS or formaldehyde in the interfacial region are not forming hydrogen bonds with each other, further reducing the intensity in the OH stretching region.

This picture is supported by both the ssp and sps data, which show large increases in the intensity due to loosely coordinated water molecules and more resolved CH peaks. It is likely that this intensity increase is due to both an increase in the surface population and the environmental restriction of being bound to SO_2 at the surface. As a relatively large, polarizable compound, HMS has the potential to hydrogen bond with water or sulfite molecules in many different configurations in solution. However, at the interface, these binding possibilities are much more limited, an interpretation supported by the narrow peaks observed here, relative to those measured after removing SO_2 , when the ions are once again solvated. For a summary of the fitting parameters used in these experiments, please see Appendix C.

8.2.3 Conclusions

From these experiments, it is clear that the interfacial environment is sensitive to the atmospherically relevant reaction between SO_2 and CH_2O . The surface perturbations introduced by the flow of SO_2 gas are quite complex, but the cartoon in Fig. 8.9. provides a simple illustration of the overall interfacial behavior. The aqueous formaldehyde shows evidence of surface-bound organic species, which are

depicted as green ovals in Fig. 8.9.. Upon exposure to SO_2 , the surface water molecules immediately form complexes with surface-bound SO_2 , and adsorbed SO_2 reacts with water in the bulk. The subsequent reaction between CH_2O and HSO_3^- occurs primarily in the bulk solution, depleting surface adsorbed formaldehyde concentrations. This is followed by the migration of HMS to the interfacial region, where it forms surface complexes with SO_2 . Like the complexes between water and SO_2 , the $\text{HMS}:\text{SO}_2$ complexes are reversible, and are only observed while the SO_2 gas is flowing over the surface.

Cooling the formaldehyde solution to an atmospherically relevant temperature results in a significant enhancement of the observed SO_2 absorption. In addition, changes to the shape and intensity of the CH peaks are consistent with a structurally more congested interface where the orientations of the surface complexes between SO_2 and HMS are more constrained. This is consistent with the increased contribution from loosely coordinated water molecules in the topmost surface region. The main spectral contributions from water are from water molecules that are either involved in complexes to SO_2 or those with weak hydrogen bonding interactions with other waters. This points to an interface that is mainly populated by surface-bound organics, ions, and other species that are loosely solvated by water. These surface species are short-lived, and the ions return to solution when the SO_2 is removed from the system. The resultant solution exhibits enhanced interfacial coordination consistent with spectra of other low pH, ion-containing solutions.

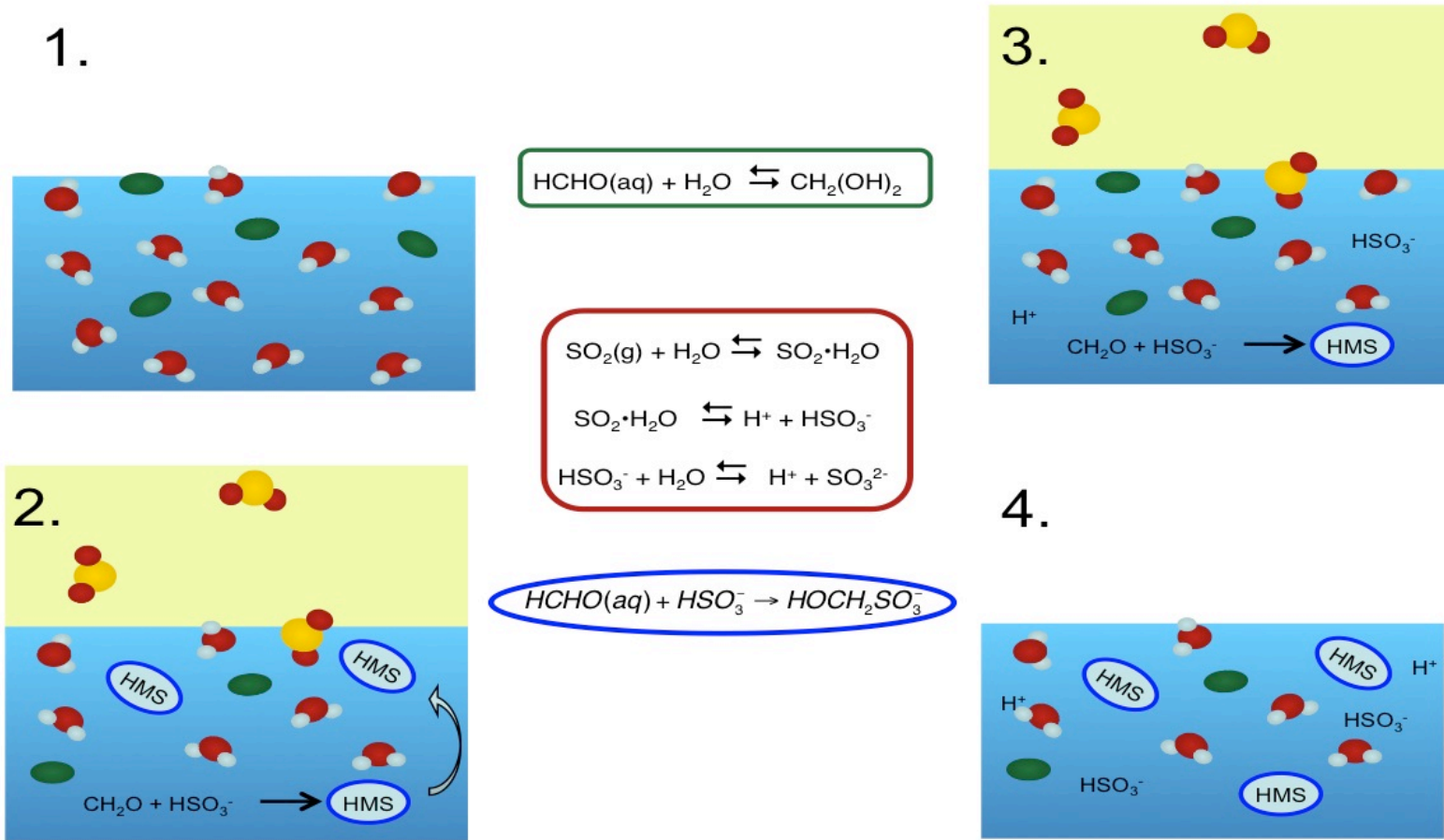


Figure 8.9 Cartoon depiction of the evolution of aqueous formaldehyde with SO₂ exposure over time. 1. Vapor/CH₂O (aq) Interface. 2. Exposure to SO₂ results in surface complexes with water and bulk reaction to form HMS. 3. Extended exposure to SO₂ results in surface complexes between SO₂ and HMS. 4. Surface complexes are reversible, but the ions formed during SO₂ exposure remain in solution.

CHAPTER IX

CONCLUSIONS

The uptake of gases by aqueous aerosols is a primary step in many atmospheric interactions, but details about the mechanisms that drive gas adsorption to water remain elusive. While surface complexes are known to form between SO_2 and H_2O , previous studies have left many questions regarding the behavior of these interfacial species unanswered. Many of the ambiguities found in earlier studies resulted from indirect indicators of surface complexation. The studies presented here provide a direct examination of surface $\text{SO}_2:\text{H}_2\text{O}$ complexation as a function of temperature, solution acidity, and organic composition under conditions relevant to tropospheric surface reactions.

The results of the uptake studies presented in Chapter V illustrate the importance of solvent temperature on the likelihood of SO_2 surface complexation. At low temperatures, the adsorption of SO_2 was significantly enhanced, resulting in the reorientation and complexation of nearly all of the water molecules in the topmost surface region.

Important new insights into the adsorption and uptake of SO_2 to acid solutions were provided in the studies presented in Chapter VI. It is well known that the uptake of SO_2 is diminished as an aqueous solution becomes more acidic. These studies show that even though the acidic ions in a bulk H_2SO_4 solution are present in the interfacial region, as manifested through their impact on the hydrogen bonding characteristics water molecules therein, the presence of these ions has no effect on the complexation of SO_2 to the water surface at either room temperature or $0\text{ }^\circ\text{C}$. Furthermore, the increased production of ions such as HSO_3^- in the interfacial region that is observed

upon exposure of SO_2 to neutral solutions is not observed in the presence of acid. Hence the chemistry occurring in the interfacial region appears to be driven by the same equilibrium behavior as the bulk solution. Overall these results suggested that the complexation behavior at the topmost layer of the surface was largely uncoupled from the rest of the interfacial region and the bulk solution.

These studies were extended to investigate the behavior that might occur in more polluted environments, where organic solutes are abundant. The results of Chapter VII illustrate the persistence of $\text{SO}_2\text{:H}_2\text{O}$ surface compounds, which continued to form when interfacial region was populated with succinic acid. Further, there was no evidence of any interaction between succinic acid and SO_2 in the interfacial region. These results raised the question of whether surface complexes were specific to water? or whether formaldehyde, a more reactive organic pollutant, might demonstrate different surface behavior when exposed to SO_2 ? These questions were explored in Chapter VIII. Formaldehyde itself demonstrated a similar insensitivity to SO_2 at the surface, and the reaction between SO_2 and CH_2O was found to occur primarily in solution. However, as the droplet composition changed, a new compound was observed at the surface. The new species was determined to be a reversible surface complex between HMS and SO_2 . Similar to the behavior observed for the clean water surface, the formation of these complexes was significantly enhanced at low temperature. Interestingly, none of the surface complexes investigated in these studies were observed after purging the cell of SO_2 . However, with the exception of the highly acidic solutions, all of solutions examined showed evidence of SO_2 absorption and reaction with water, and the formaldehyde solutions showed evidence of HMS formation. In summary, these experiments show that aqueous surfaces can act as as reservoir for SO_2 (or other gases) in the atmosphere by forming interfacial complexes

even when the aqueous composition might otherwise impede uptake. The results from these experiments point to the importance of understanding, and accounting for, surface interactions in models of atmospheric behavior. As was demonstrated with the formaldehyde system, all species, including the reaction products have the potential to influence interfacial activity and gas uptake. This study shows clear evidence of surface accumulation in the absence of bulk absorption, a phenomenon that has important implications for atmospheric chemistry. Surfaces form a platform for potential reactions with either gas phase or solvated species. In addition, surface adsorbed species are vulnerable to reactions with UV light in the atmosphere. These potential surface interactions may be especially relevant to polluted environments where there is an abundance of both SO_2 and reactive organic species.

APPENDIX A

CALCULATED CONCENTRATIONS FOR ISOTOPIC DILUTION STUDIES

The equilibrium concentrations of solutions containing H₂O, D₂O, and HOD can be closely approximated using an equilibrium constant of 4, the value used for the concentrations reported in Chapters IV and V. However, differences between the zero point energies for the three species causes a slight dependence on the initial solution concentrations. Experimental measurements, in conjunction with calculations indicate that the actual equilibrium constant can vary between 3.4 and 4.4 depending on the experimental conditions and the theoretical models used²⁰⁸ Table A.1. shows calculated concentrations, given as mole fractions, for the solutions presented in Chapters IV and V. These values were calculated using the equilibrium relationship shown in Eq. (A.1).

$$K_{eq} = \frac{[\text{HOD}]^2}{[\text{H}_2\text{O}][\text{D}_2\text{O}]} \quad (\text{A.1.})$$

For the solutions used in these experiments, the equilibrium constant is expected to be close to 3.9 based on the results of previous measurements by Libnau et al.²⁰⁸ Based on these calculations, the zero point energies are expected to have very little effect on the experimental concentrations of HOD, H₂O, and D₂O.

TABLE A.1. Calculated Isotopic Dilution Concentrations

K_{eq}	Solution 1			Solution 2			Solution 3		
	HOD	H2O	D2O	HOD	H2O	D2O	HOD	H2O	D2O
4.4	0.340	0.617	0.043	0.512	0.247	0.242	0.227	0.015	0.757
4.3	0.339	0.618	0.043	0.509	0.248	0.243	0.227	0.016	0.758
4.2	0.338	0.619	0.044	0.506	0.249	0.244	0.226	0.016	0.758
4.1	0.336	0.619	0.045	0.503	0.251	0.246	0.225	0.016	0.758
4	0.335	0.620	0.045	0.500	0.252	0.248	0.225	0.017	0.759
3.9	0.333	0.621	0.046	0.497	0.254	0.249	0.224	0.017	0.759
3.8	0.332	0.621	0.047	0.494	0.256	0.251	0.223	0.017	0.759
3.7	0.330	0.622	0.047	0.490	0.257	0.252	0.223	0.018	0.760
3.6	0.329	0.623	0.048	0.487	0.259	0.254	0.222	0.018	0.760
3.5	0.327	0.624	0.049	0.483	0.261	0.256	0.221	0.018	0.760
3.4	0.325	0.625	0.050	0.480	0.263	0.258	0.220	0.019	0.761
average	0.333	0.621	0.046	0.496	0.254	0.249	0.224	0.017	0.759
std dev	0.005	0.002	0.002	0.011	0.005	0.005	0.002	0.001	0.001

APPENDIX B

FITTING PARAMETERS FOR SUCCINIC ACID

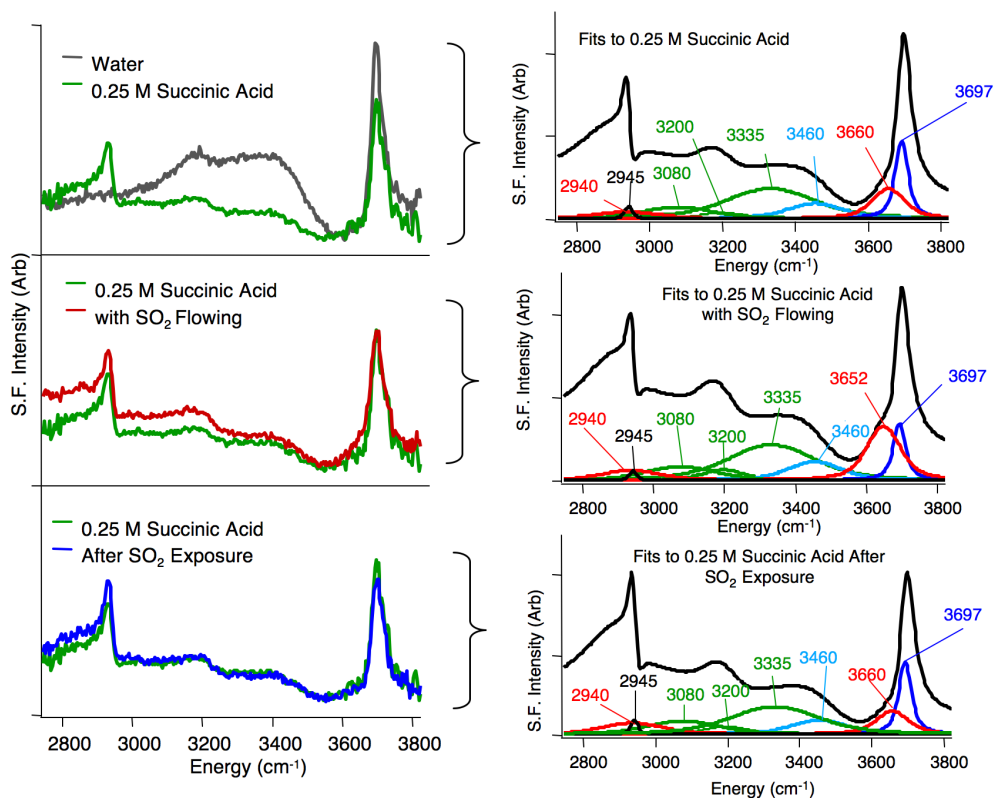


FIGURE B.1. The evolution of the interfacial region when succinic acid is exposed to SO₂. Left. ssp-polarization data. Right. Corresponding fits and resonant components.

TABLE B.1 Fitting Parameters for Succinic Acid Resonant Peaks

	Strong Coord.		Strong Coord.		Companion		Free OH		Solvation		Strong Coord.		Carboxyl OH		CH	
	ω_ν	Γ_ν	ω_ν	Γ_ν	ω_ν	Γ_ν	ω_ν	Γ_ν	ω_ν	Γ_ν	ω_ν	Γ_ν	ω_ν	Γ_ν	ω_ν	Γ_ν
H ₂ O	3200	45	3335	140	3458	88	3697	16	–	–	–	–	–	–	–	–
(DOOC(CH ₂)) ₂	–	–	–	–	–	–	2730	12	2695	40	–	–	–	–	2945	12
							(OD)									
(HOOC(CD ₂)) ₂	3200	65	3335	140	3458	85	3697	14	3660	47	3080	110	2940	90	–	–
(HOOC(CH ₂)) ₂	3200	65	3335	140	3458	85	3697	14	3660	50	3080	110	2940	95	2945	11
With SO ₂ Flowing																
	Strong Coord.		Strong Coord.		Companion		Free OH		Complexed OH		Strong Coord.		Carboxyl OH		CH	
	ω_ν	Γ_ν	ω_ν	Γ_ν	ω_ν	Γ_ν	ω_ν	Γ_ν	ω_ν	Γ_ν	ω_ν	Γ_ν	ω_ν	Γ_ν	ω_ν	Γ_ν
H ₂ O	3215	50	3335	140	3470	95	3692	13	3660	35	3140	115	–	–	–	–
(HOOC(CD ₂)) ₂	3205	70	3331	145	3465	85	3697	12	3645	75	3080	110	2940	90	–	–
(HOOC(CH ₂)) ₂	3200	65	3335	140	3458	85	3697	14	3650	50	3080	110	2940	95	2945	11
After SO ₂ Exposure																
	Strong Coord.		Strong Coord.		Companion		Free OH		Solvation		Strong Coord.		Carboxyl OH		CH	
	ω_ν	Γ_ν	ω_ν	Γ_ν	ω_ν	Γ_ν	ω_ν	Γ_ν	ω_ν	Γ_ν	ω_ν	Γ_ν	ω_ν	Γ_ν	ω_ν	Γ_ν
H ₂ O	3210	40	3330	140	3475	95	3694	10	3660	50	3140	90	–	–	–	–
(HOOC(CD ₂)) ₂	3200	65	3335	140	3458	85	3697	14	3660	47	3080	110	2940	90	–	–
(HOOC(CH ₂)) ₂	3200	65	3335	140	3458	85	3697	14	3660	50	3080	110	2940	95	2945	11

All values are given in wavenumbers. Energies are ± 10 cm⁻¹ and Gaussian widths are ± 20 cm⁻¹ for strong OH stretching

APPENDIX C

FITTING PARAMETERS FOR FORMALDEHYDE

TABLE C.1. Fitting Parameters for Formaldehyde CH-stretch Region

Room Temperature (23 °C)											
ssp-polarization						sps-polarization					
CH ₂ O		with SO ₂		after SO ₂		CH ₂ O		with SO ₂		after SO ₂	
ω_ν	Γ_ν	ω_ν	Γ_ν	ω_ν	Γ_ν	ω_ν	Γ_ν	ω_ν	Γ_ν	ω_ν	Γ_ν
2785	35	2786	45	–	–	–	–	–	–	–	–
–	–	–	–	–	–	2855	37	2855	25	2845	50
2870	45	2880	30	2875	40	–	–	–	–	–	–
–	–	–	–	–	–	2920	20	2920	30	2930	35
–	–	2930	23	2930	18	–	–	–	–	–	–
–	–	–	–	–	–	2975	30	2970	20	2980	25
2994	20	3000	16	–	–	–	–	–	–	–	–
Cold (0 °C)											
ω_ν	Γ_ν	ω_ν	Γ_ν	ω_ν	Γ_ν	ω_ν	Γ_ν	ω_ν	Γ_ν	ω_ν	Γ_ν
2785	35	2790	40	–	–	–	–	–	–	–	–
–	–	–	–	–	–	2853	37	2860	20	–	–
2870	45	2880	40	2880	45	–	–	–	–	–	–
2910	20	–	–	–	–	–	–	2910	22	–	–
–	–	2920	13	–	–	2920	20	–	–	2935	20
–	–	2945	10	2930	20	–	–	2947	20	–	–
–	–	–	–	–	–	2975	30	2970	15	2980	15
2994	20	–	–	–	–	–	–	–	–	–	–
HMS (acidic)						HMS (alkaline)					
HMS		with SO ₂		after SO ₂		HMS		with SO ₂		after SO ₂	
ω_ν	Γ_ν	ω_ν	Γ_ν	ω_ν	Γ_ν	ω_ν	Γ_ν	ω_ν	Γ_ν	ω_ν	Γ_ν
–	–	–	–	–	–	2790	55	–	–	–	–
–	–	–	–	–	–	2845	30	–	–	-2844	20
2885	40	2880	23	2870	23	–	–	2865	35	–	–
–	–	2930	25	2935	21	2935	50	2930	30	2940	45
–	–	–	–	–	–	2990	65	–	–	–	–

All values are given in wavenumbers. Energies are $\pm 5 \text{ cm}^{-1}$
 Gaussian widths are $\pm 10 \text{ cm}^{-1}$

REFERENCES CITED

- [1] Finlayson-Pitts, B. J., and Pitts, J. N., Jr. *Chemistry of the Upper and Lower Atmosphere*; Academic Press: San Diego, 2000.
- [2] Manahan, S. E. *Environmental Chemistry*, 6th ed.; Lewis Publishers: Boca Raton, FL, 1994.
- [3] Donaldson, D. J., and Vaida, V. (2006) The Influence of Organic Films at the Air-Aqueous Boundary on Atmospheric Processes. *Chem. Rev.* *106*, 1445–1461.
- [4] Molina, M. J., Molina, L. T., and Kolb, C. E. (1996) Gas-Phase and Heterogeneous Chemical Kinetics of the Troposphere and Stratosphere. *Annu. Rev. Phys. Chem.* *47*, 327–367.
- [5] Hemminger, J. C. (1999) Heterogeneous Chemistry in the Troposphere: a Modern Surface Chemistry Approach to the Study of Fundamental Processes. *Int. Rev. Phys. Chem.* *18*, 387–417.
- [6] Reid, J. P., and Sayer, R. M. (2003) Heterogeneous Atmospheric Aerosol Chemistry: Laboratory Studies of Chemistry on Water Droplets. *Chem. Soc. Rev.* *32*, 70–79.
- [7] Garrett, B. C., Schenter, G. K., and Morita, A. (2006) Molecular Simulations of the Transport of Molecules Across the Liquid/Vapor Interface of Water. *Chem. Rev.* *106*, 1355–1374.
- [8] Mundy, C. J., and Kuo, I.-F. W. (2006) First-Principles Approaches to the Structure and Reactivity of Atmospherically Relevant Aqueous Interfaces. *Chem. Rev.* *106*, 1282–1304.
- [9] Finlayson-Pitts, B. J. (2009) Reactions at Surfaces in the Atmosphere: Integration of Experiments and Theory as Necessary (but Not Necessarily Sufficient) for Predicting the Physical Chemistry of Aerosols. *Phys. Chem. Chem. Phys.* *11*, 7760–7779.
- [10] Worsnop, D. R., Zahniser, M. S., Kolb, C. E., Gardner, J. A., Watson, L. R., Van Doren, J. M., Jayne, J. T., and Davidovits, P. (1989) Temperature Dependence of Mass Accommodation of SO₂ and H₂O₂ on Aqueous Surfaces. *J. Phys. Chem.* *93*, 1159–1172.
- [11] Chu, L., Diao, G., and Chu, L. T. (2000) Heterogeneous Interaction of SO₂ on H₂O₂-Ice Films at 190–210 K. *J. Phys. Chem. A* *104*, 7565–7573.

- [12] Conklin, M. H., and Bales, R. C. (1993) SO₂ Uptake on Ice Spheres: Liquid Nature of the Ice-Air Interface. *J. Geophys. Res.* *98*, 16851–16855.
- [13] Koliadima, A., Kapolos, J., and Farmakis, L. (2009) Diffusion Coefficients of SO₂ in Water and Partition Coefficients of SO₂ in Water-Air Interface at Different Temperature and pH Values. *Instrum. Sci. Technol.* *37*, 274–283.
- [14] Boniface, J., Shi, Q., Li, T. Q., Cheung, J. L., Rattigan, O. V., Davidovits, P., Worsnop, D. R., Jayne, J. T., and Kolb, C. E. (2000) Uptake of Gas-Phase SO₂, H₂S, and CO₂ by Aqueous Solutions. *J. Phys. Chem. A* *104*, 7502–7510.
- [15] Jia, L., and Peng, X. (2004) Research on Convective Condensation Heat Transfer for a Gas Mixture in a Vertical Tube. *Heat Transfer-Asian Res.* *33*, 219–228.
- [16] Jayne, J. T., Davidovits, P., Worsnop, D. R., Zahniser, M. S., and Kolb, C. E. (1990) Uptake of SO₂(g) by Aqueous Surfaces as a Function of pH: The Effect of Chemical Reaction at the Interface. *J. Phys. Chem.* *94*, 6041–6048.
- [17] Schwartz, S. E., and Freiburg, J. E. (2007) Mass-Transport Limitation to the Rate of Reaction of Gases in Liquid Droplets: Application to Oxidation of SO₂ in Aqueous Solutions. *Atmos. Environ.* *41*, S138–S153.
- [18] Huang, C.-H. (2005) Modeling Sulfur Dioxide Absorption by Fine Water Spray. *J. Environ. Sci. Health* *40*, 2027–2039.
- [19] Hsu, C.-T., and Shih, S.-M. (1994) Simulation of SO₂ Absorption by Falling Water Drops. *Can. J. Chem. Eng.* *72*, 256–261.
- [20] Andreasen, A., and Mayer, S. (2007) Use of Seawater Scrubbing for SO₂ Removal from Marine Engine Exhaust Gas. *Energy & Fuels* *21*, 3274–3279.
- [21] Krissman, J., Siddiqi, M. A., and Lucas, K. (1997) Absorption of Sulfur Dioxide in Dilute Aqueous Solutions of Sulfuric and Hydrochloric Acid. *Fluid Phase Equilib.* *141*, 221–233.
- [22] Worsnop, D. R., Jayne, J. T., Kolb, C. E., Shi, Q., Boniface, J., Li, Y. Q., Rattigan, O. V., Swartz, E., and Davidovits, P. (1998) Uptake of Gas-Phase SO₂, H₂S, and CO₂ into Droplets and Bubbles in Aqueous Acid Solution. *J. Aerosol Sci.* *29*, s987–s988.
- [23] Rattigan, O. V., Boniface, J., Swartz, E., Davidovits, P., Jayne, J. T., Kolb, C. E., and Worsnop, D. R. (2000) Uptake of gas-phase SO₂ in Aqueous Sulfuric acid: Oxidation by H₂O₂, O₃, and HONO. *J. Geophys. Res.* *105*, 2065–29078.

- [24] Rodriguez-Sevilla, J., Alvarez, M., Liminana, G., and Diaz, M. C. (2002) Dilute SO₂ Absorption Equilibria in Aqueous HCl and NaCl Solutions at 298.15 K. *J. Chem. Eng. Data* 47, 1339–1345.
- [25] Millero, F. J., Hershey, P., Johnson, G., and Zhang, J.-Z. (1989) The Solubility of SO₂ and the Dissociation of H₂SO₃ in NaCl Solutions. *J. Atmos. Chem.* 8, 377–389.
- [26] Zimmermann, K., Pasel, C., Lukas, M., and Herbell, J.-D. (2009) Solubility of Sulphur Dioxide in Aqueous Electrolyte Solutions at Higher Ionic strengths—Chloride and Bromide Containing Systems. *Fluid Phase Equilib.* 279, 105–114.
- [27] Knipping, E. M., Lakin, M. J., Jungwirth, P., Tobias, D. J., Gerber, R. B., Dabdub, D., and Finlayson-Pitts, B. J. (2000) Experiments and Simulations of Ion Enhanced Interfacial Chemistry on Aqueous NaCl Aerosols. *Science* 288, 301–306.
- [28] Hu, J. H., Shi, Q., Davidovits, P., Worsnop, D. R., Zahniser, M. S., and Kolb, C. E. (1995) Reactive Uptake of Cl₂(g) and Br₂(g) by Aqueous Surfaces as a Function of Br⁻ and I⁻ Ion Concentration: The Effect of Chemical Reaction at the Interface. *J. Phys. Chem.* 99, 8768–8776.
- [29] George, C., Behnke, W., Scheer, V., Zetzsch, C., Magi, L., Ponche, J. L., and Mirabel, P. (1995) Fate of ClNO₂ over Aqueous Solutions Containing Iodide. *Geophys. Res. Lett.* 22, 1505–1508.
- [30] Vázquez, G., Antorrena, G., Chenlo, F., and Alvarez, E. (1991) Absorption of SO₂ by Water: the Enhancement Factor. *Chem. Biochem. Eng. Q.* 5, 163–167.
- [31] Gardner, J. A., Watson, L. R., Adewuyi, Y. G., Van Doren, J. M., Davidovits, P., Worsnop, D. R., Zahniser, M. S., and Kolb, C. E. In *Biogenic Sulfur in the Environment*; Saltzman, E. S., and Cooper, W. J., Eds.; ACS Symposium Series; American Chemical Society: Washington, DC, 1989; Vol. 393; Chapter 32, pp 504–517.
- [32] Krissman, J., Siddiqi, M. A., and Lucas, K. (1998) Thermodynamics of SO₂ Absorption in Aqueous Solutions. *Chem. Eng. Technol.* 21, 641–644.
- [33] Matteson, M. J., and Giardina, P. J. (1974) Mass Transfer of Sulfur Dioxide to Growing Droplets. *Environ. Sci. Technol.* 8, 50–55.
- [34] Raymond, E. A., Tarbuck, T. L., Brown, M. G., and Richmond, G. L. (2003) Hydrogen-Bonding Interactions at the Vapor/Water Interface Investigated by Vibrational Sum-Frequency Spectroscopy of HOD/H₂O/D₂O Mixtures and Molecular Dynamics Simulations. *J. Phys. Chem. B* 107, 546–556.

- [35] Raymond, E. A., and Richmond, G. L. (2004) Probing the Molecular Structure and Bonding of the Surface of Aqueous Salt Solutions. *J. Phys. Chem. B* 108, 5051–5059.
- [36] Tarbuck, T. L., Ota, S. T., and Richmond, G. L. (2006) Spectroscopic Studies of Solvated Hydrogen and Hydroxide Ions at Aqueous Surfaces. *J. Am. Chem. Soc.* 128, 14519–14527.
- [37] Munger, J. W., Tiller, C., and Hoffman, M. R. (1986) Identification of Hydroxymethanesulfonate in Fog Water. *Science* 231, 247–249.
- [38] Boyce, S. D., and Hoffman, M. R. (1984) Kinetics and Mechanism of the Formation of Hydroxymethanesulfonic Acid at Low pH. *J. Phys. Chem.* 88, 4740–4746.
- [39] Warneck, P. (1989) Sulfur Dioxide in Rain Clouds: Gas-Liquid Scavenging Efficiencies and Wet Deposition Rates in the Presence of Formaldehyde. *J. Atmos. Chem.* 8, 99–117.
- [40] Dong, S., and Dasgupta, P. K. (1986) On the Formaldehyde-bisulfite-hydroxymethane-sulfonate Equilibrium. *Atmos. Environ.* 20, 1635–1637.
- [41] Winkelman, J. G. M., Ottens, M., and Beenackers, A. A. C. M. (2000) The Kinetics of the Dehydration of Methylene Glycol. *Chemical Engineering Science* 55, 2065–2071.
- [42] Olson, T. M., and Hoffman, M. R. (1989) Hydroxylalkylsulfonate Formation: Its Role as a S(IV) Reservoir in Atmospheric Water Droplets. *Atmos. Environ.* 23, 985–997.
- [43] Richmond, G. L. (2002) Molecular Bonding and Interactions at Aqueous Surfaces as Probed by Vibrational Sum Frequency Spectroscopy. *Chem. Rev.* 102, 2693–2724.
- [44] Bloembergen, N. *Nonlinear Optics*; W. A. Benjamin, Inc.: New York, 1965.
- [45] Vidal, F., and Tadjeddine, A. (2005) Sum-Frequency Generation Spectroscopy of Interfaces. *Rep. Prog. Phys.* 68, 1095–1127.
- [46] Buck, M., and Himmelhaus, M. (2001) Vibrational Spectroscopy of Interfaces by Infrared-Visible Sum Frequency Generation. *J. Vac. Sci. Technol., A* 19, 2717–2736.
- [47] Lambert, A. G., Davies, P. B., and Neivandt, D. J. (2005) Implementing the Theory of Sum Frequency Generation Vibrational Spectroscopy: A Tutorial Review. *Appl. Spec. Rev.* 40, 103–145.

- [48] Guyot-Sionnest, (2005) The Mature Years of Sum-Frequency Generation Are Ahead. *Surf. Sci.* *585*, 1–2.
- [49] Voges, A. B., Al-Abadleh, H. A., and Geiger, F. M. In *Environmental Catalysis*; Grassian, V. H., Ed.; Taylor and Francis: Boca Raton, FL, 2005.
- [50] Rao, Y., Song, D., Turro, N. J., and Eisenthal, K. B. (2008) Orientational Motions of Vibrational Chromophores in Molecules at the Air/Water Interface with Time-Resolved Sum Frequency Generation. *J. Phys. Chem. B* *112*, 13572–13576.
- [51] Bloembergen, N. (1966) Second Harmonic Reflected Light. *Opt. Acta* *13*, 311–322.
- [52] Ji, N., Ostroverkhov, V., Shiu, Y.-J., and Shen, Y.-R. (2006) Toward Chiral Sum-Frequency Spectroscopy. *J. Am. Chem. Soc.* *128*, 8845–8848.
- [53] Shen, Y. R., and Ostroverkhov, V. (2006) Sum-Frequency Vibrational Spectroscopy on Water Interfaces: Polar Orientation of Water Molecules at Interfaces. *Chem. Rev.* *106*, 1140–1154.
- [54] Ishibashi, T.-A., and Onishi, H. (2002) Multiplex Infrared-Visible Sum-Frequency Spectrometer with a Phase-Conjugated Pulse Mixing Device for Narrow-Bandwidth Visible Probe Generation. *Appl. Spec.* *56*, 1298–1302.
- [55] Ostroverkhov, V., Waychunas, G. A., and Shen, Y. R. (2005) New Information on Water Interfacial Structure Revealed by Phase-Sensitive Surface Spectroscopy. *Phys. Rev. Lett.* *94*, 046102/1–046102/4.
- [56] Shen, Y. R. (2001) Exploring New opportunities with Sum-Frequency Nonlinear Optical Spectroscopy. *Pure Appl. Chem.* *73*, 1589–1598.
- [57] Miranda, P. B., and Shen, Y. R. (1999) Liquid Interfaces: A Study by Sum-Frequency Vibrational Spectroscopy. *J. Phys. Chem. B* *103*, 3292–3307.
- [58] Hirose, C., Akamatsu, N., and Domen, K. (1992) Formulas for the Analysis of the Surface SFG Spectrum and Transformation Coefficients of Cartesian SFG Tensor Components. *Appl. Spec.* *46*, 1051–1072.
- [59] Fourkas, J. T., Walker, R. A., Can, S. Z., and Gershgoren, E. (2007) Effects of Reorientation in Vibrational Sum-Frequency Spectroscopy. *J. Phys. Chem. C* *111*, 8902–8915.
- [60] Zhu, X. D., Suhr, H., and Shen, Y. R. (1987) Surface Vibrational Spectroscopy by Infrared-Visible Sum Frequency Generation. *Phys. Rev. B* *35*, 3047–3049.

- [61] Bloembergen, N., and Pershan, P. S. (1962) Light Waves at the Boundary of Nonlinear Media. *Phys. Rev.* *128*, 606–622.
- [62] Shen, Y. R. (1989) Surface Properties Probed by Second-Harmonic and Sum-Frequency Generation. *Nature* *337*, 519–525.
- [63] Bain, C. D. (1995) Sum-Frequency Vibrational Spectroscopy of the Solid/Liquid Interface. *J. Chem. Soc., Faraday Trans.* *91*, 1281–1296.
- [64] Löbau, J., and Wolfrum, K. (1997) Sum-Frequency Spectroscopy in Total Internal Reflection Geometry: Signal Enhancement and Access to Molecular Properties. *J. Opt. Soc. Am. B* *14*, 2505–2512.
- [65] McGall, S. J., Davies, P. B., and Neivandt, D. J. (2004) Interference Effects in Sum Frequency Vibrational Spectra of Thin Polymer Films: An Experimental and Modeling Investigation. *J. Phys. Chem. B* *108*, 16030–16039.
- [66] Shultz, M. J. In *Advances in Multi-Photon Processes and Spectroscopy*; Lin, S. H., Villaeys, A. A., and Fujimura, Y., Eds.; World Scientific Publishing Co.: River Edge, NJ, 2008; Vol. 18; Chapter 4, pp 133–199.
- [67] Moore, F. G., Becraft, K. A., and Richmond, G. L. (2002) Challenges in Interpreting Vibrational Sum Frequency Spectra: Deconvoluting Spectral Features as Demonstrated in the Calcium Fluoride–Water–Sodium Dodecylsulfate System. *Appl. Spec.* *56*, 1575–1578.
- [68] Bain, C. D., Davies, P. B., Ong, T. H., Ward, R. N., and Brown, M. A. (1991) Quantitative Analysis of Monolayer Composition by Sum-Frequency Vibrational Spectroscopy. *Langmuir* *7*, 1563–1566.
- [69] Raymond, E. A., Tarbuck, T. L., and Richmond, G. L. (2002) Isotopic Dilution Studies of the Vapor/Water Interface as Investigated by Vibrational Sum-Frequency Spectroscopy. *J. Phys. Chem. B* *106*, 2817–2820.
- [70] Gragson, D., McCarty, B., Richmond, G. L., and Alavi, D. S. (1996) High-Power Broadly Tunable Picosecond IR Laser System For Use In Nonlinear Spectroscopic Applications. *J. Opt. Soc. Am. B* *13*, 1075–2083.
- [71] Gragson, D., Alavi, D., and Richmond, G. L. (1995) Tunable Picosecond Infrared Laser System Based on Parametric Amplification in KTP with a Ti:Sapphire Amplifier. *Optics Lett.* *20*, 1991–1993.
- [72] Allen, H. C., Raymond, E. A., and Richmond, G. L. (2001) Surface Structural Studies of Methanesulfonic Acid at Air/Aqueous Solution Interfaces Using Vibrational Sum Frequency Spectroscopy. *J. Phys. Chem. A* *105*, 11649–1655.

- [73] Vanherzeele, H., Bierlain, J. D., and Zumsteg, F. C. (1988) Index of Refraction Measurements and Parametric Generation in Hydrothermally Grown KTiOPO_4 . *Applied Optics* 27, 3314–3316.
- [74] Fenimore, D. L., Schepler, K. L., Ramabadran, U. B., and McPherson, S. R. (1995) Infrared Corrected Sellmeier Coefficients for Potassium Titanyl Arsenate. *J. Opt. Soc. Am. B* 12, 794–706.
- [75] Finlayson-Pitts, B. J. (2003) The Tropospheric Chemistry of Sea Salt: A Molecular-Level View of the Chemistry of NaCl and NaBr. *Chem. Rev.* 103, 4801–4822.
- [76] Ellison, G. B., Tuck, A. F., and Vaida, V. (1999) Atmospheric Processing of Organic Aerosols. *J. Geophys. Res.* 104, 11,633–11,641.
- [77] Jacobson, M. C., Hansson, H. C., Noone, K. J., and Charlson, R. J. (2000) Organic Atmospheric Aerosols: Review and State of the Science. *Reviews of Geophysics* 38, 267–294.
- [78] Fuzzi, S., Decesari, S., Facchini, M. C., Matta, E., and Mircea, M. (2001) A Simplified Model of the Water Soluble Organic Component of Atmospheric Aerosols. *Geophys. Res. Lett.* 20, 4079–4082.
- [79] Rudich, Y. (2003) Laboratory Perspectives on the Chemical Transformation of Organic Matter in Atmospheric Particles. *Chem. Rev.* 103, 5097–5124.
- [80] Bianco, R., and Hynes, J. T. (2006) Heterogeneous Reactions Important in Atmospheric Ozone Depletion: A Theoretical Perspective. *Acc. Chem. Res.* 39, 159–165.
- [81] Du, Q., Superfine, R., Freysz, E., and Shen, Y. (1993) Vibrational Spectroscopy of Water at the Vapor/Water Interface. *Phys. Rev. Lett.* 70, 2313–2316.
- [82] Perry, A., Neipert, C., Ridley, C., Space, B., and Moore, P. B. (2005) Identification of a Wagging Vibrational Mode of Water Molecules at the Water/Vapor Interface. *Phys. Rev. E: Stat., Nonlinear, Soft Matter Phys.* 71, 050601/1–050601/4.
- [83] Smits, M., Ghosh, A., Sterrer, M., Müller, M., and Bonn, M. (2007) Ultrafast Vibrational Energy Transfer between Surface and Bulk Water at the Air–Water Interface. *Phys. Rev. Lett.* 98, 098302/1–09802/4.
- [84] Sovago, M., Campen, R. K., Bakker, H. J., and Bonn, M. (2009) Hydrogen Bonding Strength of Interfacial Water Determined With Surface Sum-Frequency Generation. *Chem. Phys. Lett.* 470, 7–12.

- [85] Sovago, M., Campen, R. K., Wurpel, G. W. H., Müller, M., Bakker, H. J., and Bonn, M. (2008) Vibrational Response of Hydrogen-Bonded Interfacial Water is Dominated by Intramolecular Coupling. *Phys. Rev. Lett.* *100*, 173901/1–173901/4.
- [86] Buch, V. (2005) Molecular Structure and the OH-Stretch Spectra of Liquid Water Surface. *J. Phys. Chem. B* *109*, 17771–17774.
- [87] Dang, L. X., and Chang, T.-M. (1997) Molecular Dynamics Study of Water Clusters, Liquid, Liquid-Vapor Interface of Water With Many-Body Potentials. *J. Chem. Phys.* *106*, 8149–8159.
- [88] Auer, B. M., and Skinner, J. L. (2008) Vibrational Sum-Frequency Spectroscopy of the Liquid/Vapor Interface for dilute HOD in D₂O. *J. Chem. Phys.* *129*, 214705/1–214705/14.
- [89] Tian, C.-S., and Shen, Y. R. (2009) Isotopic Dilution Study of the Water/Vapor Interface by Phase-Sensitive Sum-Frequency Vibrational Spectroscopy. *J. Am. Chem. Soc.* *131*, 2790–2791.
- [90] Tian, C. S., and Shen, Y. R. (2009) Sum-Frequency Vibrational Spectroscopic Studies of Water/Vapor Interfaces. *Chem. Phys. Lett.* *470*, 1–6.
- [91] Fan, Y., Chen, X., Yang, L., Cremer, P. S., and Gao, Y. Q. (2009) On the Structure of Water at the Aqueous/Air Interface. *J. Phys. Chem. B* *113*, 11672–11679.
- [92] Morita, A. (2006) Improved Computation of Sum Frequency Generation Spectrum of the Surface of Water. *J. Phys. Chem. B* *110*, 3158–3163.
- [93] Kuo, I.-F. W., Mundy, C. J., Eggimann, B. L., McGrath, M. J., Siepmann, J. I., Chen, B., Vieceli, J., and Tobias, D. J. (2006) Structure and Dynamics of the Aqueous Liquid–Vapor Interface: A Comprehensive Particle-Based Simulation Study. *J. Phys. Chem. B* *110*, 3738–3746.
- [94] Walker, D. S., Hore, D. K., and Richmond, G. L. (2006) Understanding the Population, Coordination, and Orientation of Water Species Contributing to the Nonlinear Optical Spectroscopy of the Vapor–Water Interface through Molecular Dynamics Simulations. *J. Phys. Chem. B* *110*, 20451–20459.
- [95] Ishiyama, T., and Morita, A. (2007) Molecular Dynamics Study of Gas-Liquid Aqueous Sodium Halide Interfaces. I. Flexible and Polarizable Molecular Modeling and Interfacial Properties. *J. Phys. Chem. C* *111*, 721–737.

- [96] Walker, D. S., and Richmond, G. L. (2007) Understanding the Effects of Hydrogen Bonding at the Vapor–Water Interface: Vibrational Sum Frequency Spectroscopy of H₂O/HOD/D₂O Mixtures Studied Using Molecular Dynamics Simulations. *J. Phys. Chem. C* *111*, 8321–8330.
- [97] Ishiyama, T., and Morita, A. (2007) Molecular Dynamics Study of Gas-Liquid Aqueous Sodium Halide Interfaces. II. Analysis of Vibrational Sum Frequency Generation Spectra. *J. Phys. Chem. C* *111*, 738–748.
- [98] Hore, D. K., Walker, D. S., and Richmond, G. L. (2008) Water at Hydrophobic Surfaces: When Weaker is Better. *J. Am. Chem. Soc.* *130*, 1800–1801.
- [99] Ishiyama, T., and Morita, A. (2009) Vibrational Spectroscopic Response of Intermolecular Orientational Correlation at the Water Surface. *J. Phys. Chem. C* *113*, 16299–16302.
- [100] Ishiyama, T., and Morita, A. (2009) Analysis of Anisotropic Local Field in Sum Frequency Generation Spectroscopy With the Charge Response Kernel Water Model. *J. Chem. Phys.* *131*, 244714/1–244717/17.
- [101] Noah-Vanhoucke, J., Smith, J. D., and Geissler, P. L. (2009) Toward a Simple Molecular Understanding of Sum Frequency Generation at Air–Water Interfaces. *J. Phys. Chem. B* *113*, 4065–4074.
- [102] Auer, B. M., and Skinner, J. L. (2009) Water: Hydrogen Bonding and Vibrational Spectroscopy, In the Bulk Liquid and at the Liquid/Vapor Interface. *Chem. Phys. Lett.* *470*, 13–20.
- [103] Kühn, T. D., Pascal, T. A., Kaxiras, E., and Jung, Y. (2011) New Insights into the Structure of the Vapor/Water Interface from Large-Scale First-Principles Simulations. *J. Phys. Chem. Lett.* *2*, 105–113.
- [104] Gan, W., Wu, D., Zhang, Z., Feng, R.-r., and Wang, H.-f. (2006) Polarization and Experimental Configuration Analyses of Sum Frequency Generation Vibrational Spectra, Structure, and Orientational Motion of the Air/Water Interface. *J. Chem. Phys.* *124*, 114705/1–114705/15.
- [105] Morita, A., and Hynes, J. T. (2002) A Theoretical Analysis of the Sum Frequency Generation Spectrum of the Water Surface. II. Time-Dependent Approach. *J. Phys. Chem. B* *106*, 673–685.
- [106] Ghosh, A., Smits, M., Sovago, M., Bredenbeck, J., Müller, M., and Bonn, M. (2008) Ultrafast vibrational dynamics of interfacial water. *Chem. Phys.* *350*, 23–30.

- [107] Auer, B. M., and Skinner, J. L. (2009) Vibrational Sum-Frequency Spectroscopy of the Water Liquid/Vapor Interface. *J. Phys. Chem. B* *113*, 4125–4130.
- [108] Bakker, H. J., and Skinner, J. L. (2010) Vibrational Spectroscopy as a Probe of Structure and Dynamics in Liquid Water. *Chem. Rev.* *110*, 1498–1517.
- [109] Sovago, M., Vartiainen, E. M., and Bonn, M. (2009) Determining Absolute Molecular Orientation at Interfaces: A Phase Retrieval Approach for Sum Frequency Generation Spectroscopy. *J. Phys. Chem. C* *113*, 6100–6106.
- [110] Tian, C. S., and Shen, Y. R. (2008) Comment on "Vibrational Response of Hydrogen-Bonded Interfacial Water is Dominated by Intermolecular Coupling". *Phys. Rev. Lett.* *101*, 139401/1.
- [111] Sovago, M., Campen, R. K., Wurfel, G. W. H., Muller, M., Bakker, H. J., and Bonn, M. (2008) Sovago *et. al.*Reply. *Phys. Rev. Lett.* *101*, 139402/1.
- [112] Stiopkin, I. V., Jayathilake, H. D., Bordenyuk, A. N., and Benderskii, A. V. (2008) Heterodyne-Detected Vibrational Sum frequency Generation Spectroscopy. *J. Am. Chem. Soc.* *130*, 2271–2275.
- [113] Schnitzer, C., Baldelli, S., and Shultz, M. J. (2000) Sum Frequency Generation of Water on NaCl, NaNO₃, KHSO₄, HCl, HNO₃, and H₂SO₄ Aqueous Solutions. *J. Phys. Chem. B* *104*, 585–590.
- [114] Wei, X., Miranda, P. B., and Shen, Y. R. (2001) Surface Vibrational Spectroscopic Study of Surface Melting of Ice. *Phys. Rev. Lett.* *86*, 1554–1557.
- [115] Wei, X., and Shen, Y. R. (2002) Vibrational Spectroscopy of Ice Interfaces. *Appl. Phys. B* *74*, 617–620.
- [116] Shen, Y. R. (1998) Sum Frequency Generation for Vibrational Spectroscopy: Applications to Water Interfaces and Films of Water and Ice. *Solid State Commun.* *108*, 399–406.
- [117] Laskin, A., Gaspar, D. J., Wang, W., Hunt, S. W., Cowin, J. P., Colson, S. D., and Finlayson-Pitts, B. J. (2003) Reactions at Interfaces As a Source of Sulfate Formation in Sea-Salt Particles. *Science* *301*, 340–344.
- [118] Alexandrova, S., Marion, M., Lepinasse, E., and Saboni, A. (2004) Mass Transfer Modeling of SO₂ into Large Water Drops. *Chem. Eng. Technol.* *27*, 676–680.
- [119] Adema, E. H., and Heeres, P. (1995) Dry deposition of Sulfur Dioxide and Ammonia on Wet Surfaces and the Surface Oxidation Kinetics of Bisulfite. *Atmos. Environ.* *29*, 1091–1103.

- [120] Chang, C. S., and Rochelle, G. T. (1981) SO₂ Absorption Into Aqueous Solutions. *AIChE J.* *27*, 292–298.
- [121] Shaka, H., Robertson, W. H., and Finlayson-Pitts, B. J. (2007) A New Approach to Studying Aqueous Reactions Using Diffuse Reflectance Infrared Fourier Transform Spectrometry: Application to the Uptake and Oxidation of SO₂ on OH-Processed Sea Salt Aerosol. *Phys. Chem. Chem. Phys.* *9*, 1980–1990.
- [122] Cotton, F. A., Wilkinson, G., Murillo, C. A., and Bochmann, M. *Advanced Inorganic Chemistry*, 6th ed.; John Wiley and Sons, Inc.: New York, 1999.
- [123] Tarbuck, T. L., and Richmond, G. L. (2006) Adsorption and Reaction of CO₂ and SO₂ at a Water Surface. *J. Am. Chem. Soc.* *128*, 3256–3267.
- [124] Tarbuck, T. L., and Richmond, G. L. (2005) SO₂:H₂O complex found at the Vapor/Water interface. *J. Am. Chem. Soc.* *127*, 16806–16807.
- [125] Baer, M., Mundy, C. J., Chang, T.-M., Tao, F.-M., and Dang, L. X. (2010) Interpreting Vibrational Sum-Frequency Spectra of Sulfur Dioxide at the Air/Water Interface: A Comprehensive Molecular Dynamics Study. *J. Phys. Chem. B* *114*, 7245–7249.
- [126] Schriver-Mazzuoli, L., Chaabouni, H., and Schriver, A. (2003) Infrared spectra of SO₂ and SO₂:H₂O Ices At Low Temperature. *J. Mol. Struct.* *644*, 151–164.
- [127] Hirabayashi, S., Ito, F., and Yamada, K. M. T. (2006) Infrared Spectra of the (H₂O)_n-SO₂ Complexes in Argon Matrices. *The Journal of Chem. Phys.* *125*, 034508/1–034508/6.
- [128] Zhang, Z., and Ewing, G. E. (2002) Infrared Spectroscopy of SO₂ Aqueous Solutions. *Spectrochim. Acta, Part A* *58*, 2105–2113.
- [129] Matsumura, K., Lovas, F. J., and Suenram, R. D. (1989) The Microwave Spectrum and Structure of the H₂O-SO₂ Complex. *J. Chem. Phys.* *91*, 5887–5894.
- [130] Donaldson, D. J., Guest, J. A., and Goh, M. C. (1995) Evidence for Adsorbed SO₂ at the Aqueous-Air Interface. *J. Phys. Chem.* *99*, 9313–9315.
- [131] Yang, H., Wright, N. J., Gagnon, A. M., Gerber, R. B., and Finlayson-Pitts, B. J. (2002) An Upper Limit to the Concentration of an SO₂ Complex at the Air-Water Interface at 298 K: Infrared Experiments and *ab-initio* Calculations. *Phys. Chem. Chem. Phys.* *4*, 1832–1838.

- [132] Voegelé, A. F., Tautermann, C. S., Rauch, C., Loerting, T., and Liedl, K. R. (2004) On the Formation of the Sulfonate Ion from Hydrated Sulfur Dioxide. *J. Phys. Chem. A* 108, 3859–3864.
- [133] Steudel, R., and Steudel, Y. (2009) Sulfur Dioxide and Water: Structures and Energies of the Hydrated Species $\text{SO}_2\text{-nH}_2\text{O}$, $[\text{HSO}_3]^- \text{-nH}_2\text{O}$, $[\text{SO}_3\text{H}]^- \text{-nH}_2\text{O}$, and $\text{H}_2\text{SO}_3\text{-nH}_2\text{O}$ ($n=0\text{--}8$). *Eur. J. Inorg. Chem.* 2009, 1393–1405.
- [134] Cukras, J., and Sadlej, J. (2007) Structure and Energetics of Weakly Bound Water-Sulfur Dioxide Complexes. *J. Mol. Struct. (Theochem)* 819, 41–51.
- [135] Cukras, J., and Sadlej, J. (2008) On the Nature of the Interaction in Ternary Water-Sulfur Dioxide Complexes. *Pol. J. Chem.* 82, 675–685.
- [136] Madsen, M. S., Gross, A., Falsig, H., Kongsted, J., Osted, A., Mikkelsen, K. V., and Christiansen, O. (2008) Determination of Rate constants for the Uptake Process Involving SO_2 and An Aerosol Particle. A Quantum Mechanics/Molecular Mechanics and Quantum Statistical Investigation. *Chem. Phys.* 348, 21–30.
- [137] Baldelli, S., Schnitzer, C., and Shultz, M. J. (1999) The Structure of Water on HCl Solutions Studied With Sum Frequency Generation. *Chem. Phys. Lett.* 302, 157–163.
- [138] Levering, L. M., Sierra-Hernández, and Allen, H. C. (2007) Observation of Hydronium Ions at the Air–Aqueous Interface: Vibrational Spectroscopic Studies of Aqueous HCl, HBr, and HI. *J. Phys. Chem. C* 111, 8814–8826.
- [139] Tian, C., Ji, N., Waychunas, G. A., and Shen, Y. R. (2008) Interfacial Structures of Acidic and Basic Aqueous Solutions. *J. Am. Chem. Soc.* 130, 13033–13039.
- [140] Miyamae, T., Morita, A., and Ouchi, Y. (2008) First Acid Dissociation at an Aqueous H_2SO_4 Interface with Sum Frequency Generation Spectroscopy. *Phys. Chem. Chem. Phys.* 10, 2010–2013.
- [141] Baldelli, S., Schnitzer, C., Campbell, D. J., and Shultz, M. J. (1999) Effect of H_2SO_4 and Alkali Metal $\text{SO}_4^-/\text{HSO}_4^-$ Salt Solutions on Surface Water Molecules Using Sum Frequency Generation. *J. Phys. Chem. B* 103, 2789–2795.
- [142] Schnitzer, C., Baldelli, S., and Shultz, M. J. (1999) Sum Frequency Generation by Water on Supercooled $\text{H}_2\text{SO}_4/\text{H}_2\text{O}$ Liquid Solutions at Stratospheric Temperature. *Chem. Phys. Lett.* 313, 416–420.
- [143] Baldelli, S., Schnitzer, C., Shultz, M. J., and Campbell, D. J. (1998) Sum Frequency Generation Investigation of Water at the Surface of $\text{H}_2\text{O}/\text{H}_2\text{SO}_4$ and $\text{H}_2\text{O}/\text{Cs}_2\text{SO}_4$ Binary Systems. *Chem. Phys. Lett.* 287, 143–147.

- [144] Baldelli, S., Schnitzer, C., and Shultz, M. J. (1997) Sum Frequency Generation Investigation of Water at the Surface of H₂O/H₂SO₄ Binary Systems. *J. Phys. Chem. B* 101, 10435–10441.
- [145] Radüge, C., Pflumio, V., and Shen, Y. R. (1997) Surface Vibrational Spectroscopy of Sulfuric Acid - Water Mixtures at the Liquid - Vapor Interface. *Chem. Phys. Lett.* 274, 149–144.
- [146] Shultz, M. J., Baldelli, S., Schnitzer, C., and Simonelli, D. (2002) Aqueous Solution/Air Interfaces Probed with Sum Frequency Generation Spectroscopy. *J. Phys. Chem. B* 106, 5313–5324.
- [147] Ming, Y., and Russell, L. M. (2004) Organic Aerosol Effects on Fog Droplet Spectra. *J. Geophys. Res.* 109, D10206/1–D10206/14.
- [148] Stephanou, E. G. (2005) The Decay of Organic Aerosols. *Nature* 434, 31.
- [149] Maria, S. F., Russell, L. M., Gilles, M. K., and Myneni, S. C. B. (2004) Organic Aerosol Growth Mechanisms and Their Climate-Forcing Implications. *Science* 306, 1921–1924.
- [150] Goss, K.-U. (2009) Predicting Adsorption of Organic Chemicals at the Air–Water Interface. *J. Phys. Chem. A* 113, 12256–12259.
- [151] Hyvärinen, A.-P., Raatikainen, T., Laaksonen, A., Viisanen, Y., and Lihavainen, H. (2005) Surface Tensions and Densities of H₂SO₄+ NH₃ + Water Solutions. *Geophys. Res. Lett.* 32, L16806.
- [152] Eliason, T. L., Gilman, J. B., and Vaida, V. (2004) Oxidation of Organic Films Relevant to Atmospheric Aerosols. *Atmos. Environ.* 38, 1367–1378.
- [153] Molina, M. J., Ivanov, A. V., Trakhtenberg, S., and Molina, L. T. (2004) Atmospheric Evolution of Organic Aerosol. *Geophys. Res. Lett.* 31, L22104–1–L22104–5.
- [154] O’Dowd, C. D., Facchini, M. C., Cavalli, F., Ceburnis, D., Decesari, S., Fuzzi, S., Yoon, J. J., and Putaud, J.-P. (2004) Biogenically Driven Organic Contribution to Marine Aerosol. *Nature* 431, 676–680.
- [155] Bluhm, H., and Siegmann, H. C. (2009) Surface Science with Aerosols. *Surf. Sci.* 603, 1969–1978.
- [156] Fuzzi, S., Andreae, M. O., Huebert, B. J., Kulmala, M., Bond, T. C., Boy, M., Doherty, S. J., Guenther, A., Kanakidou, M., Kawamura, K., Kerminen, V.-M., Lohmann, U., Russell, L. M., and Pöschl, U. (2005) Critical Assessment of the Current State of Scientific Knowledge, Terminology, and Research Needs Concerning the Role of Organic Aerosols in the Atmosphere, Climate, and Global Change. *Atmospheric Chemistry and Physics Discussions* 5.

- [157] Rudich, Y., Donahue, N. M., and Mentel, T. F. (2007) Aging of Organic Aerosol: Bridging the Gap Between Laboratory and Field Studies. *Annu. Rev. Phys. Chem.* *58*, 321–352.
- [158] Valsaraj, K. T., and Thibodeaux, L. J. (2010) On the Physicochemical Aspects of the Global Fate and Long-Range Atmospheric Transport of Persistent Organic Pollutants. *J. Phys. Chem. Lett.* *1*, 1694–1700.
- [159] Gilman, J. B., Eliason, T. L., Fast, A., and Vaida, V. (2004) Selectivity and Stability of Organic Films at the Air–Aqueous Interface. *Journal of Colloid and Interface Science* *280*, 234–243.
- [160] Jung, J., Tsalal, B., Kim, Y. J., and Kawamura, K. (2010) Organic and Inorganic Aerosol Composition in Ulaanbaatar, Mongolia, During the Cold Winter of 2007 to 2008: Dicarboxylic Acids, Ketocarboxylic Acids, and α -Dicarbonyls. *J. Geophys. Res.* *115*, D22203/1–D22203/15.
- [161] Legrand, M., Preunkert, S., Galy-Lacaux, C., Liousse, C., and Wagenback, D. (2005) Atmospheric Year-Round Records of Dicarboxylic Acids and Sulfate at Three French Sites Located Between 630 and 4360 m Elevation. *J. Geophys. Res.* *110*, 13302.
- [162] Kawamura, K., Kobayashi, M., Tsubonuma, N., Mochida, M., Watanabe, T., and Lee, M. In *Geochemical Investigations in Earth and Space Science: A Tribute to Isaac R. Kaplan*; Hill, R. J., Leventhal, J., Baedecker, M. J., Claypool, G., Eganhouse, R., Goldhaber, M., and Peters, K., Eds.; The Geochemical Society Special Publications Series 9; Elsevier: New York, 2004; pp 243–265.
- [163] Decesari, S., Facchini, M. C., Matta, E., Lettini, F., Mircea, M., Fuzzi, S., Tagliavini, E., and Putaud, J.-P. (2001) Chemical Features and Seasonal Variation of Fine Aerosol Water-Soluble Organic Compounds in the Po Valley, Italy. *Atmos. Environ.* *35*, 3691–3699.
- [164] Decesari, S., Facchini, M. C., and Fuzzi, S. (2000) Characterization of Water-Soluble Organic Compounds in Atmospheric Aerosol: A New Approach. *J. Geophys. Res.* *105*, 1481–1489.
- [165] Simoneit, B. R. T., Kobayashi, M., Mochida, M., and Kawamura, K. (2004) Aerosol Particles Collected on Aircraft Flights Over the Northwestern Pacific Region During the ACE-Asia campaign: Composition and Major Sources of the Organic Compounds. *J. Geophys. Res.* *109*, S09.
- [166] Russell, L. M., Maria, S. F., and Myneni, S. C. B. (2002) Mapping Organic Coatings on Atmospheric Particles. *Geophys. Res. Lett.* *29*, 26,1–26,4.

- [167] Prenni, A. J., De Mott, P. J., Kreidenweis, S. M., Sherman, D. E., Russell, L. M., and Ming, Y. (2001) The Effects of Low Molecular weight Dicarboxylic Acids on Cloud Formation. *J. Phys. Chem. A* 105, 11240–11248.
- [168] Bilde, M., Svenningsson, B., Mønster, J., and Rosenørn, T. (2003) Even-Odd Alternation of Evaporation Rates and Vapor Pressures of C3-C9 Dicarboxylic Acid Aerosols. *Environ. Sci. Technol.* 37, 1371–1378.
- [169] Kim, H. I., Goddard, W. A. I., and Beauchamp, J. L. (2006) Cluster Phase Chemistry: Gas-Phase Reactions of Anionic Sodium Salts of Dicarboxylic Acid Clusters With Water Molecules. *J. Phys. Chem. A* 110, 7777–7786.
- [170] Grunwald, E., Pan, K.-C., and Effio, A. (1976) Hydrogen Bonding in Polar Liquid Solutions. 4. Effect of Hydrogen-Bonding Solutes on Dielectric Constant and Solvent Structures in 1-Octanol. *The Journal of Physical Chemistry* 80, 2937–2940.
- [171] Beyer, K. D., Friesen, K., Bothe, J. R., and Palet, B. (2008) Phase Diagrams and Water Activities of Aqueous Dicarboxylic Acid Systems of Atmospheric Importance. *J. Phys. Chem. A* 112, 11704–11713.
- [172] Clegg, S. L., and Seinfeld, J. H. (2006) Thermodynamic Models of Aqueous Solutions Containing Inorganic Electrolytes and Dicarboxylic Acids at 298.15 K. 2. Systems Including Dissociation Equilibria. *J. Phys. Chem. A* 110, 5718–5734.
- [173] Rosado-Reyes, C. M., and Francisco, J. S. (2006) Atmospheric Oxidation Pathways of Acetic Acid. *J. Phys. Chem. A* 110, 4419–4433.
- [174] Freedman, M. A., Hasenkopf, C. A., Beaver, M. R., and Tolbert, M. A. (2009) Optical Properties of Internally Mixed Aerosol Particles Composed of Dicarboxylic Acids and Ammonium Sulfate. *J. Phys. Chem. A* 113, 13584–13592.
- [175] Choi, M. Y., and Chan, C. K. (2002) The Effect of Organic Species on the Hygroscopic Behaviors of Inorganic Aerosols. *Environ. Sci. Technol.* 36, 2422–2428.
- [176] Kawamura, K., and R., K. I. (1987) Motor Exhaust Emissions as a Primary Source for Dicarboxylic Acids in Los Angeles Ambient Air. *Environ. Sci. Technol.* 21, 105–110.
- [177] Wolfs, I., and Desseyn, H. O. (1996) Characteristic Vibrational Pattern for the Cyclic Dimer Carboxylic Acid Function in the Solid State. *Appl. Spec.* 50, 1000–1006.

- [178] Suzuki, M., and Shimanouchi, T. (1968) Infrared and Raman Spectra of Succinic Acid Crystal. *Journal of Molecular Spectroscopy* 28, 394–410.
- [179] Mitsui, K., and Ukaji, T. (1977) Infrared Spectra of Some Aqueous Solutions. *Ikutoku Kogyo Daigaku Kenkyu Hokoku, B: Rikogaku-hen B-2*, 77–82.
- [180] Cabaniss, S. E., Leenheer, J. A., and McVey, I. F. (1998) Aqueous Infrared Carboxylate Absorbances: Aliphatic Di-Acids. *Spectrochim. Acta, Part A* 54, 449–458.
- [181] De Gelder, J., De Gussem, K., Vandanabeele, P., and Moens, L. (2007) Reference Database of Raman Spectra of Biological Molecules. *J. Raman Spectrosc.* 38, 1133–1147.
- [182] Nunes, M. T., Gil, V. M. S., and Ascenso, J. (1981) The Conformation of Succinic Acid In Aqueous Solution Studied by ^1H and ^{13}C NMR. *Tetrahedron* 37, 611–614.
- [183] Mahiuddin, S., Minofar, B., Borah, J. M., Das, M. R., and Jungwirth, P. (2008) Propensities of Oxalic, Citric, Succinic, and Maleic acids for the Aqueous Solution/Vapour Interface: Surface Tension Measurements and Molecular Dynamics Simulations. *Chem. Phys. Lett.* 462, 217–221.
- [184] Vanhanen, J., Hyvärinen, A.-P., Viisanen, Y., and Lihavaunen, H. (2008) Ternary Solution of Sodium Chloride, Succinic Acid and Water–Surface Tension and its Influence on Cloud Droplet Activation. *Atmos. Chem. Phys. Discuss.* 8, 7189–7216.
- [185] Socrates, G. *Infrared and Raman Characteristic Group Frequencies: Tables and Charts*, 3rd ed.; John Wiley and Sons, Ltd., 2001.
- [186] Blando, J. D., and Turpin, B. J. (2000) Secondary Organic Aerosol Formation in Cloud and Fog Droplets: a Literature Evaluation of Plausibility. *Atmos. Environ.* 34, 1623–1632.
- [187] Iraci, L. T., and Tolbert, M. A. (1997) Heterogeneous Interaction of Formaldehyde with Cold Sulfuric Acid: Implications for the Upper Troposphere and Lower Stratosphere. *J. Geophys. Res.* 102, 16099–16107.
- [188] Davidovits, P., Kolb, C. E., Williams, L. R., Jayne, J. T., and Worsnop, D. R. (2006) Mass Accommodation and Chemical Reactions at Gas–Liquid Interfaces. *Chem. Rev.* 106, 1323–1354.
- [189] Whiteaker, J. R., and Prather, K. A. (2003) Hydroxymethanesulfonate as a Tracer For Fog Processing of Individual Aerosol Particles. *Atmos. Environ.* 37, 1033–1043.

- [190] Kroll, J. H., Ng, N. L., Murphy, S. M., Varutbangkul, V., Flagan, R. C., and Seinfeld, J. H. (2005) Chamber Studies of Secondary Organic Aerosol Growth by Reactive Uptake of Simple Carbonyl Compounds. *J. Geophys. Res.* *110*, D23207/1–D23207/10.
- [191] Lebrun, N., Dhamelinourt, P., Focsa, C., Chazallon, B., Destombes, J. L., and Prevost, D. (2003) Raman Analysis of Formaldehyde Aqueous Solutions as a Function of Concentration. *J. Raman Spectrosc.* *34*, 459–464.
- [192] Hibben, J. (1931) The Raman Spectra of Formaldehyde, Trioxymethylene, Ethylene Glycol, and of Some Viscous Liquids. *J. Am. Chem. Soc.* *53*, 2418.
- [193] Chazallon, B., Oancea, A., Capoen, B., and Focsa, C. (2008) Ice Mixtures Formed by Simultaneous Condensation of Formaldehyde and Water: an *in situ* Study by Micro-Raman Scattering. *Phys. Chem. Chem. Phys.* *10*, 702–712.
- [194] Hanoune, B., Paccou, L., Delcroix, P., and Guinet, Y. (2010) Raman Identification of H₂CO in Aqueous Solutions. *J. Raman Spectrosc.*
- [195] Ryabova, R. S., Voloshenko, G. I., Maiorov, V. D., and Osipova, G. F. (2002) Equilibrium Composition of Formaldehyde Oligomers in Aqueous Solutions from IR Data. *Russ. J. Appl. Chem.* *75*, 22–24.
- [196] Jayne, J. T., Worsnop, D. R., Kolb, C. E., Swartz, E., and Davidovits, P. (1996) Uptake of Gas-Phase Formaldehyde by Aqueous Acid Surfaces. *J. Phys. Chem.* *100*, 8015–8022.
- [197] Swartz, E., Boniface, J., Tchertkov, I., Rattigan, O. V., Robinson, D. V., Davidovits, P., Worsnop, D. R., Jayne, J. T., and Kolb, C. E. (1997) Horizontal Bubble Train Apparatus for Heterogeneous Chemistry Studies: Uptake of Gas-Phase Formaldehyde. *Environ. Sci. Technol.* *31*, 2634–2641.
- [198] Dimitrova, Y. (1997) Solvent Effects on Vibrational Spectra of Hydrogen-Bonded Complexes of Formaldehyde and Water: An Ab Initio Study. *J. Mol. Struct. (Theochem)* *391*, 251–257.
- [199] Barret, M., Houdier, S., and Domine, F. (2011) Thermodynamics of the Formaldehyde–Water and Formaldehyde–Ice Systems for Atmospheric Applications. *J. Phys. Chem. A* *115*, 307–317.
- [200] Oancea, A., Hanoune, B., Focsa, C., and Chazallon, B. (2009) Cross Determination of the Vapor Liquid Equilibrium of Formaldehyde Aqueous Solutions by Quadrupole Mass Spectrometry and Infrared Diode Laser Spectroscopy. *Environ. Sci. Technol.* *43*, 435–440.

- [201] Jayne, J. T., Duan, S. X., Davidovits, P., Worsnop, D. R., Zahniser, M. S., and Kolb, C. E. (1992) Uptake of Gas-Phase Aldehydes by Water Surfaces. *J. Phys. Chem.* *96*, 5452–5460.
- [202] Albert, M., Coto García, B., Kreiter, C., and Maurer, G. (1999) Vapor-Liquid and Chemical Equilibria of Formaldehyde-Water Mixtures. *AIChE J.* *45*, 2024–2033.
- [203] Munger, J. W., Jacob, D. J., and Hoffman, M. R. (1984) The Occurrence of Bisulfite-Aldehyde Addition Products in Fog- and Cloudwater. *J. Atmos. Chem.* *1*, 335–350.
- [204] Ang, C. C., Lipari, F., and Swarin, S. J. (1987) Determination of Hydroxymethanesulfonate in Wet Deposition Samples. *Environ. Sci. Technol.* *21*, 102–105.
- [205] Chazallon, B., Lebrun, N., Dhamelincourt, P., Toubin, C., and Focsa, C. (2005) Micro-Raman Investigations of the Formaldehyde-Ice System. *J. Phys. Chem. B* *109*, 432–439.
- [206] Begue, D., Elissalde, S., Pere, E., Iratcabal, P., and Pouchan, C. (2006) New Theoretical and Experimental Infrared Results on Formaldehyde in Solution. *J. Phys. Chem. A* *110*, 7793–7800.
- [207] Lu, R., Gan, W., Wu, B.-h., Chen, H., and Wang, H.-f. (2004) Vibrational Polarization Spectroscopy of CH Stretching Modes of the Methylene Group at the Vapor/Liquid Interfaces with Sum Frequency Generation. *J. Phys. Chem. B* *108*, 7297–7306.
- [208] Libnau, F., Christy, A. A., and Kvalheim, O. M. (1995) Determination of the Equilibrium Constant and Resolution of the HOD Spectrum by Alternating Least-Squares and Infrared Analysis. *Appl. Spec.* *49*, 1431–1437.